



**A University of Sussex DPhil thesis**

Available online via Sussex Research Online:

<http://eprints.sussex.ac.uk/>

This thesis is protected by copyright which belongs to the author.

This thesis cannot be reproduced or quoted extensively from without first obtaining permission in writing from the Author

The content must not be changed in any way or sold commercially in any format or medium without the formal permission of the Author

When referring to this work, full bibliographic details including the author, title, awarding institution and date of the thesis must be given

Please visit Sussex Research Online for more information and further details



University of Sussex

**Remote Applications of Electric Potential  
Sensors in Electrically Unshielded  
Environments**

**Sam Thomas Beardsmore-Rust**

Submitted for the degree of Doctor of Philosophy

University of Sussex

April 2010

# Declaration

I hereby declare that this thesis has not been and will not be submitted in whole or in part to another University for the award of any other degree.

Signature:

Sam Beardsmore-Rust

UNIVERSITY OF SUSSEX

SAM BEARDSMORE-RUST, DOCTOR OF PHILOSOPHY

SUMMARY

The electric potential sensor is a novel, ultra high impedance sensor, previously developed at the University of Sussex. These sensors have been applied to a range of applications, including electrophysiology, non destructive testing of composite materials and novel nuclear magnetic resonance NMR probes.

Some of these measurements can be made in a strongly coupled ( $\geq 100\text{pF}$ ) mode, where the coupling capacitance is reasonably large and well defined, and ambient noise is therefore less problematic. However for many applications, there exists a requirement for this coupling to be much weaker. This weak and poorly defined coupling creates substantial problems with ambient noise often causing sensors to saturate and become unusable. In the past, therefore, these measurements have all been made inside electrically screened rooms and enclosures.

The work discussed in this thesis explores the possibility of operating these sensors outside of electrically screened environments. A number of techniques for resilience against noise are explored and experiments to fully analyse and characterise the performance of the sensors are discussed. As a result of this work, further results are then shown for a number of experiments carried out in a busy lab environment, in the presence of noise sources, and with little or minimal screening used. In this case, data is shown for the collection of remote cardiac and respiratory data, imaging of the spatial distribution of charge on insulating materials, detecting electric field disturbances for movement sensing and early results for a microscopic XY scanning application.

# Acknowledgements

It is with some sense of relief, and a little of trepidation, that I arrive at the acknowledgements page. I must firstly thank Prof Robert Prance and Dr Helen Prance for their endless enthusiasm, support, encouragement and optimism. Their guidance, patience and support has, and I suspect will continue to be, invaluable and inspiring, and for it I am truly grateful. I must also thank Martin Nock, who has provided not only invaluable technical advice, but been a friend and colleague without whom coming to work would not have been the same. Without his support, sense of humour, expert guidance and amazing smoked trout, I am sure I would have been lost.

The past few years would not have been the same without the others in the lab, particularly Phil, whose advice and afternoons of collaboration have always proved incalculably helpful. I must thank Shrijit for his friendship and support, and of course Ahmet and Jacob for advice, friendship and great games of Unihoc. It is with pleasure that I wish Tash and Philip good luck as they embark upon a journey I am confident they will find as enjoyable and rewarding as I have.

Thanks of course to our mechanical technician Dave Smith, whose workmanship is so incredible as to be beyond superlatives, and to Dr Peter Stiffell, for developing COMSOL simulations that were of great help.

Finally I must thank my wife Megan, for her encouragement, support, patience and for putting up with my long hours spent at work. Of course thanks to my parents Ann and Mel and my brother Ben.

To all those above, and so many others for your support and good times, Zoe, Rosie, Megan, Jessica, Tim, Shailen, Ginge, Charlotte, Steve, Angela, Clare, Karli, Tom, Balaji, Akber, Diane, Matthew and all those students who I have had the pleasure to teach, and be taught so much by. Thank you, I will not forget.

# Contents

<b>List of Publications</b>	<b>x</b>
<b>List of Tables</b>	<b>x</b>
<b>List of Figures</b>	<b>xvi</b>
<b>1 Introduction and Background</b>	<b>1</b>
1.1 Electric Field Measurement Techniques . . . . .	2
1.1.1 Electrometer based measurement . . . . .	3
1.1.2 Field Mill measurements . . . . .	5
1.1.3 Optical and Electro-optical Measurement . . . . .	6
1.2 A Brief Overview of Electric Potential Sensors . . . . .	7
1.3 Applications of an Electric Potential Sensor . . . . .	9
1.3.1 Electric Fields . . . . .	9
1.3.2 Movement Sensing . . . . .	10
1.3.3 Electrophysiological Sensing . . . . .	13
1.3.4 Materials Testing . . . . .	14
<b>2 Digital Control of Sensor Characteristics and Phase Space Mapping</b>	<b>18</b>
2.1 Introduction . . . . .	18
2.2 Positive Feedback Techniques for Enhancing Instrumentation Performance .	19
2.2.1 Bootstrapping . . . . .	19
2.2.2 Neutralization . . . . .	20
2.2.3 Guarding . . . . .	20
2.2.4 Positive Feedback in an EPS Sensor . . . . .	20
2.3 Programmable Sensor . . . . .	22
2.3.1 Results . . . . .	22
2.3.2 Simulations of Bootstrapping and Neutralization . . . . .	29

2.4	Conclusions . . . . .	32
<b>3</b>	<b>Tuned Sensors</b>	<b>37</b>
3.1	Introduction . . . . .	37
3.2	Signal specific sensors . . . . .	38
3.2.1	Tuned Sensor Architecture . . . . .	40
3.2.2	Real-Time Adaptability . . . . .	40
3.2.3	Circuit design . . . . .	44
3.2.4	Results . . . . .	45
3.2.5	Settling times and Aliasing . . . . .	48
3.3	Noise immune sensors . . . . .	50
3.3.1	Sensor design . . . . .	52
3.3.2	Results . . . . .	52
3.4	Conclusions . . . . .	53
<b>4</b>	<b>A Remote Cardiac Measurement</b>	<b>58</b>
4.1	Introduction . . . . .	58
4.2	Remote Electrophysiological Signals . . . . .	58
4.2.1	Introduction . . . . .	58
4.2.2	Methodology . . . . .	60
4.2.3	Results . . . . .	61
4.3	Future work . . . . .	63
<b>5</b>	<b>Detecting electric field disturbances for passive through wall movement and proximity sensing</b>	<b>65</b>
5.1	Introduction . . . . .	65
5.1.1	Method . . . . .	67
5.1.2	Experimental Results . . . . .	70
5.1.3	Simulation . . . . .	75
5.2	Further two-dimensional movement detection for gesture recognition and analysis . . . . .	79
5.2.1	Method . . . . .	79
5.2.2	Future work . . . . .	85
5.3	Conclusions . . . . .	87

<b>6</b>	<b>Materials Characterisation</b>	<b>89</b>
6.1	Introduction . . . . .	89
6.2	Measurement of charge on insulating materials . . . . .	90
6.2.1	Introduction . . . . .	90
6.2.2	Overview of the charge scanner . . . . .	92
6.2.3	Experimental Results . . . . .	97
6.3	Measuring tribo-charging phenomena . . . . .	102
6.3.1	Introduction . . . . .	102
6.3.2	Overview of the experiment . . . . .	102
6.3.3	Quantitative tribocharging results . . . . .	103
6.4	Conclusions . . . . .	106
<b>7</b>	<b>High resolution material surface measurement system</b>	<b>108</b>
7.1	Introduction . . . . .	108
7.2	Methodology . . . . .	109
7.3	Results . . . . .	112
7.4	Conclusions and future work . . . . .	113
<b>8</b>	<b>Conclusions</b>	<b>115</b>
	<b>References</b>	<b>120</b>
<b>A</b>	<b>Labview VIs</b>	<b>130</b>
<b>B</b>	<b>Microprocessor Assembler Code</b>	<b>146</b>

# List of Publications

I have published the following papers in Journals and Conferences as shown.

- [P1] **S. T. Beardsmore-Rust**, P. Watson, R. J. Prance, C. J. Harland and H. Prance, “Imaging of charge spatial density on insulating materials” in *Measurement Science and Technology*, vol.20, 2009
- [P2] R. J. Prance, **S. T. Beardsmore-Rust**, P. Watson, C. J. Harland and H. Prance, “Remote detection of human electrophysiological signals using electric potential sensors” in *Applied Physics Letters*, vol.93, 2008
- [P3] **S. Beardsmore-Rust**, P. B. Stiffell, H. Prance, R. J. Prance and P. Watson, “Passive tracking of targets using electric field sensors” in *SPIE Defence Security and Sensing*, Orlando, USA, April 2010
- [P4] **S. T. Beardsmore-Rust** and R. J. Prance, “Non-contact charge imaging and remote tracking of dielectric objects” in *Early Career Research in Electrostatics and Dielectrics*, London, England, 15 December 2009
- [P5] **S. T. Beardsmore-Rust**, R. J. Prance, A. Aydin, H. Prance, C. J. Harland and P. B. Stiffell, “Signal specific electric potential sensors for operation in noisy environments” in *Journal of Physics: Conference Series*, vol.178, Edinburgh, Scotland, 5-7 October 2009
- [P6] **S. T. Beardsmore-Rust**, P. Watson, R. J. Prance, C. J. Harland and H. Prance, “Quantitative measurement of tribo-electric charging phenomena of dielectric materials” in *Proc. ESA Annual Meeting on Electrostatics 2009*, Boston, USA, June 2009

- [P7] **S. Beardsmore-Rust**, P. Watson, P. B. Stiffell, R. J. Prance, C. J. Harland and H. Prance, “Detecting electric field disturbances for passive through-wall movement and proximity sensing” in *SPIE Defence Security and Sensing*, vol.7313, Orlando, USA, April 2009
- [P8] R. J. Prance, **S. Beardsmore-Rust**, H. Prance, C. J. Harland and P B Stiffell, “Adaptive electric potential sensors for smart signal acquisition and processing” in *Journal of Physics: Conference Series*, vol.76, Liverpool, England, October 2007
- [P9] H. Prance, P. Watson, R. J. Prance, C. J. Harland, **S. T. Beardsmore-Rust** and A Aydin, “High spatial resolution, dry-electrode surface EMG acquisition system” in *Proceedings of AAATE 2009*, Florence, Italy, 31 August – 2 September, 2009

# List of Tables

3.1	Switched Capacitor Filter Mode Table [67] . . . . .	43
6.1	Samples and charge after tribo-charging . . . . .	93
6.2	Sample materials and dimensions . . . . .	102
6.3	Measurements of total charge deposited using standardized tribo-charging process . . . . .	105
6.4	Materials tested, in order they appear on other tribo-electric series (positive to negative charging) and charge as measured by the charge imaging scanner	105

# List of Figures

1.1	The induction probe electric field measurement approach . . . . .	3
1.2	High impedance measurement of charge through voltage on a capacitor . . .	4
1.3	Virtual earth charge measurement circuit . . . . .	4
1.4	The field mill electric field measurement approach . . . . .	5
1.5	The EPS sensor schematic . . . . .	8
2.1	Guarded and unguarded configuration . . . . .	21
2.2	Digital potentiometers used to allow automated reconfiguration of sensor characteristics . . . . .	23
2.3	Varying positive feedback techniques in isolation . . . . .	24
2.4	Frequency response with 50% bootstrap setting and varied guarding . . . . .	25
2.5	Frequency response with 80% bootstrap and varied guarding . . . . .	26
2.6	Frequency response with 97% bootstrap and varied guarding . . . . .	26
2.7	Frequency response with 110% Guarding and variable bootstrap . . . . .	27
2.8	Frequency response with 117.5% Guarding and variable bootstrap . . . . .	28
2.9	Frequency response with 120% Guarding and variable bootstrap . . . . .	28
2.10	Bootstrap simulation circuit . . . . .	29
2.11	Neutralization simulation circuit . . . . .	30
2.12	Frequency response with no bootstrapping applied to the input, with signal applied through 100fF coupling capacitance . . . . .	31
2.13	Frequency response with bootstrapping applied in order to gain maximum flat low frequency response, with signal applied through 100fF coupling capacitance . . . . .	32
2.14	Frequency response with maximum possible bootstrapping applied before instability occurs, with signal applied through 100fF coupling capacitance .	33
2.15	Frequency response with unity guarding thus no neutralisation of input capacitance, with signal applied through 100fF coupling capacitance . . . . .	34

2.16	Frequency response at mid point between unity guard and maximum stable guard, with signal applied through 100fF coupling capacitance . . . . .	35
2.17	Frequency response when guard at maximum stable value and maximum amount of input capacitance neutralised, with signal applied through 100fF coupling capacitance . . . . .	36
3.1	Block diagram showing an electric potential sensor with four band-stop(notch) filters incorporated into the feedback loop . . . . .	38
3.2	The nested feedback approach used to avoid the requirement that digital filters be placed in series . . . . .	41
3.3	The clock generator circuit . . . . .	42
3.4	The filter circuit . . . . .	44
3.5	The modular architecture used . . . . .	46
3.6	Measured response for an EPS with two switched capacitor filters incorporated into the feedback loop . . . . .	47
3.7	Measured response for an EPS with four switched capacitor filters incorporated into the feedback loop, configured for movement immunity experiment	47
3.8	Arrangement of reciprocating electrode . . . . .	48
3.9	Output from untuned sensor showing a large amount of movement interference at 2.4Hz with a small 18Hz signal superimposed . . . . .	49
3.10	Output from tuned sensor showing large 18Hz signal and small 2.4Hz ripple as a result of movement . . . . .	50
3.11	Settling of sensor output when signal at tuned frequency is activated . . . .	51
3.12	Settling of sensor output when signal at tuned frequency is deactivated . . .	51
3.13	Architecture of noise immune sensor based around broadband response containing multiple notches . . . . .	55
3.14	Frequency response of sensor with notched response showing >95dB rejection	56
3.15	Frequency response of multiple notch noise immune sensor taken through 15cm air gap . . . . .	56
3.16	Human heart signal measured at a distance of 40 cm from the front of the body in a noisy unshielded environment. This is raw data with no signal averaging or digital signal processing applied. . . . .	57
4.1	The experimental sensor arrangement . . . . .	61

4.2 Data collected from the front of the subject with a 40cm air gap between the sensing electrode and the surface of the body. Data taken in an open unshielded environment, with the subject holding their breath for the duration of the measurement. . . . . 62

4.3 Data collected from the back of the subject with a 10cm air gap between the sensing electrode and the surface of the body. Data taken in an open unshielded environment, with the subject holding their breath for the duration of the measurement. . . . . 62

4.4 Raw data, with no analogue or digital signal processing applied, showing both the respiration and heart signal collected from the front sensor. Sensor positioned 40cm away from the front surface of the body. . . . . 64

4.5 The result of applying a digital FIR filter technique to separate the low frequency respiration signal from the higher frequency cardiac signal. (a) 1Hz low pass filter applied to the data of Fig. 4.4 showing the signal due to respiration and (b) 1Hz high pass filter applied to the data of Fig. 4.4 revealing the cardiac component. . . . . 64

5.1 (a)The vertical potential distribution above the earth, (b)The disturbance to this potential distribution caused by a human body. Figure taken from The Feynman Lectures on Physics[79] . . . . . 66

5.2 The 8 element sensor array - schematic . . . . . 68

5.3 The 8 element sensor array - photo . . . . . 69

5.4 The 8 element electrode array . . . . . 69

5.5 (a) - Experimental data from pendulum (b) - Theoretical data from finite element model . . . . . 70

5.6 Arrangement of sensors and pendulum sample . . . . . 71

5.7 Frames of data from visualisation program arranged to show pendulous motion. Scale shown using white when no disturbance is present, and increasing grayscale for positive and negative disturbances. . . . . 72

5.8 Motion visualised by selecting sensor with largest output signal . . . . . 73

5.9 Plot of position against time calculated from sensor data . . . . . 74

5.10 A finite element model showing equipotential lines induced by a field which occurs as a result of the presence of a charged object. The linear array of field measurement points is also shown. . . . . 75

5.11	Data shown for sensor at one end of experimental linear array commencing after initial transients as a result of setting the pendulum in motion have died away. Amplitude is shown referred to voltage at the input of the sensor.	76
5.12	Data from simulation for measurement point positioned as for Fig.5.11 . . .	76
5.13	Data shown for sensor approximately in centre of experimental linear array commencing after initial transients as a result of setting the pendulum in motion have been allowed to die away. Amplitude is shown referred to voltage at the input of the sensor. . . . .	77
5.14	Data from simulation for point positioned as for Fig.5.13 . . . . .	77
5.15	Data shown for sensor at opposite end of experimental linear array commencing after initial transients as a result of setting the pendulum in motion have been allowed to die away. Amplitude is shown referred to voltage at the input of the sensor. . . . .	78
5.16	Data from simulation for point positioned as for Fig.5.15 . . . . .	78
5.17	Arrangement for two-dimensional pendulum movement sensing experiment	81
5.18	Data as a result of movement in x axis . . . . .	83
5.19	Data as a result of movement in y axis . . . . .	83
5.20	Data collected as a result of circular movement within XY sensor space . .	84
5.21	Result of simulation of positioning of charged object based on electric field detection. Red dot shows position of object as calculated in simulation. . .	85
5.22	A possible arrangement of sensors, with corners being used and position of a person triangulated based on relative signal amplitudes . . . . .	86
5.23	A grid arrangement of sensors for hand gesture detection . . . . .	86
6.1	(a) Cross section of flatbed charge scanner instrument (b) Arrangement of electrode head with guarding shown for each electrode . . . . .	95
6.2	The charge scanner . . . . .	96
6.3	Discharge of Mylar sheet over 8 days, with spot measurements compared against continuously measured data and overlaid with exponential fits to data	98
6.4	Charge decay of Mylar, Acetate and Polythene samples. Inset shows charge decay on acetate rescaled to improve visibility . . . . .	99
6.5	Discharge of charged island on Mylar sheet over 8 days . . . . .	99
6.6	Image of a Q shape charge distribution on PVC (a)raw integrated data (b)data interpolated and smoothed using Matlab . . . . .	100

6.7	Image of a Q shape charge distribution on acetate, shown discharging over an 8 hour period . . . . .	101
6.8	A Mylar sample imaged after being charged by the carbon fibre brush within the scanner . . . . .	104
7.1	XY Electric Potential Topography System . . . . .	110
7.2	XY System Overview . . . . .	111
7.3	XY Data compared with photograph. (a) Optical image, (b) raw data from scanner, (c) data after post processing/smoothing . . . . .	112
7.4	Three dimensional rendering of the data collected by the XY scanner . . . .	113
A.1	Pendulum Movement Experiment Front Panel . . . . .	131
A.2	Pendulum Movement Experiment Block Diagram . . . . .	132
A.3	2D Movement Experiment Front Panel . . . . .	133
A.4	2D Movement Experiment Block Diagram . . . . .	134
A.5	The Charge Scanner Virtual Instrument Front Panel . . . . .	135
A.6	The Charge Scanner Virtual Instrument . . . . .	136
A.7	The Charge Scanner Virtual Instrument - detail 1 of 9 . . . . .	137
A.8	The Charge Scanner Virtual Instrument - detail 2 of 9 . . . . .	138
A.9	The Charge Scanner Virtual Instrument - detail 3 of 9 . . . . .	139
A.10	The Charge Scanner Virtual Instrument - detail 4 of 9 . . . . .	140
A.11	The Charge Scanner Virtual Instrument - detail 5 of 9 . . . . .	141
A.12	The Charge Scanner Virtual Instrument - detail 6 of 9 . . . . .	142
A.13	The Charge Scanner Virtual Instrument - detail 7 of 9 . . . . .	143
A.14	The Charge Scanner Virtual Instrument - detail 8 of 9 . . . . .	144
A.15	The Charge Scanner Virtual Instrument - detail 9 of 9 . . . . .	145
B.1	XY Scanner Motor Control and LCD Display code - 1 of 15 . . . . .	147
B.2	XY Scanner Motor Control and LCD Display code - 2 of 15 . . . . .	148
B.3	XY Scanner Motor Control and LCD Display code - 3 of 15 . . . . .	149
B.4	XY Scanner Motor Control and LCD Display code - 4 of 15 . . . . .	150
B.5	XY Scanner Motor Control and LCD Display code - 5 of 15 . . . . .	151
B.6	XY Scanner Motor Control and LCD Display code - 6 of 15 . . . . .	152
B.7	XY Scanner Motor Control and LCD Display code - 7 of 15 . . . . .	153
B.8	XY Scanner Motor Control and LCD Display code - 8 of 15 . . . . .	154
B.9	XY Scanner Motor Control and LCD Display code - 9 of 15 . . . . .	155

B.10 XY Scanner Motor Control and LCD Display code - 10 of 15 . . . . .	156
B.11 XY Scanner Motor Control and LCD Display code - 11 of 15 . . . . .	157
B.12 XY Scanner Motor Control and LCD Display code - 12 of 15 . . . . .	158
B.13 XY Scanner Motor Control and LCD Display code - 13 of 15 . . . . .	159
B.14 XY Scanner Motor Control and LCD Display code - 14 of 15 . . . . .	160
B.15 XY Scanner Motor Control and LCD Display code - 15 of 15 . . . . .	161
B.16 Tuned Sensor Controller code - 1 of 5 . . . . .	162
B.17 Tuned Sensor Controller code - 2 of 5 . . . . .	163
B.18 Tuned Sensor Controller code - 3 of 5 . . . . .	164
B.19 Tuned Sensor Controller code - 4 of 5 . . . . .	165
B.20 Tuned Sensor Controller code - 5 of 5 . . . . .	166
B.21 Tuned Sensor Controller code - 1 of 3 . . . . .	167
B.22 Tuned Sensor Controller code - 2 of 3 . . . . .	168
B.23 Tuned Sensor Controller code - 3 of 3 . . . . .	169

# Chapter 1

## Introduction and Background

*"I wish to tell you of a new but terrible experiment which I advise you never to attempt yourself." - Pieter van Musschenbroek in a letter to Ren Raumur, 1746[1].*

In 1746, Musschenbroek, a professor at Leiden University, began a letter to a colleague in Paris to describe a recent discovery. The ability to generate static electrical energy using friction based machines was already known, but at the time there was no known way to store this energy. Musschenbroek had constructed a device, consisting of a glass jar coated inside and out with a conducting metal foil, in an attempt to store some of this energy. After charging the device, Musschenbroek had received such a powerful shock that he felt compelled to begin his letter describing the discovery with a warning of considerable magnitude. This device would later become known as the Leyden Jar, Volta would go on to call it a condenser, and today it is known as a capacitor.

Later, in 1786, Luigi Galvani observed that a dissected frog leg twitched when connected to the output from an electrostatic generating machine[2], work that would later inspire the study of electrical properties of the human body and the entire field of bioelectricity and electrophysiology. Many others, including Volta, Oerstad, Ampère, Faraday, Ohm and Henry would contribute to this growing field, before in 1865, James Clerk Maxwell published a paper called "A Dynamical Theory of the Electromagnetic Field"[3]. The discovery of electromagnetic fields, and the ability to detect, generate and manipulate these fields, resulted in revolutionary applications and the development of the discipline of electrical and electronic engineering, as well as a huge branch of modern physics.

## 1.1 Electric Field Measurement Techniques

The measurement of static and low frequency electric fields is, perhaps surprisingly, a difficult measurement to make in an accurate and repeatable way, despite the vast array of modern technology available to current scientists and researchers. In the case of an electrostatic scenario, where the interest is in the presence rather than movement of some quantity of charge, the measurement can be conceived in a number of ways. In some cases it is easier to consider the measurement of the charge directly; at other times a measurement of electric field strength is more appropriate; sometimes it is more useful to measure the actual spatial distribution of the charge; and on occasion, none of these measurements are practicable. This results in the absence of a standard technique for making this measurement, and instead there exist a range of common, and less common, measurement approaches available to those seeking to observe and establish the properties of a quantity of electrostatic charge.

Despite this statement, it is nevertheless the case that there is some commonality between measurement types. The charge  $Q$  induced on a surface, with area  $A(m^2)$  at which the electric field  $E(Vm^{-1})$  is

$$Q = \epsilon_0 \epsilon_r EA \quad (1.1)$$

where  $\epsilon_0$  = permittivity of free space and  $\epsilon_r$  = relative permittivity of the medium. This relationship, combined with the fact that capacitance  $C$  is defined as the quotient of the charge on a capacitor with the voltage present on the capacitor plates

$$C = \frac{Q}{V} \quad (1.2)$$

creates a measurable quantity. In most cases, a known capacitance of value  $C$  is allowed to charge in a field of strength  $E$ , resulting in a voltage  $V$  which can ideally be measured in some way without affecting the quantity of charge on the capacitor. This relationship, between electric field strength, measurement capacitance, probe dimensions and sensor output voltage can be expressed as:

$$V_{sensor} = S * \frac{\epsilon_0 \epsilon_r AE}{C} \quad (1.3)$$

where  $S$  is a constant, or calibration factor, which varies with sensitivity and gain of the measurement circuit.

### 1.1.1 Electrometer based measurement

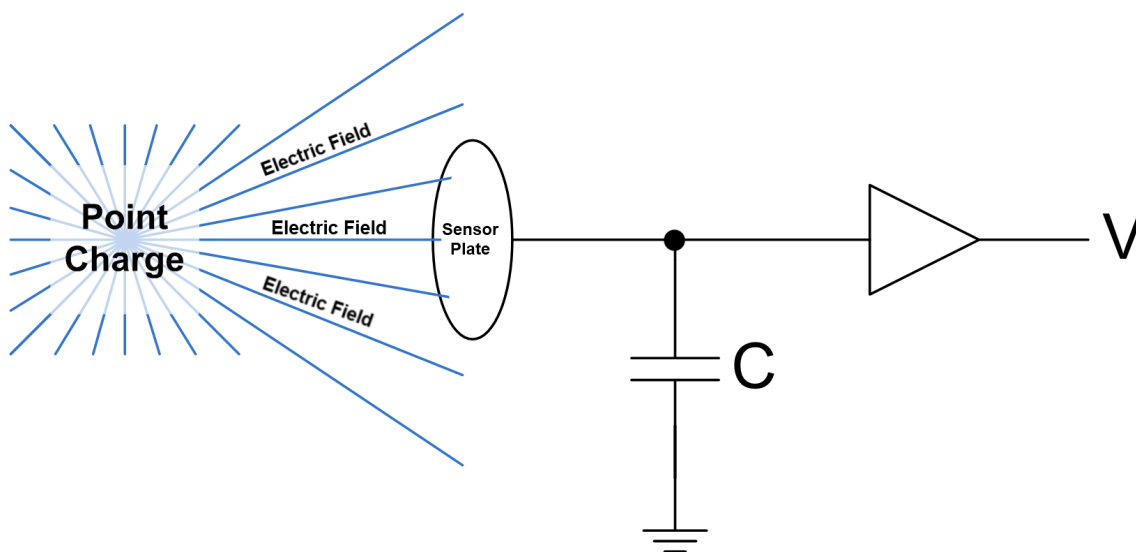


Figure 1.1: The induction probe electric field measurement approach

Induction, or induced charge[4], electric field meters are perhaps the simplest of all conventional electric field measurement circuits. This approach, involves a sensor electrode, shunted through a well defined capacitance, and connected to a specially designed charge amplifier. The arrangement described is shown in Figure 1.1. The meter must first be zeroed in the absence of an electric field, or in the presence of a field for which the strength is well known. The sensor plate is then introduced into the field to be measured, and a voltage occurs on the output of the amplifier which is directly proportional to the strength of the field, as described in Eqn 1.3 There are two typical styles of induction probe input stage, involving either a measurement of induced charge across a known input capacitor, or the use of a virtual earth charge measurement circuit. These are shown in Figure 1.2 and 1.3. There are, however, some shortcomings of these conventional measurement circuits. A suitable amplifier must be designed such that it provides minimal discharging of the front end input capacitor. In reality, maintaining the extremely high input impedances required of these amplifiers is not a trivial task, and is often impossible. Furthermore, not only must they be initially zeroed in a known field, but this zero point can drift over time, and so must be verified after the measurement as well to ensure that drift has not occurred.

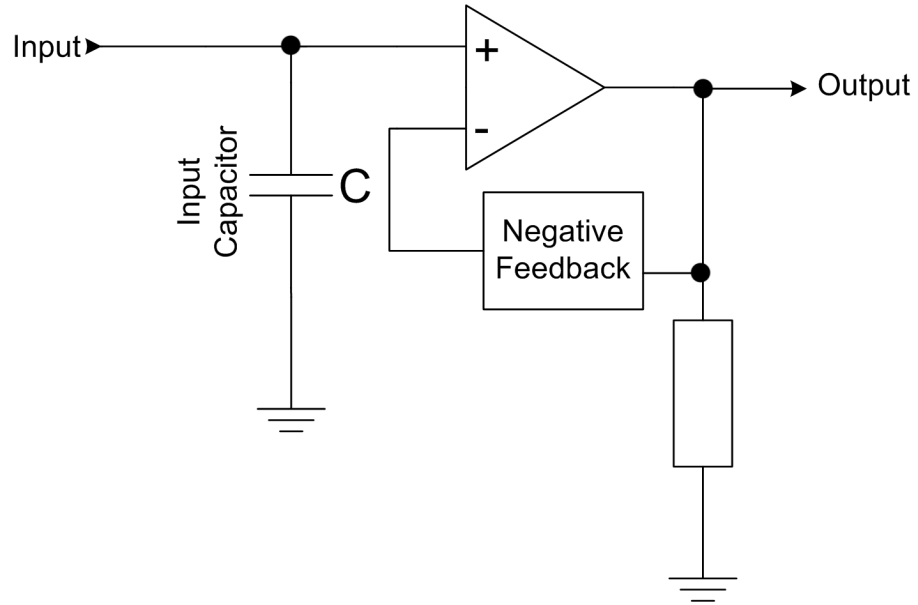


Figure 1.2: High impedance measurement of charge through voltage on a capacitor

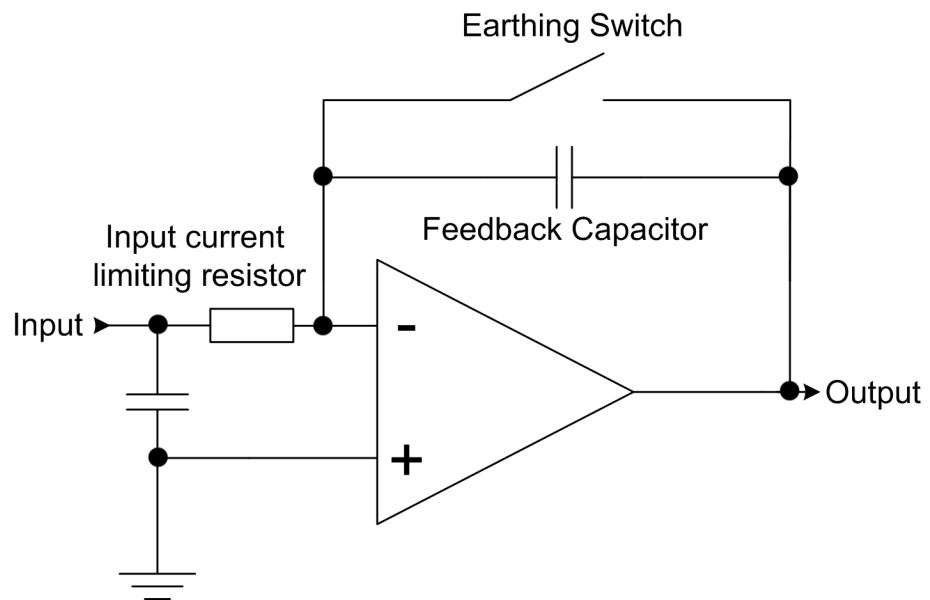


Figure 1.3: Virtual earth charge measurement circuit

### 1.1.2 Field Mill measurements

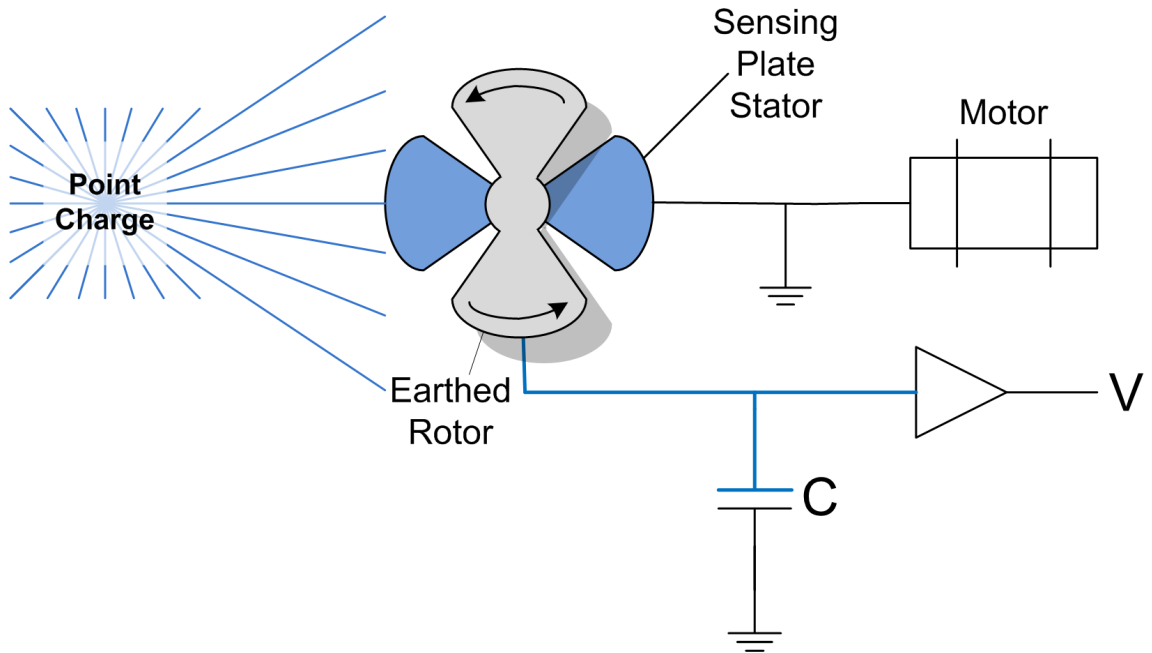


Figure 1.4: The field mill electric field measurement approach

When accurate and high quality measurements of electric field are needed, a common measurement involves the use of a type of field meter known as a field mill, a typical design for which is shown in Figure 1.4. These instruments typically involve a sample or electrode surface which is exposed to the electric field being measured. As a result, a charge is allowed to build up on the electrode, and a voltage proportional to this charge is generated with a charge amplifier circuit of some kind. This probe or electrode must then be discharged with respect to a reference, before being allowed to charge again. In this way, a DC field is "chopped" to become an AC signal which is relatively straightforward to measure. This system benefits from being straightforward in design, and makes use of a conventional charge amplifier circuit which need not have extreme input characteristics or DC drift stability, and is therefore relatively simple. These field meters exist in, essentially, two categories. Those which involve a mechanically based chopper system, often known as field mills, and those which instead vibrate a capacitive probe.

By ensuring that the coupling conditions between the field and the probe surface change cyclically it is possible to mechanically chop the signal generated by the static electric field, and thus produce an alternating signal. This has the effect of providing a constant reference with which to relate the strength of the field, and therefore avoid problems which

might otherwise arise as a result of a drifting zero point. Furthermore, it reduces the necessity to maintain an extremely high input resistance and maintain very long settling times, as an earthed plate is repeatedly placed between the field and the sensor plate. The result is an electric field sensor with, effectively, an infinitely long settling time. The only requirement is that the leakage discharge time of the probe surface is substantially longer than the modulation speed. Furthermore, since this measurement is based on sampling the field at discrete intervals, the field must be changing at a rate less than half the sampling/modulation rate of the field mill. Since the modulation is brought about by a mechanically rotated rotor, this rate is clearly limited by the speed of the motor. Provided these conditions are maintained, there will be a direct relationship between the probe voltage  $V$  and the electric field, as described in Eqn 1.3. Typical sensitivities for such a system range from around  $1kVm^{-1}$  through to around  $1000kVm^{-1}$  [5] however greater sensitivities than this have been demonstrated[6].

A similar effect to that described in the section above can also be achieved by vibrating an electrode perpendicular to an electric field. The amplitude of these vibrations must be kept consistent in order to maintain accuracy, since the amplitude of the resulting signal is proportional to the distance moved within the field. Various feedback techniques can be used to null any variation caused by changes in modulation amplitude. This approach means probes can be made significantly smaller than those requiring a mechanically driven rotor, perhaps as small as a few cubic centimetres[7]. Use of small apertures can reduce this to  $< 1mm$

### 1.1.3 Optical and Electro-optical Measurement

A more recently developed approach for measuring electric field involves the use of fibre optic based techniques. The use of field mill electric field meters mandates the introduction of earthed surfaces into an electric field. This will, at least, have the effect of disturbing and distorting the field which they seek to measure. The range of electro-optical and optical based techniques are therefore appealing because, as inherently non electrical devices, they present little risk of modifying the field and are immune from electromagnetic interference. These probes make use of a range of effects, with many being based on an electro-optical phenomena known as the Pockels effect; this describes birefringence in an

optical media produced by some crystalline materials when in the presence of static or changing electric field[8]. Another form of optical electric field measurement technique exploits piezoelectric [9] or electrostrictive [10] materials in combination with a fibre optic interferometry technique to obtain electric field measurements. In comparison to the Electric Potential Sensor technique, described below, these approaches are complex and better suited to a laboratory environment than to other general purpose applications.

## 1.2 A Brief Overview of Electric Potential Sensors

This thesis will discuss a range of possible applications for a series of novel electric potential sensors (EPS), developed and patented at the University of Sussex[11, 12, 13]. These sensors detect, passively, changes in spatial potential (electric field) created by capacitively coupling to an electric field. They are, in many respects, similar to the induction probes described earlier in this chapter. However, through the use of several types of positive feedback, guarding and active electrode techniques it has become possible to boost the effective input impedance, (i.e. electronically manipulated resistance) to values as high as  $10^{15}\Omega$  and capacitance to values as low as  $10^{-16}F$ . These values are more commonly associated with laboratory electrometers, and allow these active probes to be remarkably sensitive to electrostatic and low frequency electric fields. Unlike conventional laboratory electrometers however, these sensors maintain a stable DC bias point, and therefore do not suffer from drift problems more commonly associated with these devices. These properties allow them to find a range of applications in the sensing of electric fields and spatial electric potential, and thus to measure and observe many physical properties, including movement, biologically originating electrical signals, material properties and the presence of charge. A block diagram based schematic, showing the positive feedback techniques employed to achieve this input impedance boost, is given in Figure 1.5. The operating bandwidth depends on the particular design, coupling conditions and other requirements such as noise performance, but in various versions these sensors can operate from  $<1$  mHz to  $>100$  MHz. Furthermore, by employing methods based on some of the techniques described in the section above, it is possible to make the sensors effective at measuring static fields in some instances.

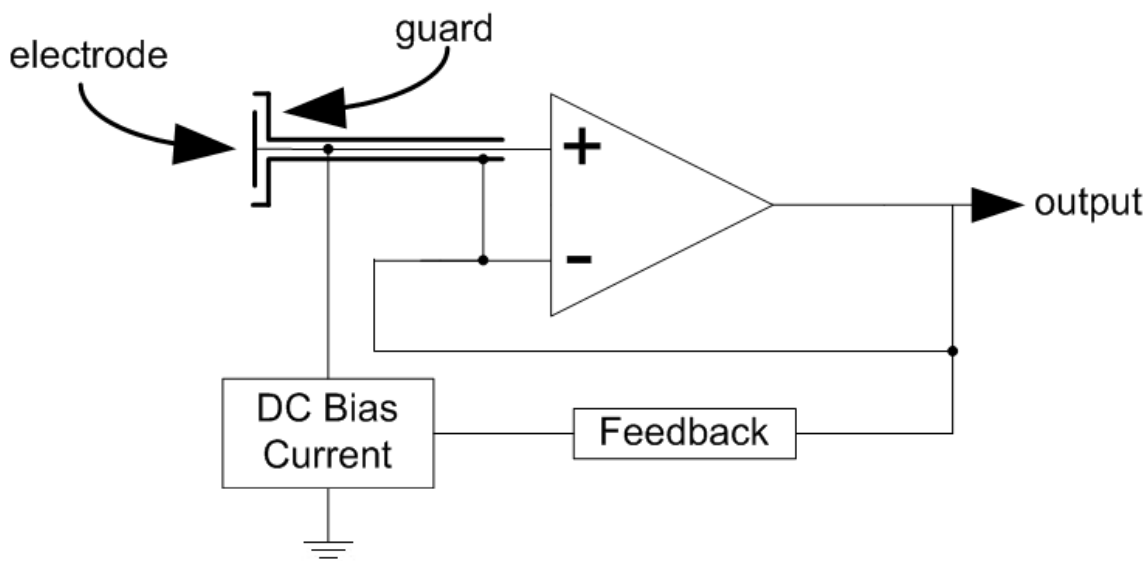


Figure 1.5: The EPS sensor schematic

These probes can therefore be seen either as capacitively coupled probes, where the sensor is coupled through a known or well defined capacitance to a source, or as electric field probes, where the coupling capacitance is less well defined and the performance is dictated by the combination of the leakage capacitance between the probe electrode and ground, and the input capacitance of the front end electrometer. In this case, their application is closer to charge amplifiers and induction probes. The first scenario is referred to as *contact mode*, since the sensors are generally in close physical contact (though not conductive contact) with the signal source. The second scenario, where there is a physical spacing between sensor and source, is known as *remote mode*.

To date we have already demonstrated proof of principle in many areas of interest, including body electrophysiology[14, 15], novel nuclear magnetic resonance NMR probes[16], non destructive testing of composite materials[17], as well as in a range of other fields[18, 19].

## 1.3 Applications of an Electric Potential Sensor

### 1.3.1 Electric Fields

When one considers the sensing of electric fields, it is perhaps most common to think of the range of high frequency RF applications. These techniques form the basis of modern digital communications and broadcast technologies and make up the vast majority of remote electric field sensing applications. It is usual to think of this type of sensing as taking place at MHz frequencies and above, and design considerations are typically focused around impedance matching and antenna design. Some people might also think of manufacturing-related electrostatic applications; the sensing of fields related to static charge on insulating materials for the purposes of preventing electrostatic discharge damage or when handling and storing potentially explosive substances. It seems likely that few would, when asked about electric field sensing, immediately identify applications which operate in the range of low frequency (0.1Hz - 1kHz), low intensity fields. This is perhaps because sensors which operate in this region, with both the required bandwidth and sensitivity to make useful measurements of ambient electric field at these frequencies and intensities have not been commonly available outside of the laboratory.

Despite this, it would not be accurate to say no applications currently exist for the sensing of low frequency electric fields. In the field of communications, very low frequency communications systems have been developed which operate in this band. Both the United States of America, and Russia, are known to have developed extremely low frequency (ELF) communication systems for communicating with submarines without the requirement for them to surface[20]. These applications exploit the fact that, while most electromagnetic waves would be screened out by the presence of large volumes of conducting seawater, very low frequency signals can penetrate through these materials. Further to these communication applications, there are a number of other sources, both natural and man-made, of ELF (Extremely Low Frequency 3Hz - 3kHz) and VLF (Very Low Frequency 3kHz - 30kHz) electromagnetic waves, which are reviewed by Barr[21]. There has also been substantial work carried out to investigate the health implications of human exposure to low frequency electric and magnetic fields, such as those present in

the vicinity of power transmission systems[22]. In all these cases, however, the signals and fields detected are of a substantial field strength.

In comparison, for the case of low strength, low frequency electric fields surprisingly little prior work exists. It is perhaps unusual that while animals are known to exploit the information which can be gathered from electric fields for both orientation, communication and other critical behaviours[23], the current technological use of electric field sensors for these applications is relatively rare, with other approaches usually being adopted.

This thesis will discuss the modification and application of an electric potential sensor for use in detecting a range of signals generated some distance from the sensor. This includes detection of the movement of large dielectric objects such as the human body (0.1Hz - 30Hz)[24]; the remote sensing of a cardiac (1Hz - 30Hz) and respiratory (0.1Hz - 5Hz) signals in an open, unshielded laboratory some distance from the body[25]; the imaging of the spatial distribution of charge on the surface of an insulating material (frequency dictated by movement but typically  $< 1\text{kHz}$ )[26, 27]; and the topography of a material sample using the sensing of electric potential. There is existing work[13, 12, 19, 18, 15, 28, 29, 30, 17, 31, 16] in all of these applications, but this thesis will specifically explore the potential for applying highly sensitive low frequency electric potential sensors to these areas and the role that these sensors have to play.

### **1.3.2 Movement Sensing**

The ability to detect subject presence and movement, despite obstruction by walls and other structures, would clearly be of particular interest to those working in areas of law enforcement, search and rescue and the military. As a result of this need, there has been substantial work done in this area[32, 33] with technologies being regularly reviewed by defence and security organizations as early prototype products begin to appear commercially[33]. In a number of these applications, it is sufficient to be aware when a given space is occupied by an individual or individuals and to obtain information about their movements around, into and out of the space. In such cases, there is often a requirement for long term, unattended, surveillance systems which do not generate excess

data or false alarms[34, 35]. In many such cases, existing sensor technologies are capable of meeting the requirements for monitoring of this kind, however existing approaches are either active (Radar, LIDAR) or have a requirement for maintaining line of sight (optical, PIR).

There is also considerable interest in human motion analysis, and the information it may be possible to extract from human motion for a range of general applications spanning human machine interfaces, security and sports medicine[36]. Furthermore, the ability to detect movement, and identify hand gestures, has attracted research interest as a possible option for intuitive user interfaces, where it could represent an alternative to conventional methods for interface and control, particularly in applications where existing approaches are not ideal[37]. Much research effort has been dedicated to this topic, but has been focused around image recognition techniques applied to video data collected with cameras[38, 39]. The ability to sense touch, movement and gestures allows for the design of complex and powerful user interfaces. Furthermore, if interfacing could be carried out remotely without any need for physical contact with the sensor, this would be particularly powerful.

There have been previous examples of control schemes based around electric field sensors. The best known, perhaps, is the work done by Lord Theremin[40] resulting in the invention of the Theremin musical instrument in 1922. The reason why much further work in this field did not take place until recently is somewhat unknown, but perhaps the explanation lies in a combination of the lack of electronic devices requiring advanced control interfaces at the time the Theremin was invented, combined with the fact that, in some cases, the computational solutions required to build complex interfaces would have rendered the control scheme impractical.

More recently, the application of electric field sensing to this area has yielded significant progress, and substantial work has been carried out[41] to explore the possibilities of these applications. Previously it has been shown that it is possible to use electric fields to control a range of electronic based musical instruments other than a Theremin[42], as well as develop a mouse style control system using electric fields[43]. Some commercialization of these technologies has taken place, with at least one integrated circuit on the market based on these techniques [44]. Notably, in these cases, an active measurement approach

is adopted, whereby a subject or object is connected directly to a generated field. A capacitive effect is then observed and measured by a sensor as, for example when a human hand comes in close proximity to the object, thereby enabling position information to be inferred.

Use of Radar for small, short range movement detection has also been commercialised, with several types of Doppler module (e.g.8960 series modules[45]) brought to market. These are sold with suggested applications including intruder alarms, speed measurement, vibration measurement and proximity switches. These devices are based on the detection of Doppler-shift in reflected microwave radiation, generated at a frequency of approximately 10 Ghz.

Existing passive techniques have previously tended to focus on either optical or infrared sensors[46]. Both types of sensor can be obscured by objects, walls and poor visibility. Moreover, where used in video imaging systems, the data sets generated are extremely large, complex to analyse and may contain significantly more information than is required for the application. Active techniques have therefore been favoured for through-wall tracking and detection applications, however to date, much of this work has focused on the use of RF Radar approaches for identifying movement through walls and debris [47, 48]. As active techniques, while clearly effective, these methods have some disadvantages. Passive techniques, in comparison, provide compatibility with a need for covert surveillance, the removal of potential hazards due to irradiation, light weight construction, reduced power requirements and a capability for extended use.

The sensors described in this thesis have been demonstrated as being sensitive enough, in certain applications, to detect signals created by movement, at distances of at least 5-10 m, without any need for an applied field. These electric field signals are generated by measuring perturbations in the ambient electric field. Furthermore, as the measurement made is of perturbations in the ambient electric field, it is unaffected by the presence of walls or structures consisting of non-conducting material, or where any conducting material is suitably electrically isolated from earth. As a result this creates the possibility of detecting movement through concrete walls in an entirely passive way.

In this thesis, it is shown that by arranging arrays of sensors, it is possible to detect both the presence and direction of movement, in such a way that real-time, passive gesture

detection becomes a realistic prospect. A very early prototype is presented which clearly demonstrates the possibility of sensing direction and speed of movement, by measuring the perturbations in the electric field created by a small dielectric object; in this case a small 120 ml plastic bottle of water, swinging in a pendulous fashion perpendicular to a linear array of 8 electric potential sensors. With basic visualization in Labview, it becomes clear that this information includes both velocity and direction information.

Data is then presented for a two dimensional experiment, in which the ability to reproduce limited position information within a two-dimensional space is shown. Proof of principle is provided for an application using only four sensors to infer position within a two dimensional plane and shows that it would be possible to reproduce x and y location, and velocity, using sensors in this arrangement. In this way, it is suggested that a human body, or human hand, could be tracked within a two dimensional space to give position and velocity information, and this information used to extract and detect gestures and movements for the purposes of interfacing with a computer controlled device.

### **1.3.3 Electrophysiological Sensing**

Much research effort has been invested in exploring techniques for measuring physiological characteristics and information remotely. This information has a wide range of possible uses, with applications in biometric identification, security, healthcare monitoring at home, as well as the monitoring of people carrying out safety critical tasks.

The identification of an individual using only biometric information is considered perhaps the ultimate goal of a substantial area of security related research[49]. Biometric data has the unusual and useful property of being completely unrevokable[50]. A metric of this kind could be used either for identification of an individual, from a large database of possible users, or for the authentication of a user who has identified themselves[51]. At present, the most popular metrics on which research is focused span fingerprint recognition[52], iris scanning, facial feature identification, and voice recognition[53], with some research taking place on the possibility of using other techniques such as key stroke timing and pressure pattern recognition[54]. In this thesis it is suggested that data presented implies

it may be possible to make a biometric measurement using an electric field sensor. This opens up the possibility of acquiring electrophysiological signals remotely, in particular a cardiac signal, without any need for physical contact with the body.

The remote measurement of electrophysiological signals is also clearly of interest within a healthcare setting, whether that be for the monitoring of long term medical conditions within the home or for the monitoring of pilots, drivers, soldiers and others in safety critical situations. Data is presented in this thesis to demonstrate that it is possible to monitor, passively, a combination of electrical and movement related signals and that, by comparing signals acquired from the front and back of a subject, it is possible to separate signals as a result of respiration and cardiac activity. Alternative methods of achieving this result include optical vibrocardiology[55] and microwave Doppler radar[56]. These techniques are both active, and require the irradiation of a subject with either a laser or microwave source. Furthermore, these approaches both yield a signal related only to the movement of the chest, and infer information about a heartbeat on that basis. This potentially limits their usefulness to very specific parts of the body, typically the front and often only the neck. In contrast, a technique based around electric field sensing has the potential to detect the electro-physiological signal due to the heart directly, and therefore provide more information as well as being relatively independent of sensor orientation.

### 1.3.4 Materials Testing

The need to characterize and study materials, as well as analyse them for potential changes or faults which are not visible on the surface, creates a requirement for imaging and measurement techniques and instrumentation. Many approaches exist for measuring and imaging the properties of materials at the micrometre and nanometre scales, and the list of imaging techniques at this scale is expansive. Many nano scale techniques are based around the principles of scanning tunnelling microscopy[57]. In this case, a conducting tip is brought to within approximately 10Å of the surface, at which point electrons begin to "tunnel" between the sample and the probe, where the tunnelling current ( $I_t$ ) is given by an exponential function of the distance:

$$I_t = e^{-kd} \tag{1.4}$$

This exponential relationship gives the scanning tunnelling microscope (STM) remarkable sensitivity, and allows measurements to be made at a sub nanometre scale. Significantly, however, samples must be conductors or semiconductors in order for this measurement to work.

Further development of these techniques led to the invention of the Atomic Force Microscope (AFM) [57], which adopts a similar approach based around a mechanical cantilever system. These methods can be applied to monitor the surface properties of insulating materials, using a mechanical probe and cantilever to measure the surface structure by exploiting the response to repulsive Coulomb interactions which exist between the probe and the sample when the separation distance between them is very small. Many variations on these atomic force microscopy techniques have then been explored for a variety of possible applications. Scanning thermal microscopy[58] measures and images temperature variations on the surface of a sample using a temperature sensitive thermal tip as part of a Wheatstone bridge in addition to conventional AFM techniques. Another AFM related technique, known as Scanning Capacitance Microscopy[59], allows for the characterization and imaging of semiconductor devices by measuring variations in capacitance between a probe and semiconductor sample surface.

The disadvantage, however, of many of these techniques is that they rely on atomic forces which exist only at extremely small separation distances between probe and sample. If imaging is needed both at a very small scale, and simultaneously at a larger microscopic or even macroscopic scale, these techniques are not suitable as scanning large areas (mm scale or above) would take an extremely long time.

In this thesis, two different materials testing applications of the EPS sensor are described. A technique is discussed in chapter 6 involving the development, based on an EPS, of a charge scanning instrument capable of imaging spatial charge distribution on insulating materials at a macroscopic scale. This measurement is entirely passive, involving no excitation signal being applied to the sample. Instead the measurement involves making a DC measurement of static charge on a surface by moving the highly sensitive Electric Potential Sensors over the sample area to create an AC signal which they can measure.

The process by which charge can be built up on insulating materials as a result of rubbing or contact is known as tribo-charging. Through this process it is possible for very large

voltages to exist on these materials. This tribo-charging appears to be a combination of an effect due to movement, as well as an equilibrium effect[60]. Tribo-charging, as a phenomenon, is not well understood. One possible explanation often given is that a temperature gradient is formed between the rubbing and rubbed surfaces and that this gives rise to the movement based component of the charging effect[60]. Opinions are more widely divided on the cause of the contact electrification component of the charging, a comprehensive review of the field is given by Fuhrmann[61]

Industrial processes involving electrostatics are typically based around the controlled charging of particles and/or surfaces. There is often a requirement, therefore, to measure the charge on particles, or collections of particles, and a measurement involving a Faraday cup or Faraday pail is often used[62]. The charge density on an electret, or surface of an insulating material, can be measured using a dissectible capacitor[63] and is discussed and described by Sessler[64]. However, when a measurement of the spatial distribution of charge on a surface is required, a different technique is often employed. This typically involves bringing a low impedance field meter close to a charged surface, such that it represents the closest earthed object coupling to the surface charge. As a result, field lines will terminate on the electrode of the meter and a measurement will be made[65]. By moving this electrode, or applying some kind of aperture, it is possible to obtain a crude measurement of the spatial distribution of the charge. This technique, however, has limitations if more than one sensing electrode is to be used simultaneously. In this case, field lines will terminate on both electrodes, and the presence of a second electrode will compromise the measurement being taken by the other electrode, thereby making large arrays of this type of sensor an unattractive proposition.

In this thesis, measurements are reported, taken on samples of Mylar, Kapton and PTFE sheet, which demonstrate the imaging of the spatial charge distribution on these sheets which occurs as a result of tribo-charging, by an earthed lead and by a human finger. These measurements are compared with several published tribo-electric series[66] and, by comparing measurements taken on various samples and thicknesses of material, we show that it is possible to make fully quantitative measurements of the tribo-electrically generated charge density and therefore to establish a quantitative tribo-electric series. This opens up the possibility of absolute, rather than simply relative, positioning of materials within a tribo-electric series using a repeatable and calibrated measurement technique.

The ability to image charge distribution is shown, and complex distributions of tribo-electrically generated charge 'drawn' on these materials with an earthed lead can be clearly identified. The measurement results in no measurable sample discharging effects, and therefore can be used to investigate rates of decay of tribo-electrically generated charge on varying material samples. In many cases, the periods of time over which these decays occur span several days.

In contrast, an active measurement is described in chapter 7, whereby an AC signal is applied to a conducting sample, and a capacitively coupled EP sensor used to measure this signal as the sensor is moved over the sample surface at a constant height. A signal proportional to the spacing between the conducting sample and the probe will exist and since, as the surface topography changes the coupling capacitance and therefore amplitude of the signal will change, this results in the ability to establish the shape of the sample surface. The sensitivity of these sensors means that extremely small probes, in the order of microns, can be used. In contrast to the methods described above, this technique can be applied at a range of scales from  $1\ \mu m$  to several metres.

## Chapter 2

# Digital Control of Sensor Characteristics and Phase Space Mapping

### 2.1 Introduction

When operated in an open, remote and unscreened environment, noise can often saturate the electric potential sensor and prevent signal acquisition. If saturation occurs at the same time as a signal of interest, that information will be lost and cannot be recovered through post processing. If, however, the sensor is not saturated, it should be possible to recover small signals from within large noisy ones through the use of post processing techniques. It is crucial, therefore, that these sensors operate with sufficient dynamic range to prevent saturation under any potential operating conditions. There are many possible solutions to this problem. One is the use of modified feedback paths to reduce or enhance sensitivity at noise and signal frequencies respectively, as discussed in Chapter 3. While these techniques provide solutions under some circumstances, it was clear from the experiments carried out and the data shown and discussed in that chapter that they would not provide a generic solution for all applications. As such, other approaches must be considered. One possible approach is the expansion of voltage rails through the use

of discrete transistor based designs which allow much wider power supply rails whilst maintaining sensitivity. This is being explored by another member of the group. Another possible solution is clearly the reduction in gain of the sensor, in such a way that signal to noise ratio is not compromised. This requires that the sensitivity does not decrease to the point that the noise inherent in the sensor is sufficiently large as to overwhelm the signal of interest.

## **2.2 Positive Feedback Techniques for Enhancing Instrumentation Performance**

In order to discuss the effect of positive feedback techniques used to enhance the input characteristics of the sensor, they must first be defined in some detail. As such, this section will begin by defining what is meant by the terms Bootstrapping, Neutralization and Guarding.

### **2.2.1 Bootstrapping**

Bootstrapping[67] is the name given to a positive feedback technique used to increase the effective input resistance of an amplifier circuit. In this case, the signal at the output of the amplifier is fed back and used to ensure that the presence of external components on the input of the amplifier, necessary for dc biasing, does not compromise the input resistance of the circuit. If the feedback is configured such that the signal voltage across the component connected to the input is zero (i.e. the voltage on both sides of the component is equal) and thus the component is arranged to draw no current from the input, then the component can be seen to have effectively infinite resistance. Feedback in excess of this value creates instability, so in practice the need to ensure this does not occur limits the maximum effective input resistance which it is possible to reach with this technique. Despite this, significant increases in input resistance may be achieved at the signal frequency.

### 2.2.2 Neutralization

Input capacitance can also be reduced (or cancelled) using a similar positive feedback technique known as neutralization[67]. In this case, current is fed back from the output through a feedback capacitor. This compensates for the input current which is shunted by the input capacitance and nulls its effect. In much the same way as with bootstrap, it is possible for this to be configured so that the input capacitance is completely cancelled, but at a risk of instability.

### 2.2.3 Guarding

In order to screen against noise, the input of an electrometer or amplifier is often surrounded by an earthed layer. This applies whether the input is an electrode, or in the more common case where a coaxial cable is used to connect the input to a source. The use of a dielectric spacer introduces a leakage resistance between the input of the electrometer and ground which, while large, can compromise the input impedance of very high impedance circuits. This creates a problem since, in the absence of any screening, it is clear that noise would be increased by local sources. The solution involves the use of a technique known as guarding[68] and is illustrated in Figure 2.1. The shielding, whether it be the outer of a coaxial cable or a shield on the electrode and around the input on the printed circuit board, is driven with a voltage that is approximately equal to the input voltage, thus making the effective leakage resistance extremely large.

### 2.2.4 Positive Feedback in an EPS Sensor

To date, the need to overcome extremely large coupling impedances when operating the EPS in a remote mode has meant that bootstrapping, neutralization and guarding have all been employed for any application in which the sensor might find itself very weakly coupled to a signal. The implications of using these techniques were not well understood, particularly with regard to their effect on signal to noise ratio, however it had been

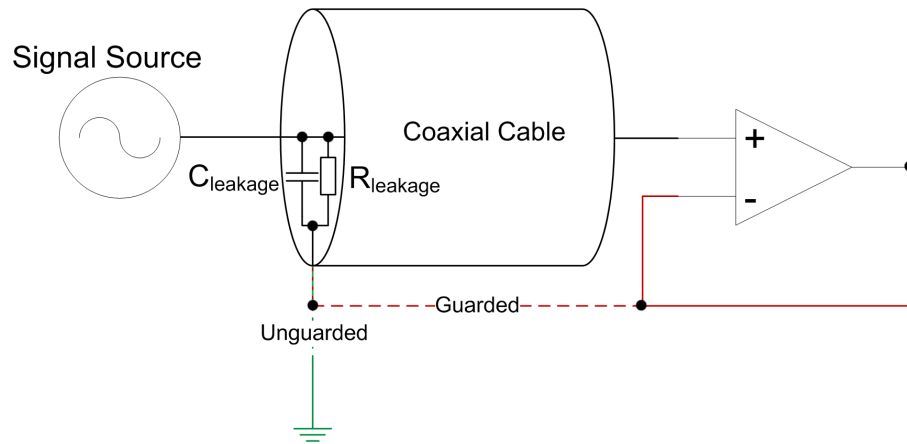


Figure 2.1: Guarded and unguarded configuration

presumed that these techniques all resulted in improved performance. In this chapter, the effects of combining all these techniques will be explored. Results will be presented from a series of experiments designed to map out the sensor characteristics, showing the effects of varying these positive feedback parameters in an EPS.

Since these are positive feedback techniques, their use dictates relatively high levels of gain in the sensors. If these techniques yielded an improvement in signal to noise ratio, then clearly they were highly beneficial to the design of the sensor. Conversely, if it could be shown that under some circumstances they yielded no benefit, then these feedback techniques would be compromising the performance of the sensor both by limiting the dynamic range and restricting the usable bandwidth.

Since a capacitance is formed between the guard and input of a sensor, the application of positive feedback through use of guarding at ratios of greater than unity is indistinguishable from the use of neutralization. The leakage capacitance and resistance which exists between the inner and outer of the co-axial cable is shown pictorially in Figure 2.1. With unity guarding, it is possible to neutralize the capacitance that would otherwise exist between the input and the outer of the electrode. If greater than unity guarding is applied, it is theoretically also possible to neutralize the input capacitance of the sensor and increase sensitivity. However, if the noise level is also increased at a level equal to the improvement in sensitivity, no improvement in signal to noise ratio is yielded.

With this in mind, a sensor was designed which would allow for automated digital control of bootstrapping and guarding. In addition, a number of fixed value capacitors were

constructed to provide well defined coupling capacitances of similar magnitude to that experienced when using the sensors remotely. This allowed the automated mapping of the sensor parameter space, by varying the amounts of guarding, neutralization and bootstrapping, and plotting the effect these had on a frequency response. The objective was to establish under which conditions these techniques provided a benefit to the sensor, and under which they undermined performance by restricting dynamic range.

## 2.3 Programmable Sensor

A sensor was designed using digital potentiometers (Analog Devices 5290) [69] to provide variable levels of bootstrapping and guarding. These devices are 256 position digital potentiometers which are controlled using an SPI serial bus interface. A testing and development board was designed and constructed in such a way that sensors of this type could be easily connected. A microcontroller was used to adjust the potentiometers and interface with a keypad, LCD display and USB data acquisition card [70]. This acquisition card was in turn connected to a PC running Labview[70]. Microprocessor code was written to facilitate communication between Labview and the sensor and allow manual settings using the keypad, with adjustments indicated on the LCD display. The system described is shown diagrammatically in Figure 2.2

A Rohde and Schwarz function generator (Model AFGU) was used to provide a reference signal. A Labview VI was written to control the reference signal from the function generator, feed this through a well defined capacitance into the sensor, acquire data from the output of the sensor and calculate a frequency response. In this way, a frequency response could be measured for every stable value of bootstrapping and guarding, and a data set taken for several different coupling capacitances.

### 2.3.1 Results

Once data had been collected for all stable values of bootstrap and guarding, many plots could be generated in order to visually present the effect of the controlled feedback

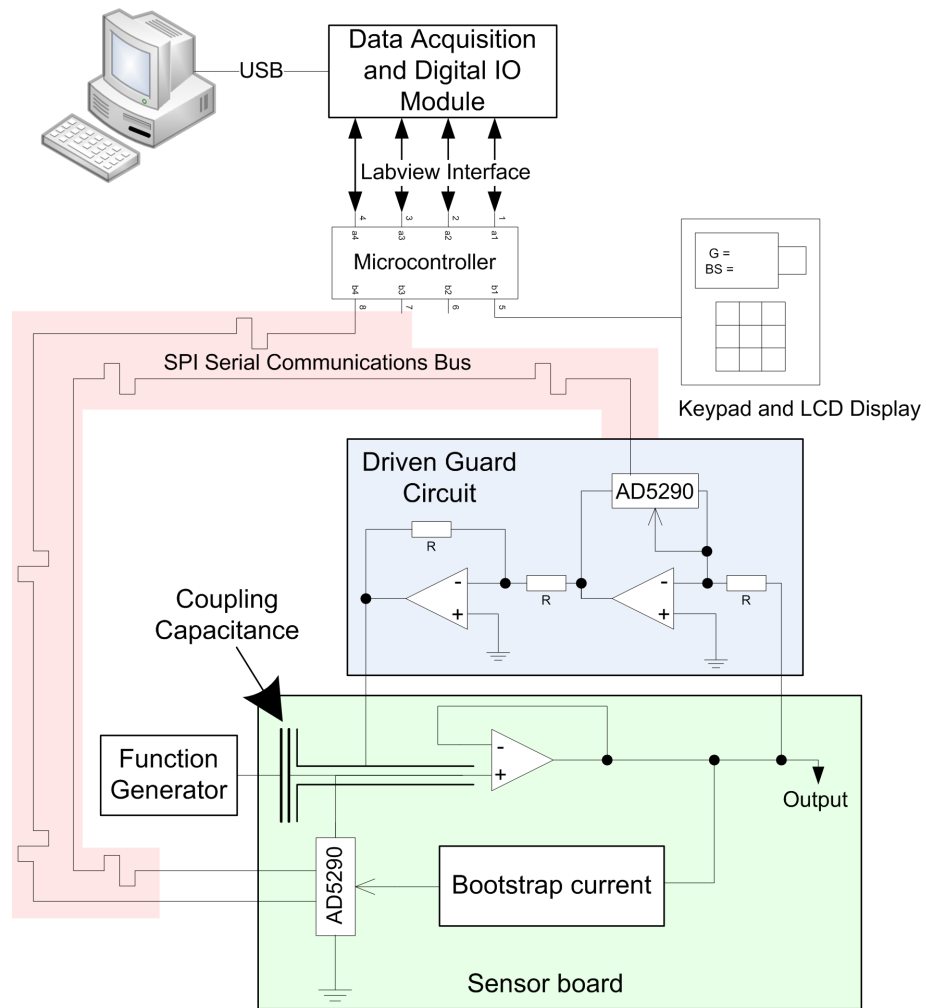
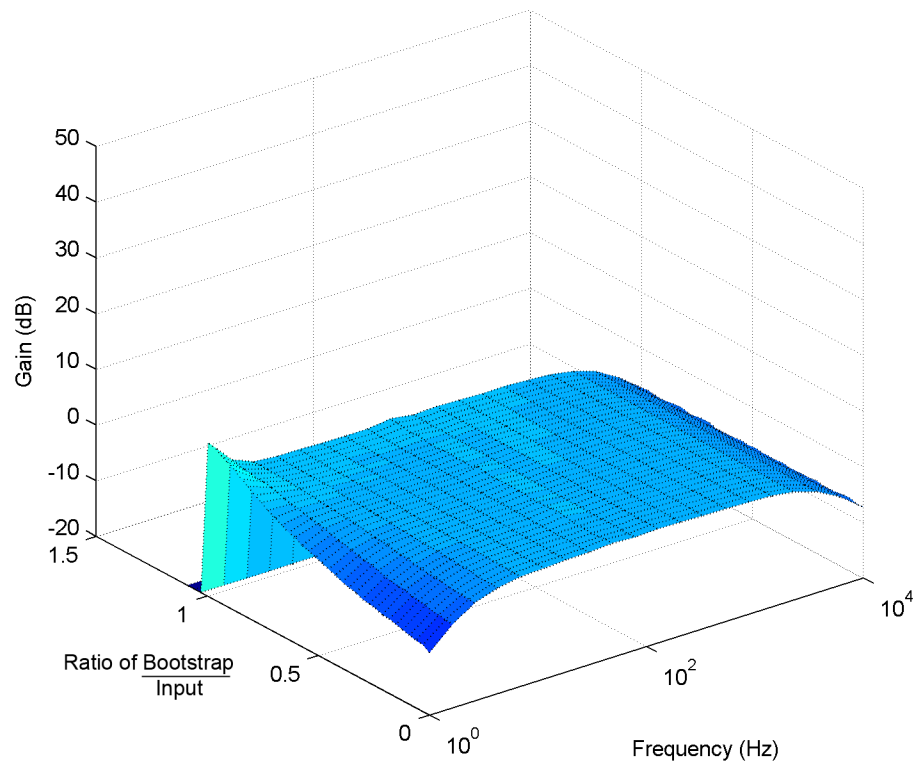


Figure 2.2: Digital potentiometers used to allow automated reconfiguration of sensor characteristics

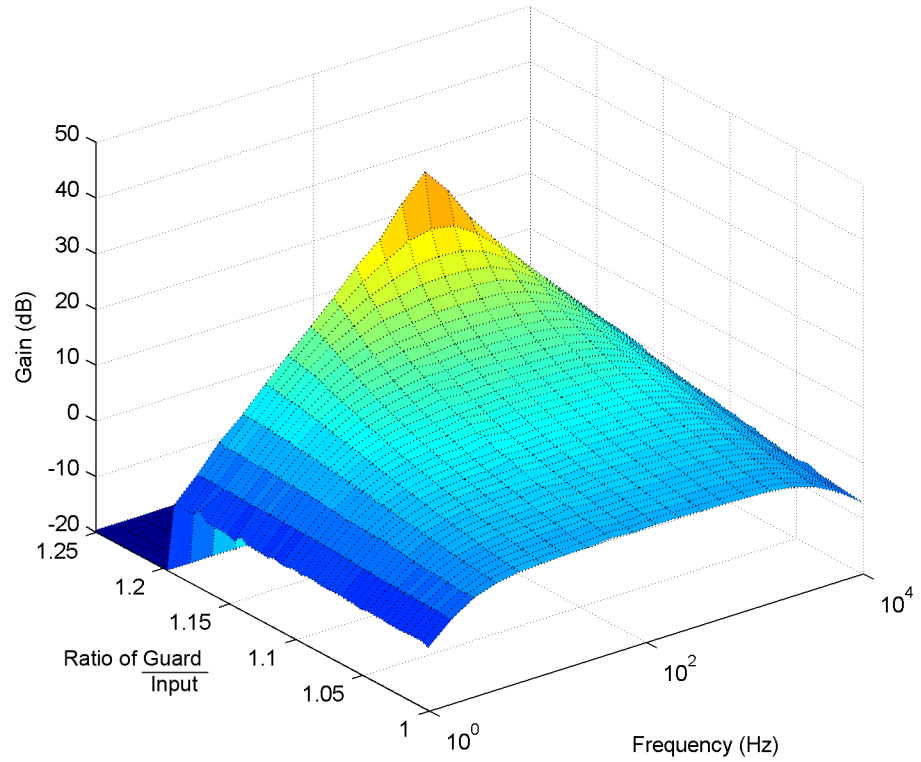
techniques on a frequency response. Two dimensional surface plots were generated as a result of varying frequency and either bootstrap or guarding, while the other parameter was kept constant. This allowed these techniques to be analysed both individually, but also in combination.

The plots in Figure 2.3(a) and 2.3(b) demonstrate the effect of bootstrapping and guarding acting independently of each other. Specifically, in Figure 2.3(b) the flat frequency response at values of guarding close to unity can be seen narrowing, with the 3dB points moving towards the middle of the frequency range as the level of guarding is increased.

This is perhaps to be expected, as a capacitance exists between the guard and the input of the electrometer. In this way, with positive feedback applied through a capacitor, the



(a) Varying amount of bootstrapping with only unity guarding present (i.e. no neutralisation of input capacitance)



(b) Varying amount of guarding with no bootstrapping present

Figure 2.3: Varying positive feedback techniques in isolation

input capacitance of the sensor can be largely neutralized, resulting in the observable improvement in gain at mid band frequencies. The fixed level of input resistance becomes the limiting factor at lower frequencies. In these cases, it can clearly be observed that guarding, in addition to the screening effect, also has an effect similar to neutralization when at levels greater than unity.

Bootstrapping, on the other hand, increases the effective input resistance, but only at low frequencies, since the input capacitance is the dominating characteristic at frequencies above the 3dB point. This is seen in Figure 2.3(a). As the level of bootstrapping is increased, it can be seen that in the absence of other positive feedback techniques a point is reached where the frequency response has become flat. It should be noted that there must still exist a lower cut off frequency, as the input resistance will always maintain a finite value, but in this case it is below the lowest 1Hz frequency at which a measurement is made. If bootstrapping is increased further, it is apparent that the response begins to turn up at the low frequency end, eventually to the point of becoming tuned to very low frequencies.

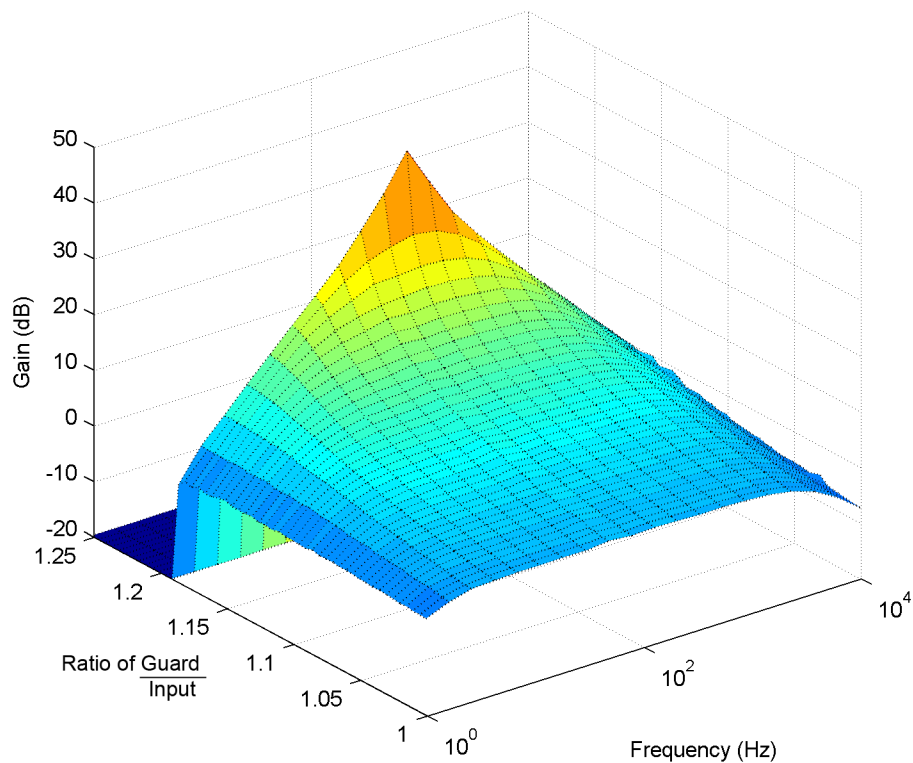


Figure 2.4: Frequency response with 50% bootstrap setting and varied guarding

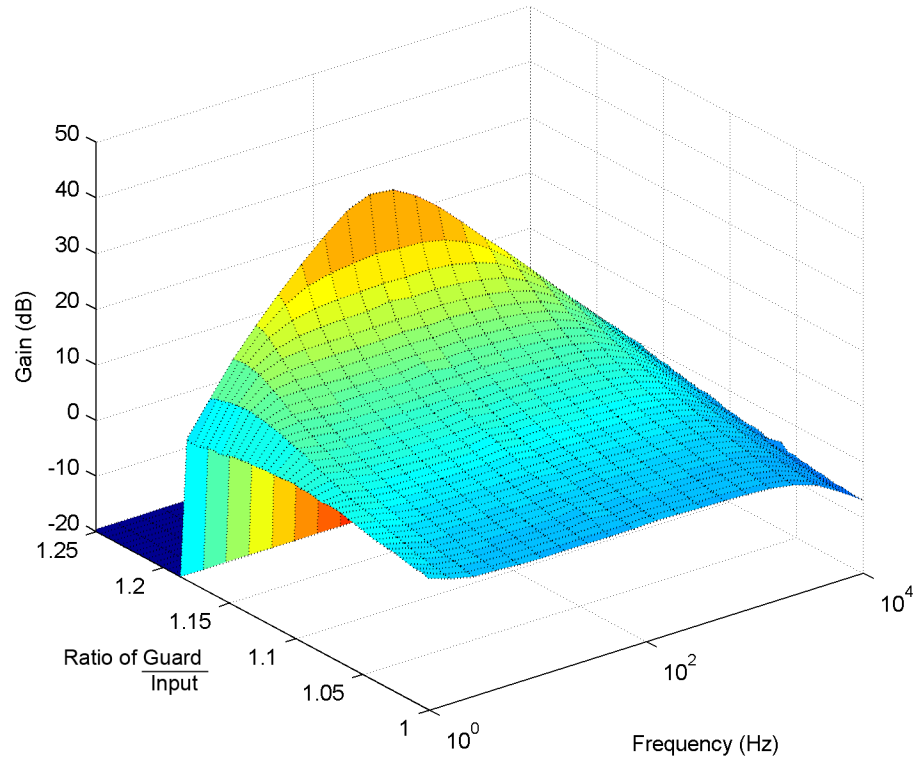


Figure 2.5: Frequency response with 80% bootstrap and varied guarding

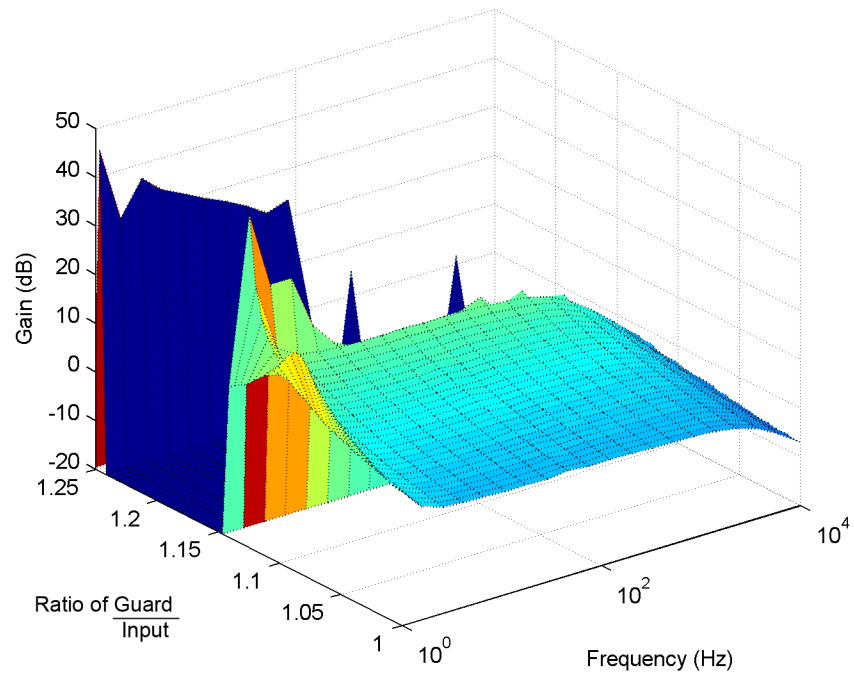


Figure 2.6: Frequency response with 97% bootstrap and varied guarding

Figures 2.4, 2.5 and 2.6 show the effect of varying guarding at increasing levels of bootstrap. Applying bootstrap current has the effect of improving the low frequency response and flattening out the peakiness in the response caused by the application of increased levels of guarding. The ideal level of bootstrapping appears to vary depending on how much neutralisation, provided by guarding, is applied. Once the level of bootstrapping becomes very high (close to 100%) the combination of bootstrap and neutralisation brought about by high levels of guarding causes the sensor to become unstable as a result of positive feedback. This is visible in Figure 2.6 where the instability point can be seen to occur at a far lower level of guarding than is present at other levels of bootstrap.

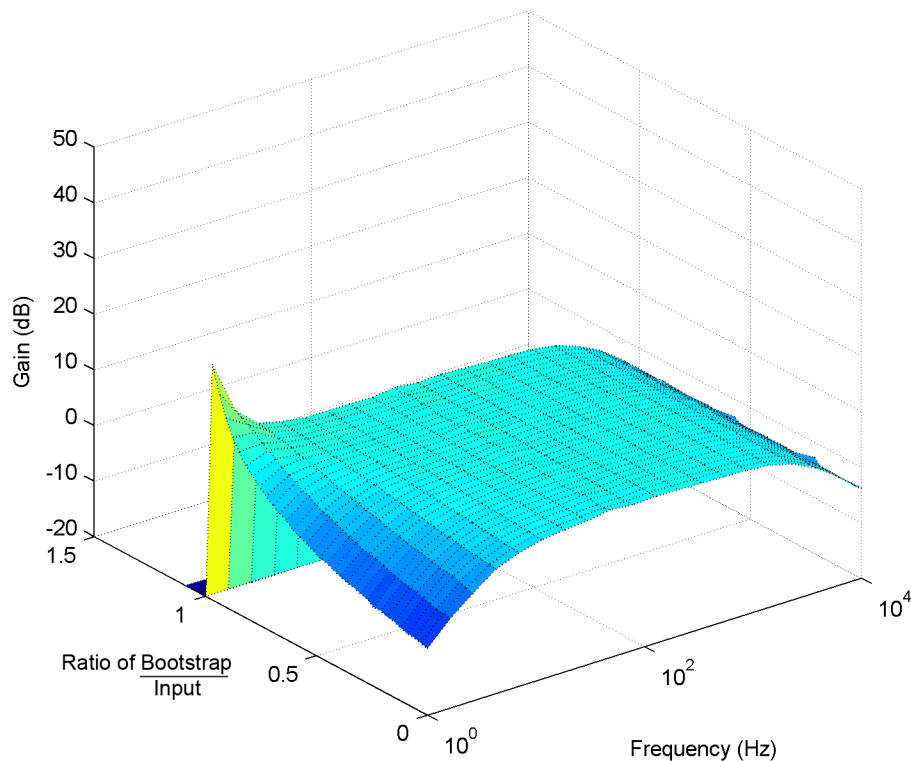


Figure 2.7: Frequency response with 110% Guarding and variable bootstrap

Figures 2.7, 2.8 and 2.9 show that applying varying levels of bootstrapping while maintaining constant values of guarding yields similar results. It can be seen in Figure 2.7 that additional guarding has resulted in increased gain, when compared to Figure 2.3(a), as a result of the reduction in effective input capacitance brought about by this neutralization current. As the bootstrap current is increased, the low frequency gain is increased and the frequency response flattened out until, as bootstrap is increased yet further, the response turns up at lower frequencies. As the level of guarding is increased further, it becomes impossible to completely flatten the response using bootstrapping

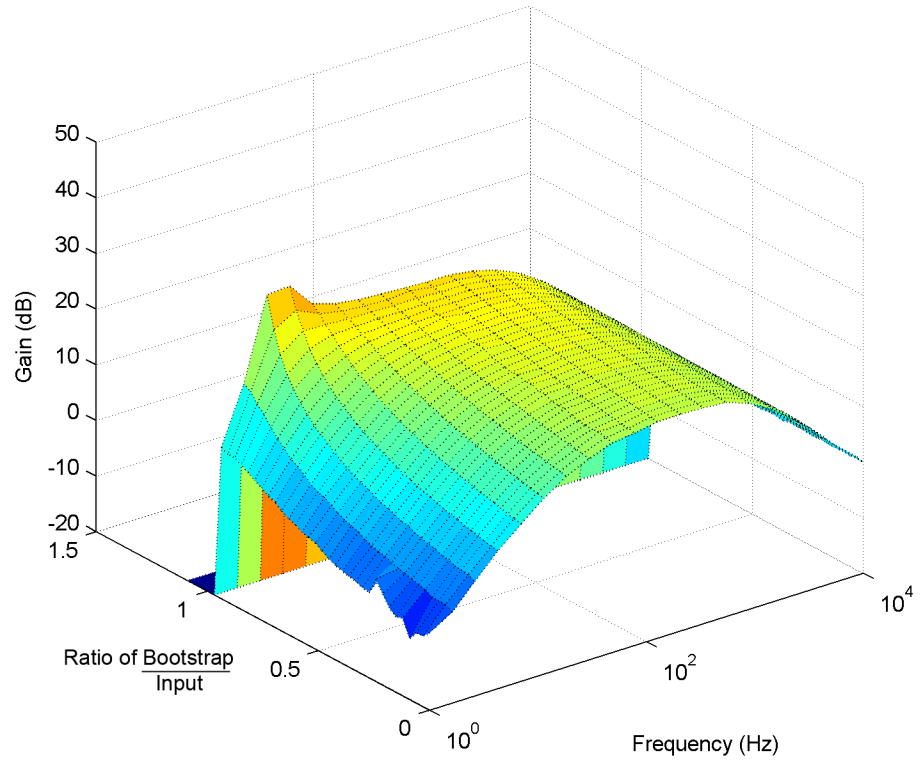


Figure 2.8: Frequency response with 117.5% Guarding and variable bootstrap

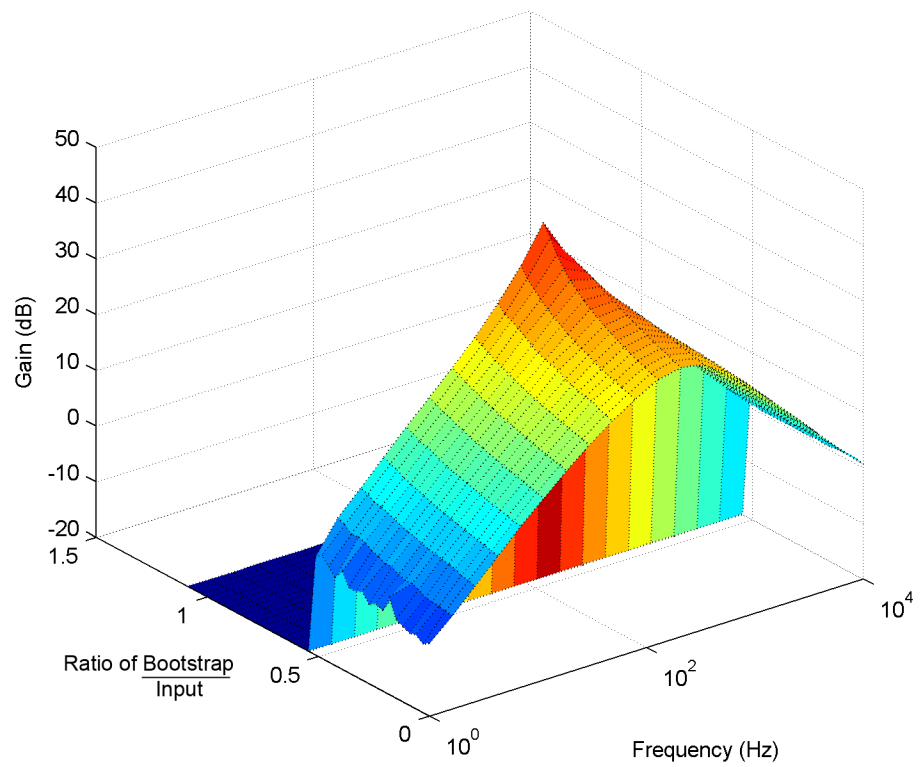


Figure 2.9: Frequency response with 120% Guarding and variable bootstrap

without causing instability, as seen in Figure 2.8. Ultimately, once guarding is increased to close to its stability limit, the maximum amount of bootstrapping that can be applied without causing instability becomes limited as shown in Figure 2.9.

### 2.3.2 Simulations of Bootstrapping and Neutralization

It is possible to analyse bootstrapping and neutralization as techniques within a Spice simulation. This allows a comparison to be made between the predicted effect these techniques would have on the frequency response and performance of a sensor, and the effect measured and observed when these parameters were varied in the way described in this chapter. Two simulation circuits were designed to model the sensor's input characteristics and provide adjustable bootstrapping or neutralization respectively. The input capacitance was fixed at 1pF to be representative of standard sensor performance, while the coupling capacitance was set at 100fF to represent a weakly coupled scenario in which bootstrapping and neutralization had a significant effect on sensor performance. These are shown in Figure 2.10 and 2.11.

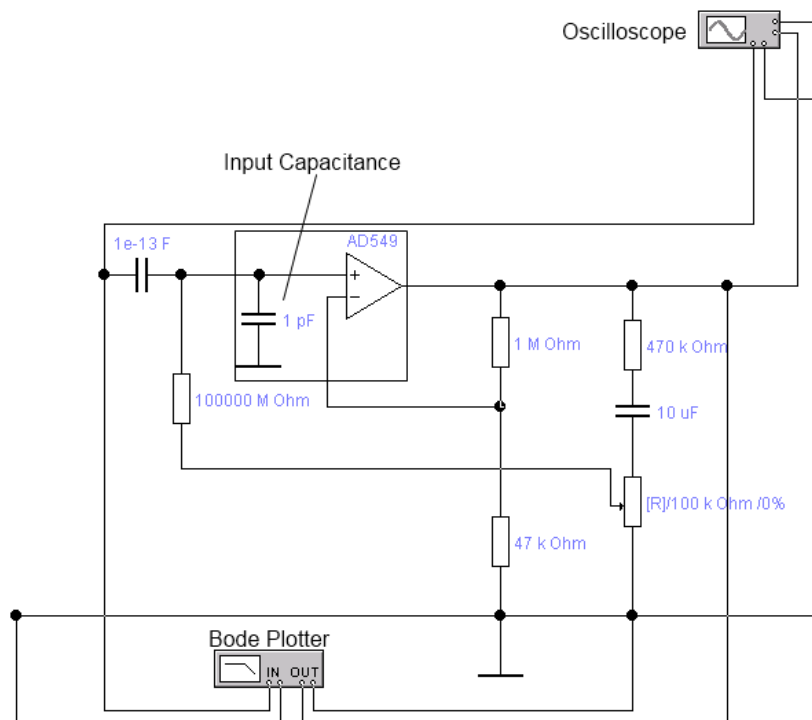


Figure 2.10: Bootstrap simulation circuit

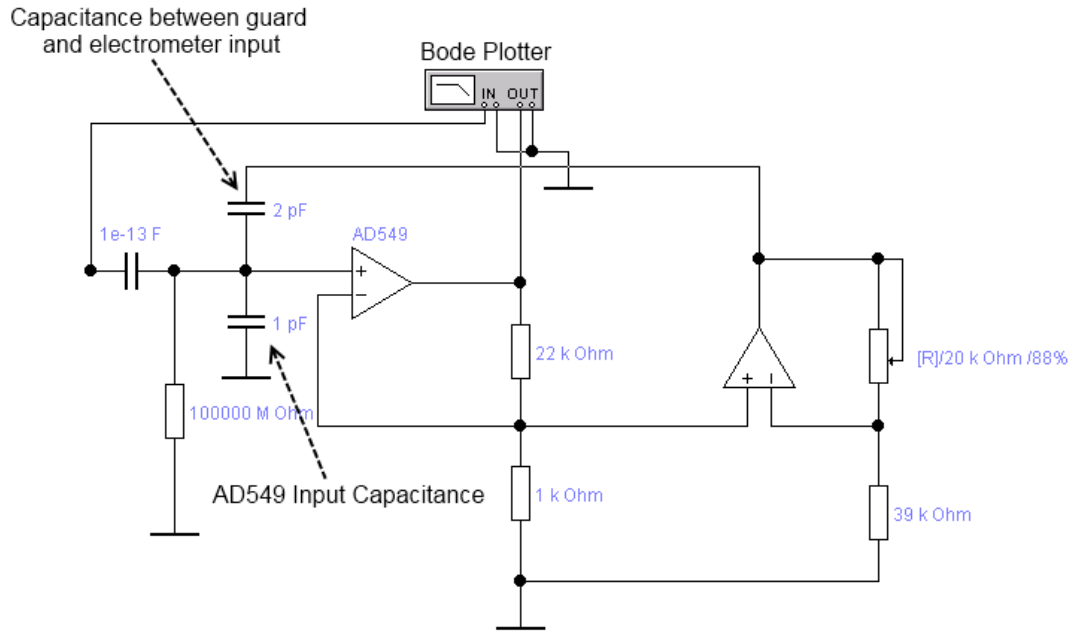


Figure 2.11: Neutralization simulation circuit

Using these circuits it is possible to generate simulated frequency responses for different amounts of applied bootstrap. The circuits shown are simplified significantly from final sensor designs, but demonstrate the application of these techniques individually. This should allow these effects to be isolated and tested in simulation. Figure 2.12 shows a frequency response generated from this circuit with no bootstrapping applied.

Applying bootstrapping increases the effective input resistance and thereby extends the usable bandwidth towards the low frequency end of the response. This was observed in the experimentally collected data, and is reproduced in simulations as shown in Figure 2.13. In this case, bootstrapping is applied in amounts large enough to flatten the low frequency response as much as possible and give maximum usable bandwidth at the low end. It should be noted that this results in a large phase shift at low frequencies, which could represent a serious problem if attempting to collect and analyse electrophysiological signals such as an ECG.

Applying further bootstrapping creates a peak in the response at low frequencies, before ultimately the circuit begins to oscillate. Again, this was observed experimentally, and the effect on the frequency response of applying the maximum amount of bootstrapping possible before oscillation occurs is shown in Figure 2.14.

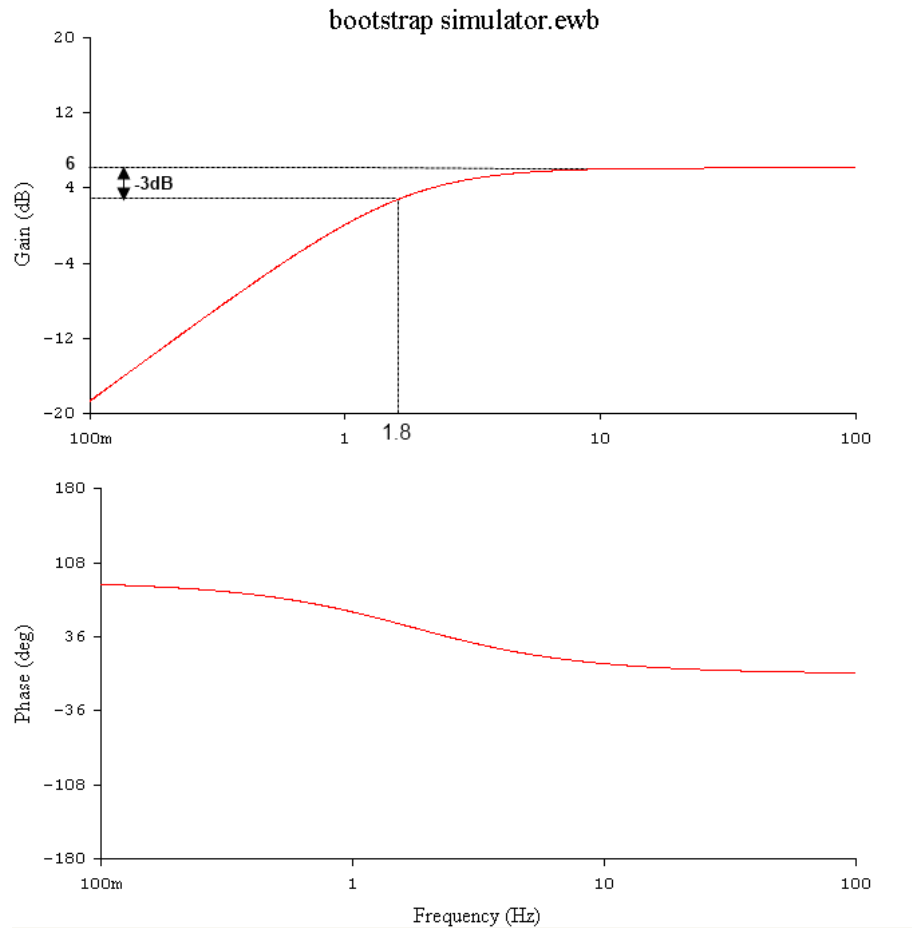


Figure 2.12: Frequency response with no bootstrapping applied to the input, with signal applied through 100fF coupling capacitance

Neutralisation of input capacitance also occurs when positive feedback is applied through a capacitance to the input of the sensor. This effect becomes similar to guarding when a guarding signal of amplitude more than 1.0 x input voltage is applied. This enables guarding and neutralization to be combined as a technique, leading to a significantly simplified circuit design. As with the bootstrapping, the results obtained from the experimental sensor are largely reproduced in simulation. Figure 2.15 shows a frequency response with unity guarding applied. In this case, only the capacitance between the input and the outer of any connectors and electrodes is neutralised, while the input capacitance of the sensor remains unaffected.

By adding more guarding, it is possible to neutralise some of the input capacitance of the sensor, thereby increasing the gain at mid band frequencies. This is shown to some extent in Figure 2.16. Adding more neutralisation allows more of the input capacitance to be neutralised until gain reaches a level almost commensurate with an input capacitance of

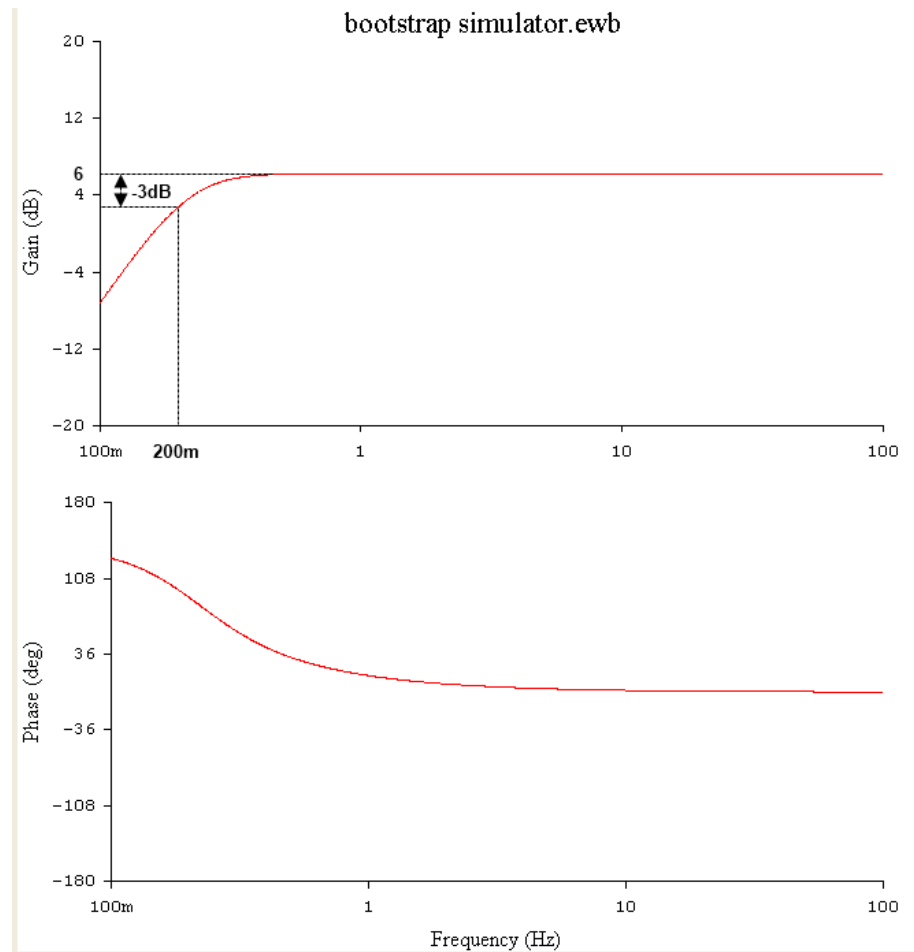


Figure 2.13: Frequency response with bootstrapping applied in order to gain maximum flat low frequency response, with signal applied through 100fF coupling capacitance

zero Farads. This is shown in Figure 2.17. After this point, the circuit quickly becomes unstable.

## 2.4 Conclusions

The application of positive feedback techniques can be demonstrated, both experimentally and in simulation, to increase the input impedance characteristics significantly. As a result, it could therefore be concluded that since the use of bootstrap and neutralization techniques appear to boost the input resistance and decrease the input capacitance respectively, that these techniques result in an improved sensor and should therefore always be applied. This has always been the assumption made when constructing EPS sensors

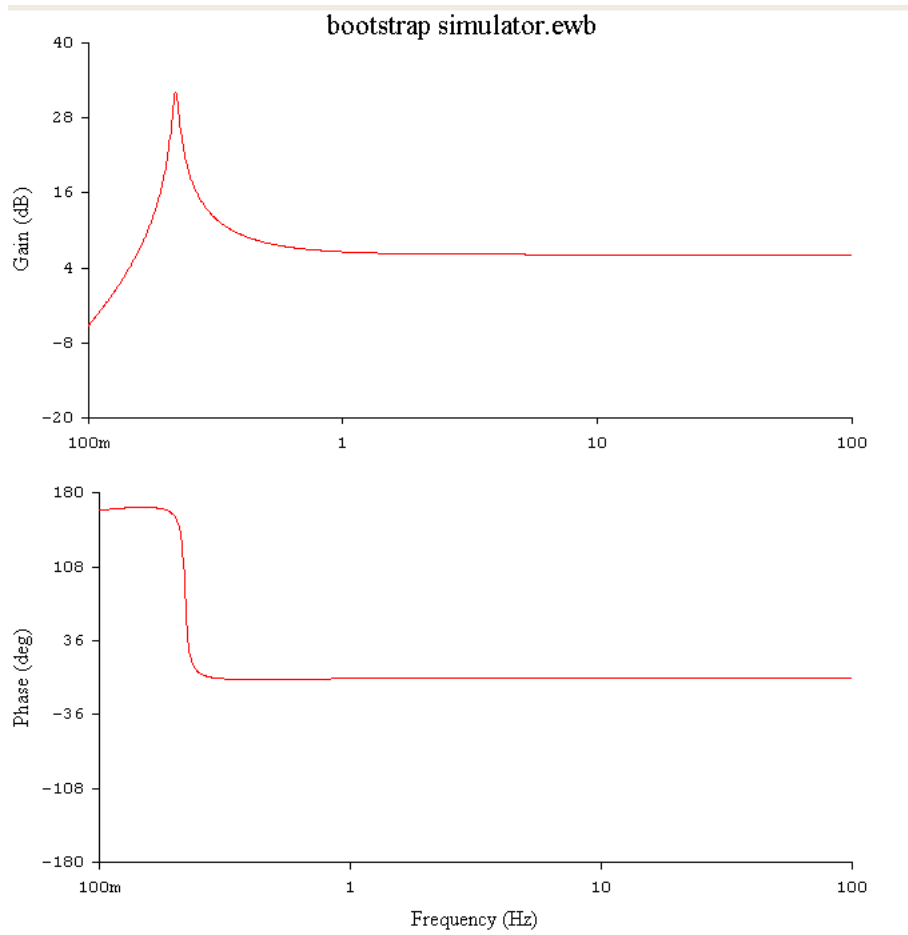


Figure 2.14: Frequency response with maximum possible bootstrapping applied before instability occurs, with signal applied through 100fF coupling capacitance

for a variety of applications in the past. However, the nature of these techniques as positive feedback techniques means that, in almost all cases, these improvements in input impedance do not yield concomitant increases in signal to noise. Since noise, as well as signal, which is present on the output of the sensor is fed back, there will be no signal to noise improvement unless a lower noise or noiseless source can be used to bootstrap or neutralize the input.

However, where these techniques can be extremely helpful is in the modification of the response to fit the requirements of the signal being acquired. Where a particularly low frequency signal remains of interest, the ability to maintain a flat response down to very low, in some cases almost DC, frequencies proves beneficial. Furthermore, where a very low coupling capacitance exists, the ability to boost the gain at mid band frequencies has the potential to increase gain, while simultaneously reducing sensitivity to potential noise sources such as low frequency movement related signals.

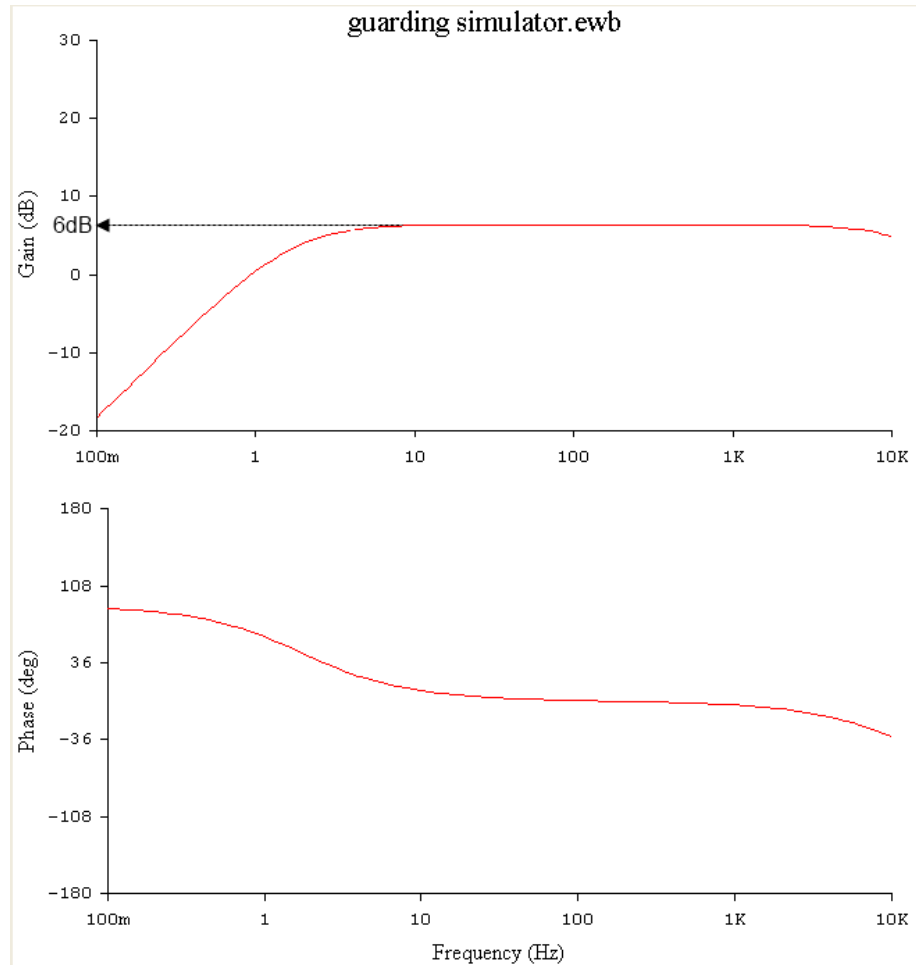


Figure 2.15: Frequency response with unity guarding thus no neutralisation of input capacitance, with signal applied through 100fF coupling capacitance

These increases in gain, however, come at the cost of reduced dynamic range. It will be shown in later chapters that this creates a problem, and it is a lack of dynamic range, more than other characteristics, that limits performance in a significant number of remote applications. In these cases, it is arguably better to avoid the use of neutralisation, and to some extent bootstrapping. This has the effect of improving dynamic range, since gain is reduced, without compromising signal to noise ratio.

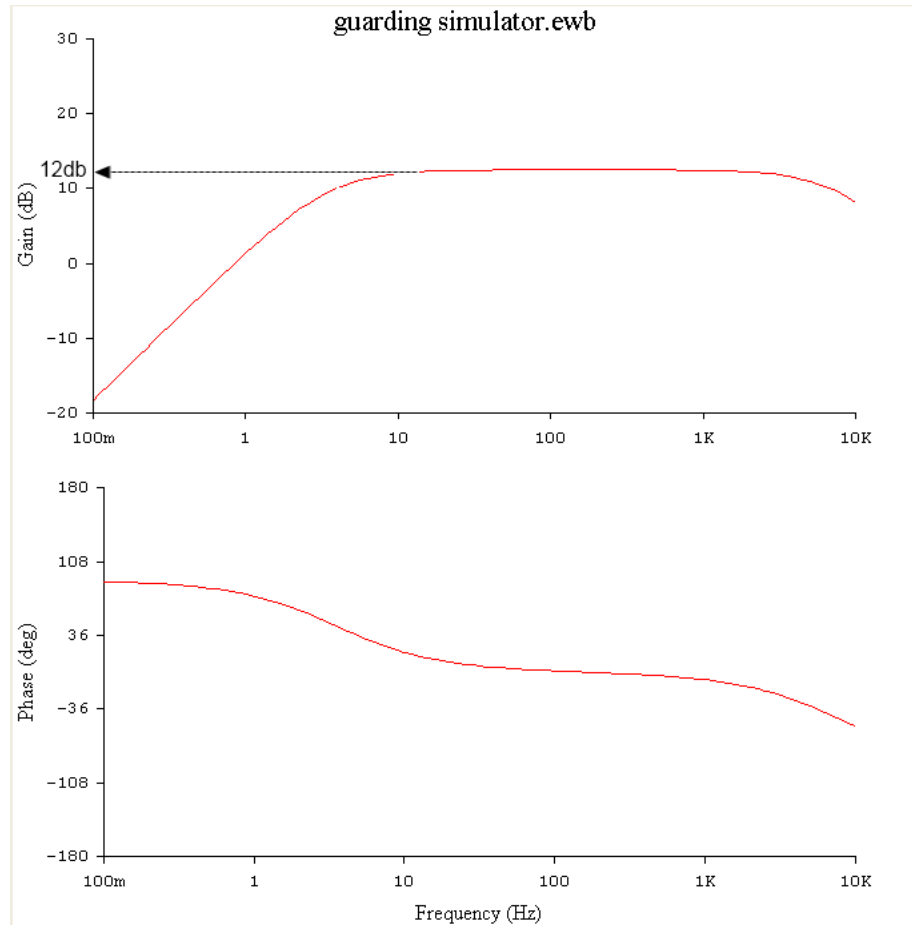


Figure 2.16: Frequency response at mid point between unity guard and maximum stable guard, with signal applied through 100fF coupling capacitance

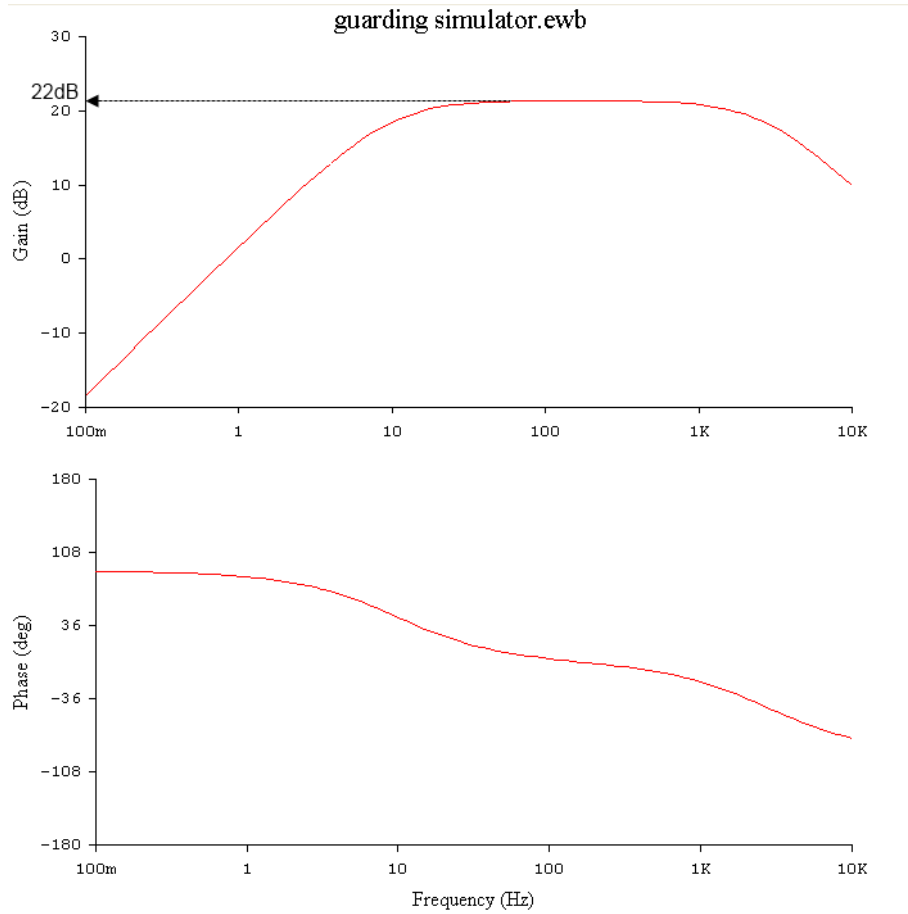


Figure 2.17: Frequency response when guard at maximum stable value and maximum amount of input capacitance neutralised, with signal applied through 100fF coupling capacitance

## Chapter 3

# Tuned Sensors

### 3.1 Introduction

It has previously been shown that it is possible to operate the EP Sensors in a remote mode, where the coupling capacitance between the sensor and the source is sufficiently small as to be dominated by the self capacitance of the sensors[15]. This enables the sensors to act in a manner analogous to a magnetometer measuring a magnetic field. When doing so, however, the ability of the EPS to operate in an open and unshielded environment is seriously compromised. In contact mode, the proximity of the sensor to the signal source ensures that the coupling capacitance is relatively large (1pF to 1nF), and sufficient self-screening from external sources of noise is in place. However, in remote applications, where a substantial spatial gap is present between the sensor and the source, no self screening effect is present. The result of this is that the sensor must either be operated within a screened environment, as required in earlier work when a remote ECG was measured[15], or with a significantly reduced sensitivity in order to prevent external noise, often mains related noise, from saturating the sensor and preventing any measurement. It is worth noting that no amount of conventional post acquisition signal processing, whether analogue or digital, would be capable of recovering a signal from regions of saturation.

### 3.2 Signal specific sensors

One possible solution to this problem is to implement a sensor design which is sensitive only at frequencies of interest. The technique described in this section involves the use of filter networks, incorporated into the feedback loop of the sensor. This allows the tailoring of the frequency response of the sensor to match the frequency components of signals of interest. There are two very clear and immediate advantages to this approach when compared to the conventional solution of applying signal processing to the output of the sensor. Significantly, the effective bandwidth of the sensor is reduced substantially, leading to a concomitant improvement in signal to noise ratio. Furthermore, since all sources of noise which do not coincide with one of the selected Fourier components are excluded, they cannot cause the sensor to saturate.

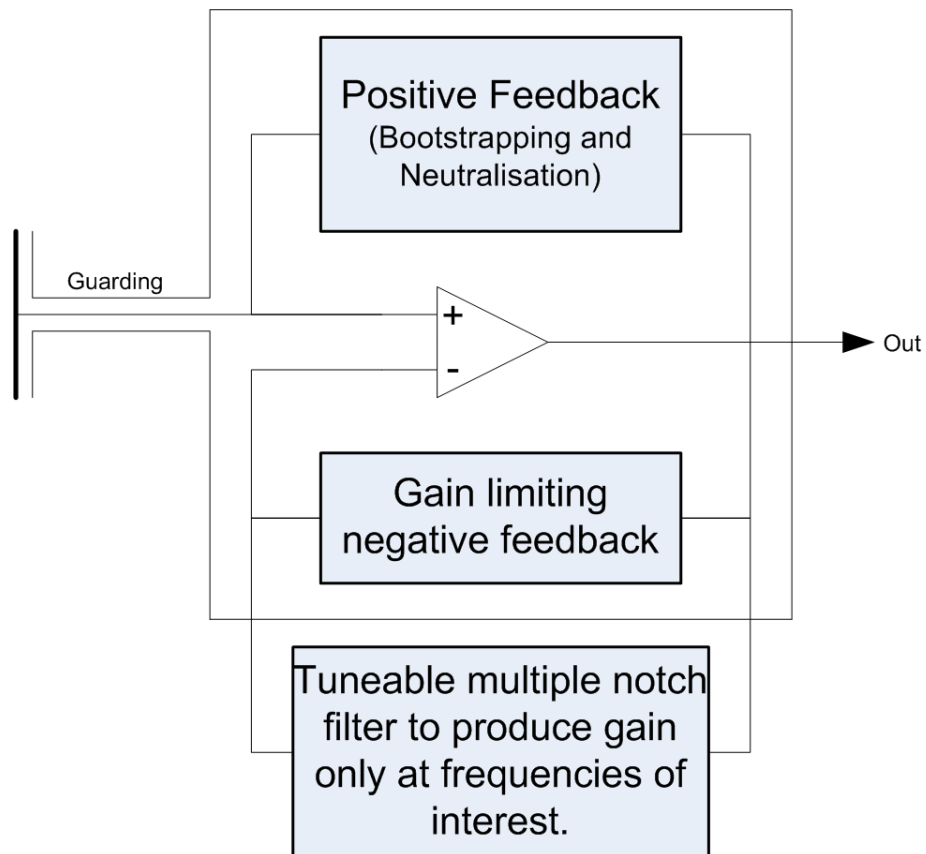


Figure 3.1: Block diagram showing an electric potential sensor with four bandstop(notch) filters incorporated into the feedback loop

Figure 3.1 shows a typical schematic for a sensor capable of responding to a signal containing four distinct frequency components. In reality these would normally be harmonically related for periodic signals, thus simplifying the implementation considerably. In this way the bandstop(notch) filter functions are transformed into a set of bandpass functions in the response of the sensor. The technique of using multiple high quality factor (Q) filters, which is proposed here, results in a substantial reduction in the bandwidth of the sensor required to obtain a signal with a large number of harmonics. For example, a signal consisting of a fundamental at 1kHz and harmonics at 3, 5, 7, and 9kHz would require 10kHz of bandwidth. However, if acquired using a tuned sensor, with a Q of 50, centred on these five frequencies would require a total bandwidth of

$$20 + 60 + 100 + 140 + 180 = 500Hz$$

This reduction in signal bandwidth from 9kHz to 500Hz, assuming noise is white (flat in the frequency domain) yields an improvement in signal to noise ratio by a factor of

$$\sqrt{\frac{9000}{500}} = 4.24 = 12.5dB$$

If the Q factor of the filters involved is increased beyond this, the improvement is also increased and becomes even more significant. With a Q factor in the filters of 100, the bandwidth for the sensor reduces to just 250Hz, yielding a further improvement in the signal to noise ratio of 6 dB. With a Q in the order of 1000, the bandwidth becomes just 25Hz, yielding a signal to noise ratio improvement of nineteen, or 26dB. Furthermore, these calculations rely on the assumption that background noise is white and therefore uniformly distributed across the frequency spectrum. In reality, this is rarely the case. The primary concern, as discussed, is that of large amplitude noise signals which potentially drive the sensor into saturation and limit the dynamic range. The techniques discussed here could potentially reduce these signals by 60dB, which would yield a much larger dynamic range provided that noise exists at frequencies which do not overlap those of interest.

In practice, these large noise signals are often the result of movement, either of a subject or sample being measured, or of the sensor itself. The ability to differentiate between a signal of interest and the large low frequency movement-related noise components would be particularly helpful in enhancing the usability of the sensor for remote electro-physiological applications.

In order to explore this possibility, switched capacitor filters (LMF100[71]) were used to create a series of filters, the centre frequency of which was controlled by a variable clock frequency for each filter. Furthermore, the Q factor of each filter can be adjusted using a digital potentiometer. These filters were integrated into the feedback loop of an audio frequency sensor with a bandwidth of 1Hz to 100kHz. With these filters in feedback, the sensor had a flat low gain response, with high gain peaks occurring at the filter centre frequencies. This results in the sensor having high sensitivity at these frequencies, and a flat, low level of sensitivity, across the rest of the sensor's frequency range.

### 3.2.1 Tuned Sensor Architecture

In order to achieve a tuned signal selective sensor architecture, a multiple notch filter was needed in the feedback path, thus ensuring gain only at the centre frequencies of these notches. Several possible approaches exist when designing such a filter. Clearly, notch filters could be placed in series to create a multiple notch response. In this case, however, the digital nature of these filters made this impractical. Anti aliasing filters would need to exist between each stage, in order to prevent noise from the clock of one filter feeding directly into the input of the next. This would introduce phase shifts which could not be tolerated in a feedback network without introducing oscillation. An alternative approach was therefore selected, by which band pass filters were placed in parallel in the feedback loop of an operational amplifier, to create an active multiple notch filter. This filter was then used in the sensor feedback network to result in a multiple band pass (or multiple inverted notch) response. This arrangement is shown in Figure 3.2

### 3.2.2 Real-Time Adaptability

A programmable waveform generator (Analog Devices AD9833) IC was used to generate programmatically variable clock signals with a high degree of precision. This device is capable of generating a clock signal by dividing a given master clock ( $f_{MCLK}$ ), by  $2^{28}$  then multiplying the result by a value stored in a serially programmable register ( $FREQREG$ ). This technique could be used to generate programmatically variable centre frequencies



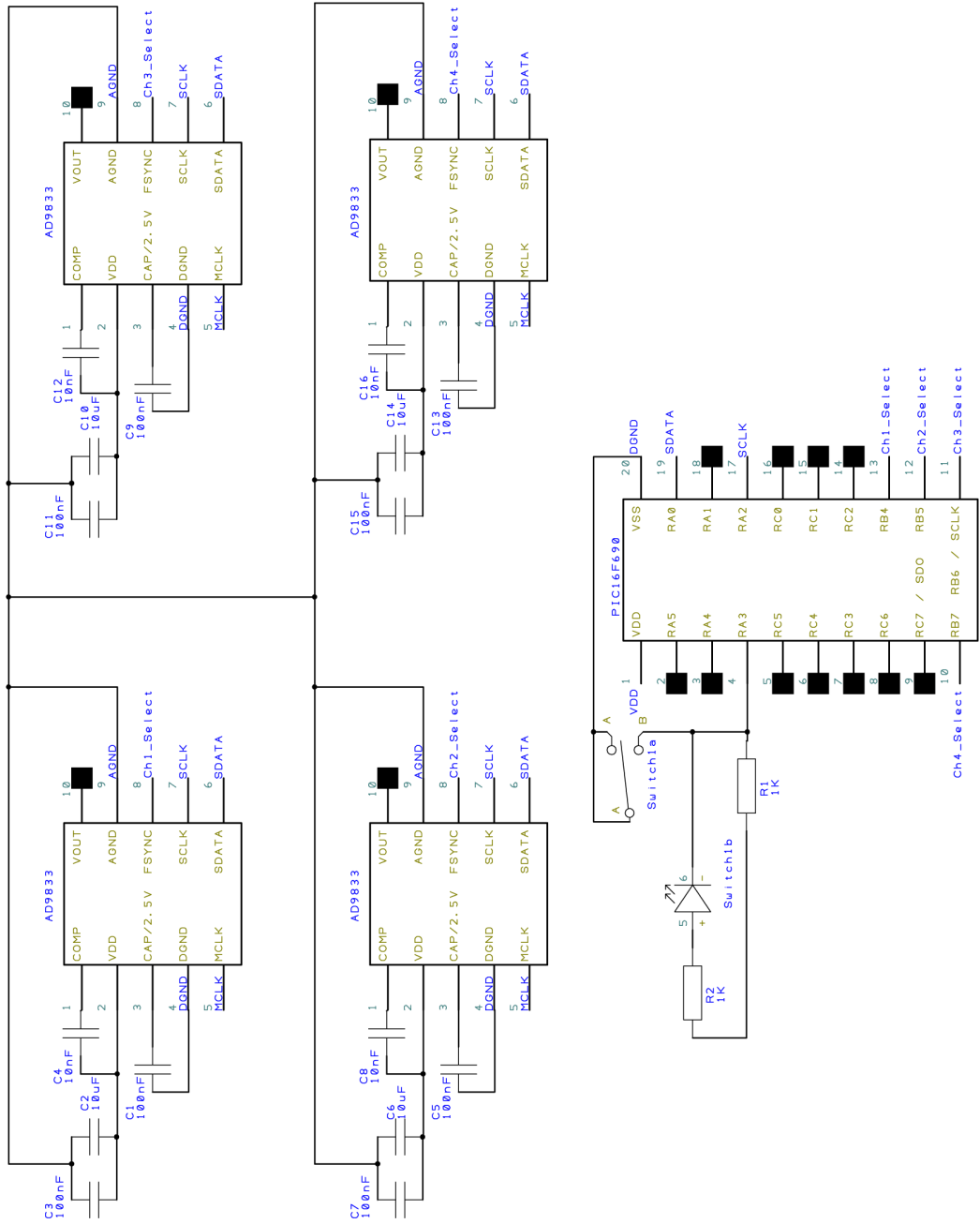


Figure 3.3: The clock generator circuit

Table 3.1: Switched Capacitor Filter Mode Table [67]

Mode	BP	LP	HP	N	AP	Number of Resistors	Adjustable $\frac{f_{cLk}}{f_0}$	Notes
1	Yes	Yes	No	Yes	No	3	No	
1a	$H_{OBP1} = -Q$ $H_{OBP2} = +1$	$H_{OLP} = +1$	No	No	No	2	No	May need input buffer Poor dynamics for high Q
1b	Yes	Yes	No	Yes	No	3	No	Useful for high frequency applications
2	Yes	Yes	No	Yes	No	3	Yes (Above $\frac{f_{cLk}}{50}$ or $\frac{f_{cLk}}{100}$ )	
3	Yes	Yes	Yes	No	No	4	Yes	Universal state variable filter Best general-purpose mode
3a	Yes	Yes	Yes	Yes	No	7	Yes	As above, but also includes resistor tunable notch
4	Yes	Yes	No	No	Yes	3	No	Gives allpass response with $H_{OAP} = -1$ and $H_{OLP} = -2$
5	Yes	Yes	No	No	Yes	4	Yes	Gives flatter allpass response than above if $R_1 = R_2 = 0.02R_4$
6a	No	Yes	Yes	No	No	3	Yes	Single pole
6b	No	$H_{OLP1} = +1$ $H_{OLP2} = \frac{-R_3}{R_2}$	No	No	No	2	Yes	Single pole
6c	No	Yes	No	No	Yes	3	No	Single pole
7	No	No	No	No	No	2	Yes	Summing integrator with adjustable time constant

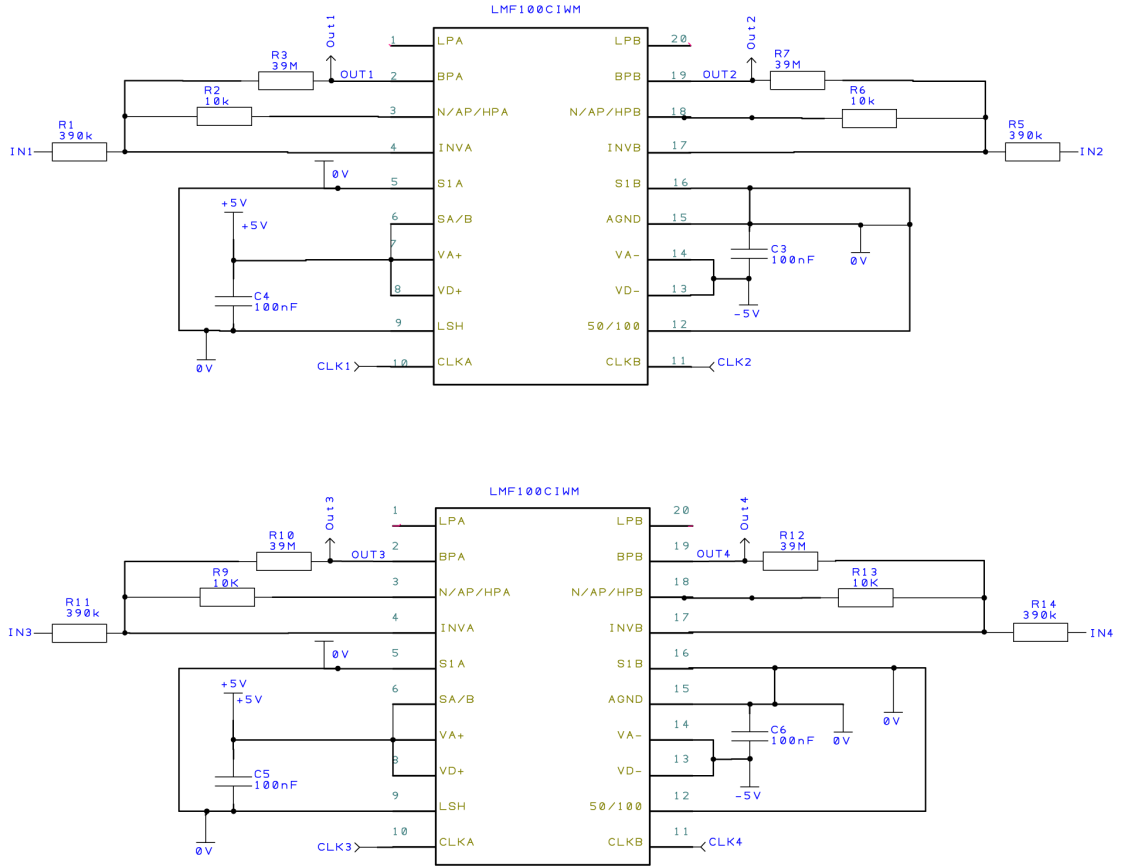


Figure 3.4: The filter circuit

In this case, the filters were configured to operate in Mode 1, as this allowed for independent control over the  $Q$ , gain, and centre frequency of the filter. The design equations used were  $Q = \frac{f_0}{BW} = \frac{R3}{R2}$  and band pass gain ( $H_{OBP}$ ) =  $-\frac{R3}{R1}$  as given by the data sheet [71]. This allowed configuration as band pass filters, while maintaining independent control over the  $Q$  (Quality Factor) of the filters, and the band pass gain ( $H_{OBP}$ ). The circuit used can be seen in Figure 3.4.

### 3.2.3 Circuit design

A sensor was designed which incorporated connections to a number of sockets for attaching additional modular boards to allow for the planned modifications. Four sockets were used to allow the attachment of a clock generation board (Figure 3.3); two filter boards, where each was capable of containing four filters; and a summing amplifier board to sum these signals together before they were fed back into the electrometer. Designing the

electrometer in this modular way, as shown in Figure 3.5, ensured that each section was capable of being developed separately; redesigned and replaced if necessary; and that small design changes to one section did not require a complete rebuild of a very complex system.

This first version of the electrometer involved just a single filter in the feedback loop to create sensitivity at a single frequency. This allowed the concept to be explored and ensured that no major problems were immediately apparent. Having constructed and tested this version of the system, and verified its operation, the filter board was then modified to include first two and then four filters.

### 3.2.4 Results

Discrimination between the sensitivity at frequencies of interest and the background noise level, and the ability to achieve distinct, adjacent peaks in sensitivity at harmonically related frequencies are two of the most important characteristics in determining the performance of the combined filter and sensory system. Preliminary results have been presented using an EPS with two switched capacitor filters incorporated into the feedback loop [72]. Figure 3.6 shows a typical frequency response for such a system. In this case a multiple band pass function has been successfully implemented, and two harmonically related frequencies (100Hz and 400Hz) selected for the purposes of demonstrating the technique. The measured discrimination shown is in excess of 50dB, and the centre frequency adjustable over a frequency range spanning from 10Hz to 10kHz, in steps of 0.01Hz. Adjusting this centre frequency has the effect of adjusting both frequencies and maintaining their harmonic relationship, however independent adjustment of frequencies is also achievable. The system Q measured is of the order of 1000, with the sensor weakly coupled (coupling capacitance of 2pf) to the tracking generator output of the signal analyser.

Further filters were added to the feedback loop to create a sensor with four harmonically related frequencies. A frequency response for such a sensor, with centre frequencies of 9, 18, 27 and 36 Hz is shown in Figure 3.7. Clearly 50dB of differentiation can be seen between signals at these frequencies, which have a gain of 25dB, and sensitivity at other frequencies, with a gain of -25dB.

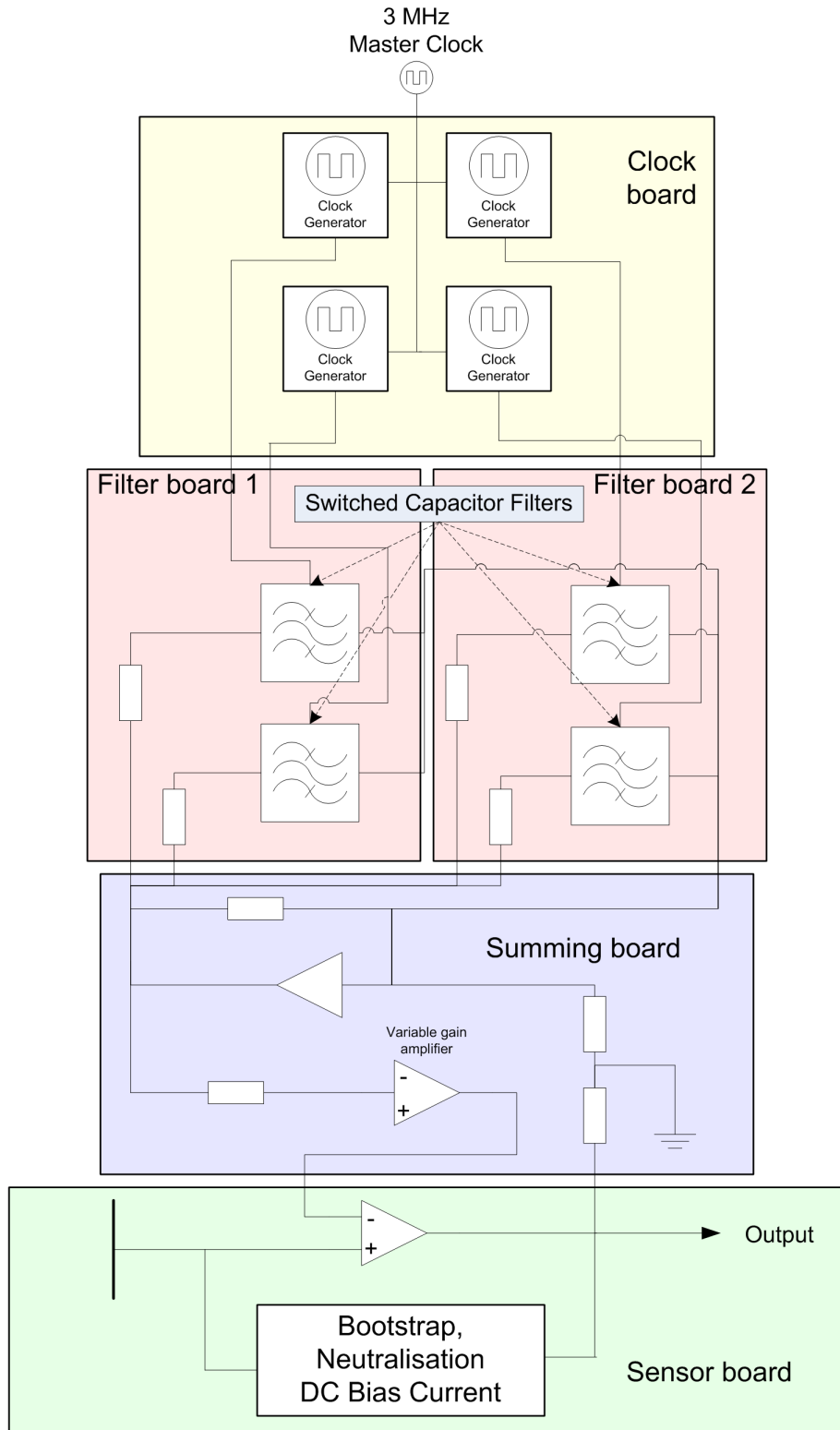


Figure 3.5: The modular architecture used

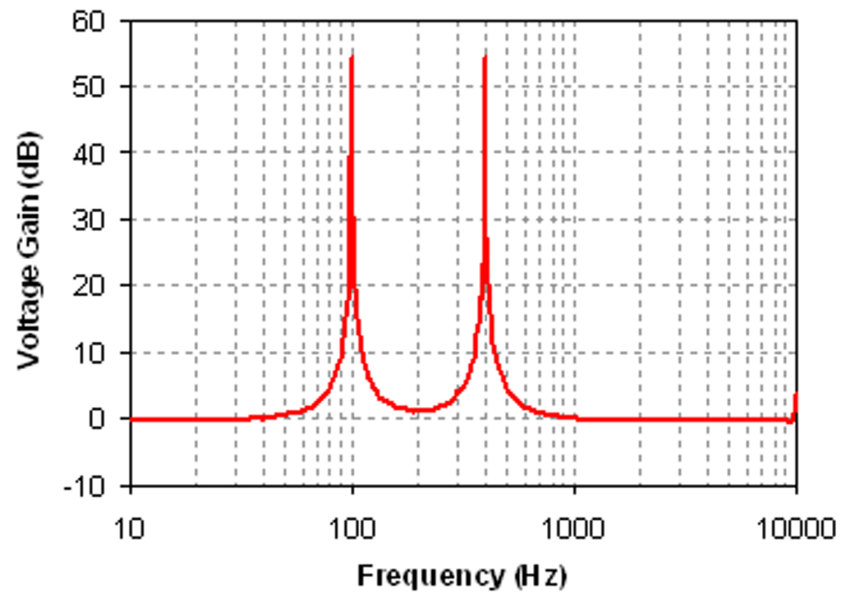


Figure 3.6: Measured response for an EPS with two switched capacitor filters incorporated into the feedback loop

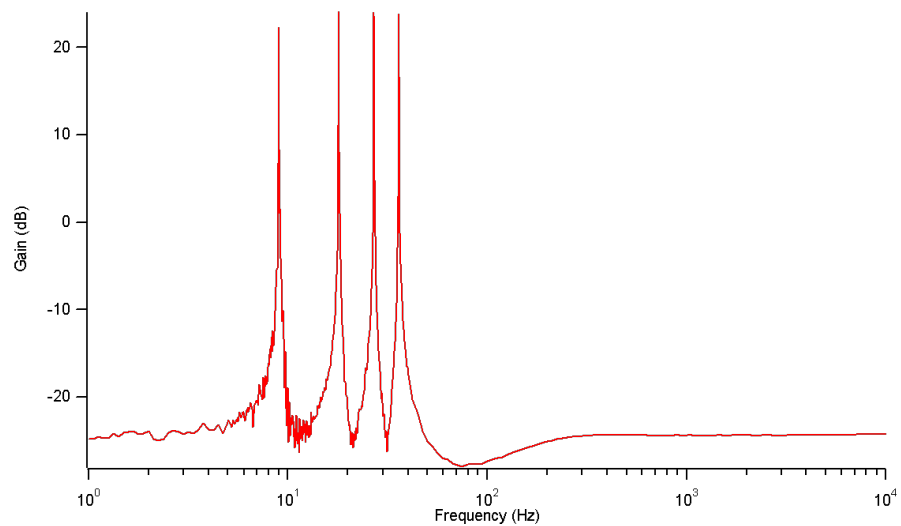


Figure 3.7: Measured response for an EPS with four switched capacitor filters incorporated into the feedback loop, configured for movement immunity experiment

This sensor was then used in an experiment designed to test the performance of the system in terms of discriminating between a low frequency movement signal and a higher frequency in band signal from a source electrode. An electrode was attached to reciprocating arm, and moved back and forth in a sinusoidal fashion towards and away from the sensor. The arrangement is shown in Figure 3.8. The arm was moved at a frequency of 2.4 Hz, over a distance of between 20mm and 30mm from the sensor. A 12 V motor was used to drive the arm, and a signal applied to the electrode with a frequency of 18 Hz, and an amplitude of 0.15 V.

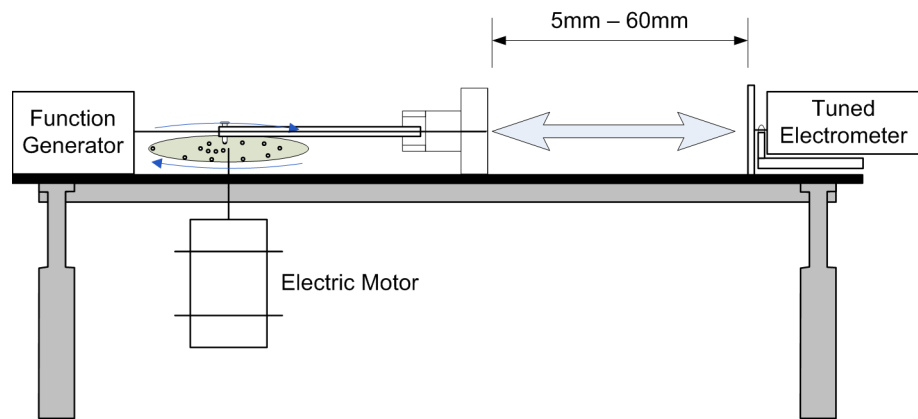


Figure 3.8: Arrangement of reciprocating electrode

Figures 3.9 and 3.10 show data collected from the sensor with 4Hz high pass and 30Hz low pass filtering applied to the sensor output. Signal to noise ratios were compared both with and without the presence of the tuned feedback electronics, and the improvement yielded as a result of the tuned sensor electronics was clearly visible. The same sensor was used for both measurements.

### 3.2.5 Settling times and Aliasing

The highly tuned nature of the signal specific sensors introduced a number of issues related to settling time which should be discussed for a full assessment of these techniques. The extremely long settling times associated with these techniques present a serious issue and an impediment to their use in a large number of applications. Depending on the  $Q$  selected for the filters, settling times can reach hundreds of time periods of the tuned frequency,

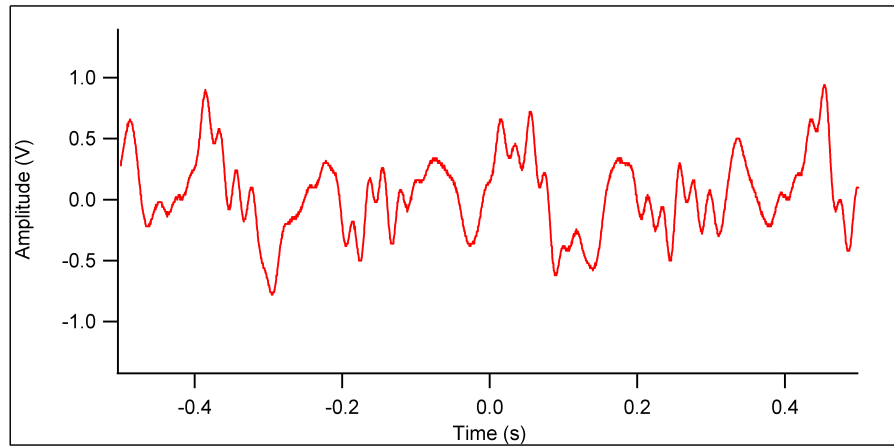


Figure 3.9: Output from untuned sensor showing a large amount of movement interference at 2.4Hz with a small 18Hz signal superimposed

limiting the usefulness of these techniques in sensors intended to detect quasi periodic signals such as those occurring due to a human heart beat. Figure 3.11 shows the time domain response of a tuned filter, with a tuned frequency of 9Hz, responding to the introduction of a 9Hz signal in the vicinity of the sensor. Similarly, Figure 3.12 shows the settling time after the 9Hz signal is removed.

In this case settling times were in the region of approximately 60 seconds. By adjusting the Q of the filters in the feedback loop it was possible to reduce this settling time, at the cost of sensor selectivity, but in order to ensure a useful level of selectivity in the sensors a settling time of several seconds was still required.

Furthermore, despite addressing some of the aliasing issues, these filters were still susceptible to aliasing problems as a result of leakage from clock lines into the inputs of the filters. This would typically be addressed using low pass anti aliasing pre filters on the inputs of these integrated circuits. However, since these were being used in a feedback loop where phase shift was crucial, it was not possible to use this technique. This compounded settling time and instability problems.

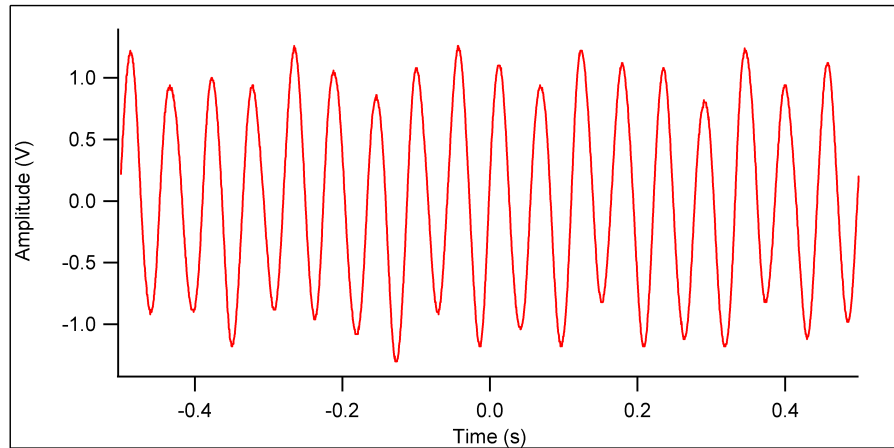


Figure 3.10: Output from tuned sensor showing large 18Hz signal and small 2.4Hz ripple as a result of movement

### 3.3 Noise immune sensors

The EPS is capable of detecting small changes in an ambient electric field which occur as a result of a wide range of phenomena. These include electro-physiological signals, movement signals, and variations in an actively generated electric field which has been actively created for the purposes of materials testing and characterization. All of these measurements, however, have in common the requirement that they involve looking for small signals in the presence of much larger ambient fields. In particular, the presence of mains electrical noise at a frequency of 50Hz and multiples thereof, and the large signals which occur as a result of movement in the vicinity of the sensor, pose a problem if these sensors are to be used in open, unshielded environments.

One solution has been to explore the performance of these sensors inside an electro-magnetically screened room [15]. Another possible solution is to explore the use of sensors designed to be sensitive only at specific frequencies of interest, as described above. However, an option remains to design a sensor which is conditioned to be insensitive to specific frequencies identified as noise. Unlike the design above, such a sensor would feature a broadband frequency response, but contain notches in the response at particular frequencies. This would be particularly suitable for reducing the problems posed by mains noise, which can in some applications saturate the sensor and therefore preclude the detection of a signal.

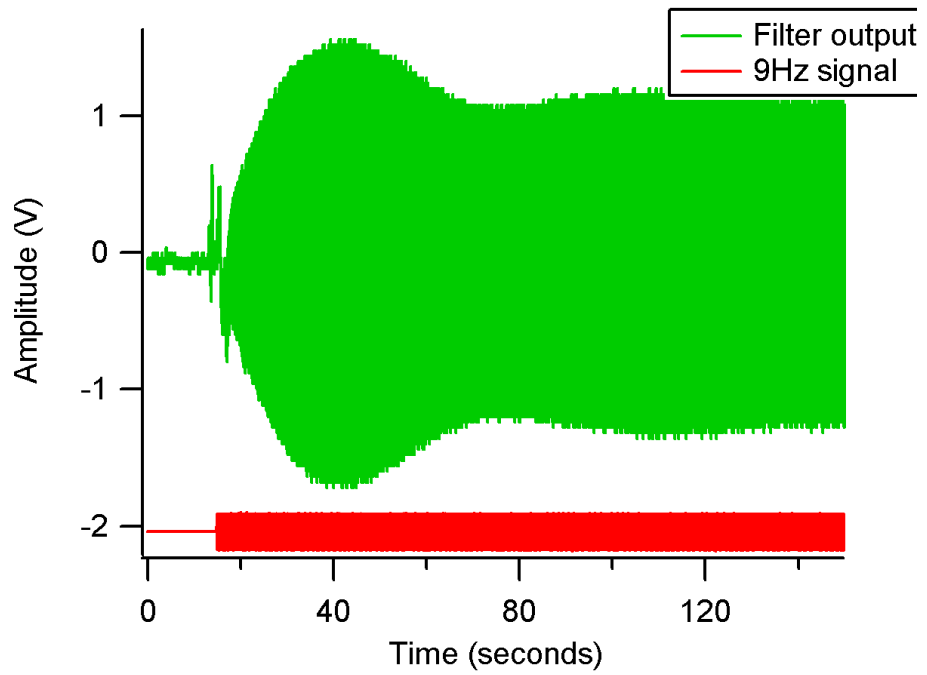


Figure 3.11: Settling of sensor output when signal at tuned frequency is activated

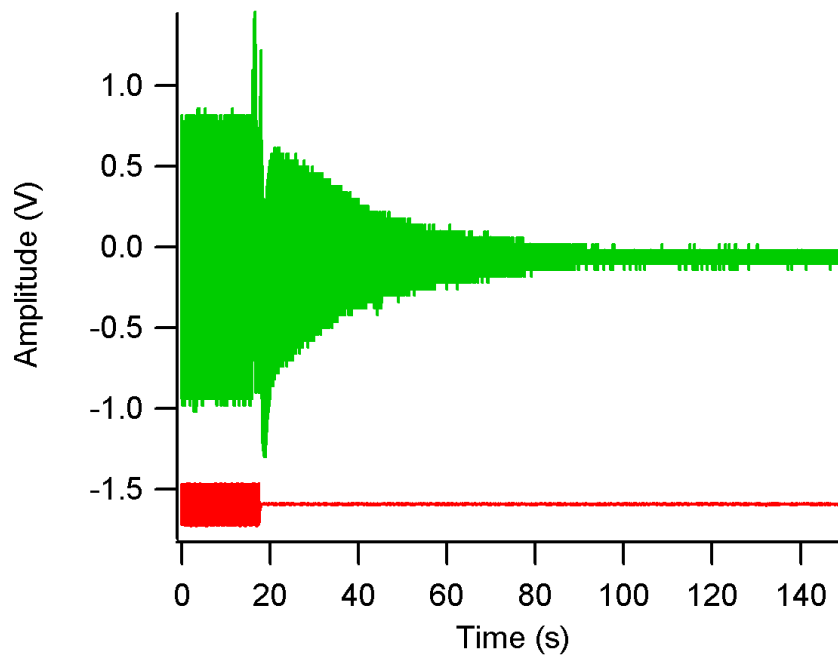


Figure 3.12: Settling of sensor output when signal at tuned frequency is deactivated

Creating a sensor insensitive to large noise signals is preferable to post-processing in the case where the high sensitivity required would cause this noise to saturate the sensor. Since the output of a saturated sensor does not contain a signal, no amount of post-processing can recover information which has been lost in this way. By using these techniques, it is possible to increase the dynamic range of the sensor by a factor approaching the rejection ratio. In addition the settling time of the filters will not cause ringing of the signal frequency, as was the case in the previous section.

### 3.3.1 Sensor design

The modular design described in the previous section allowed the filters to be replaced with multiple band pass filters, while the rest of the sensor was left unchanged. This resulted in a sensor with a multiple notch response as described above. Since a multiple notch response was required, the problems described in Section 3.2.1 did not exist, and band pass filters could simply be placed in parallel, directly in the feedback loop of the sensor to create the desired response. This resulted in a much simpler implementation than was required for the signal selective sensor as described in section 3.2. The new sensor architecture is shown in Figure 3.13

As with the signal specific sensor, the centre frequencies of the notches are dictated by a clock signal, which is derived for each filter from a master clock and an AD9833 programmable waveform generator. This allows the notches to be positioned at frequencies containing the largest noise components, and moved to track changes in noise frequencies which might occur over time (for example a drifting mains frequency).

### 3.3.2 Results

The concept was tested in much the same way as the tunable sensor. Initially a sensor with a single notch in the response was designed and constructed. The resulting frequency response is shown in Figure 3.14. This shows a rejection of 95 dB achieved at 50 Hz with a -3 dB bandwidth of only 4 Hz. This measurement is made through a 0.1pF capacitor

A frequency response for a filter with multiple notches applied is shown in Figure 3.15. In this case, the measurement is made through a well defined 0.1pF capacitor. Later, in chapter 4, a response is shown for a very similar sensor being applied to a remote physiological sensing application, where the response is measured through a 15cm air gap in order to provide data more representative of the applications for which this sensor may be useful. The bandwidth, as dictated by the -3dB points, can be seen to be 0.8Hz to 1.5kHz. This bandwidth is dictated by the characteristics of the sensor (input resistance and input capacitance), the feedback techniques used (bootstrapping, neutralization, guarding) and the coupling conditions.

The four notch frequencies are set to 50, 100, 150 and 200 Hz in this case, but could easily be set to any desired combination of frequencies within the operational bandwidth of the EPS by modifying the clock frequencies in the PIC start-up routine. The depth of the measured notches appears significantly reduced from that seen in the data of Figure 3.14, however this is an artefact due to the limited frequency resolution of the analyser when spanning a large range of frequency space. Clearly if the predicted attenuation figures of 95 dB are obtained with each of the notch filters it should be feasible to operate the sensor in an open unscreened environment in the presence of electrical noise related to the mains supply frequency and harmonics

This response allowed the remote measurement of a human heart beat as shown here in Figure 3.16, and this application and data is discussed in more detail in chapter 4.

### 3.4 Conclusions

Two novel approaches to the design of an adaptive sensor, capable of being configured to respond only to signals of interest, or alternatively to reject signals which can be identified as noise or interference, are described in this chapter. An adaptive sensor designed to respond only to a particular mix of harmonics and which is tunable over a large range of frequencies, has many possible benefits. This selectivity greatly enhances the effective dynamic range of the sensor and also impacts significantly on the signal to noise ratio. Preliminary results have been presented for a simple implementation using four switched

capacitor filters. The frequency and Q of the filters, and hence the sensor, are controlled by a PIC microcontroller. This allows for combinations of harmonics to be specified, and the response of the sensor and the amount of selectivity to be varied for different applications

In this chapter a number of techniques have been discussed which aim to provide the ability to use high impedance electric field sensors in open and electrically unshielded environments, where the presence of large amounts of electrical noise is inevitable. Signal specific feedback techniques have been described to dictate the response of the sensor. In this case, feedback is either used to ensure sensitivity only at frequencies of interest, and therefore to signals of interest, or to ensure sensitivity is reduced at frequencies known to contain large noise components, allowing a broadband frequency response with resilience against large noise components. Clearly both approaches have limitations which make them unsuitable for general use across any generic application, but equally are useful and beneficial under certain conditions. In the event that a signal is periodic and continuous over long periods of time, a signal specific sensor could be shown to have a number of advantages over a broadband sensor. However, issues are apparent due to the long settling times that these sensors exhibit. Where high sensitivity is required, and noise can be identified as existing only at fixed and well known frequencies, an alternative approach of reducing sensitivity to signals known to be noise related can be used. This can provide high levels of immunity to some types of noise, such as mains noise, but is less helpful when dealing with other noise signals, for example the large signals which arise due to movement of large dielectric objects in the vicinity of the sensor.

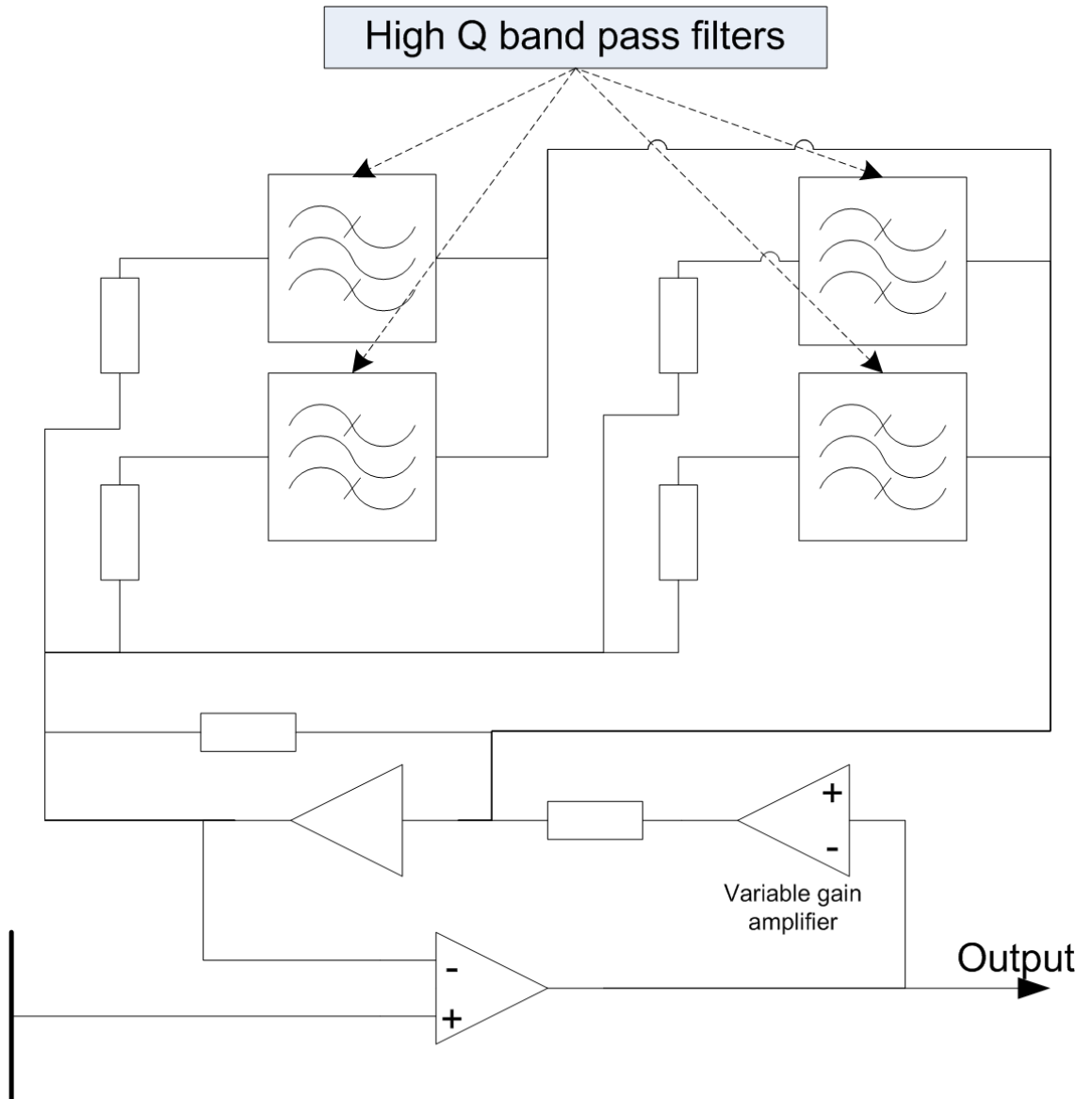


Figure 3.13: Architecture of noise immune sensor based around broadband response containing multiple notches

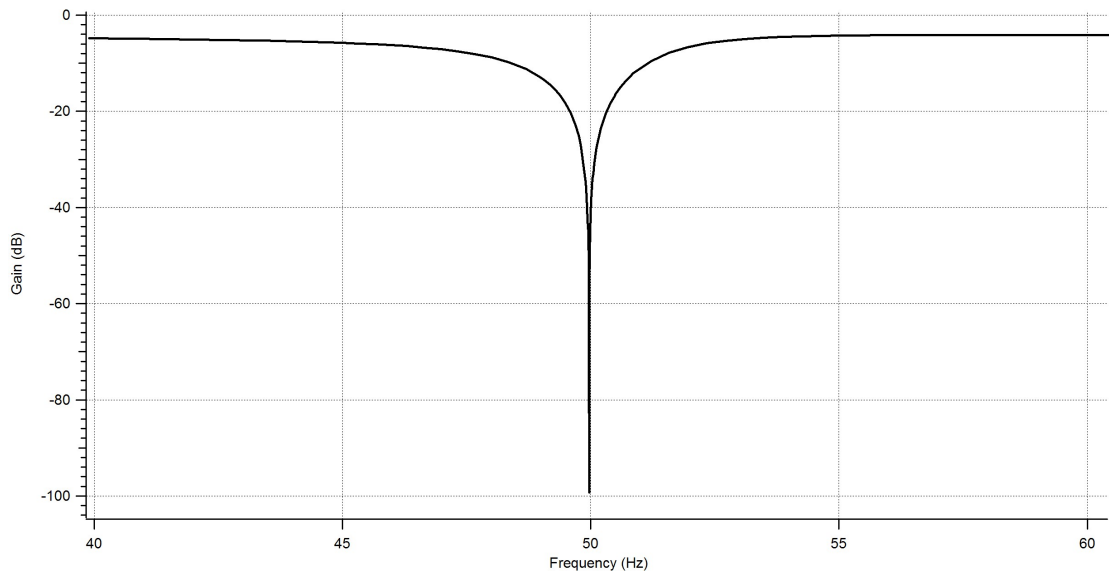


Figure 3.14: Frequency response of sensor with notched response showing  $>95\text{dB}$  rejection

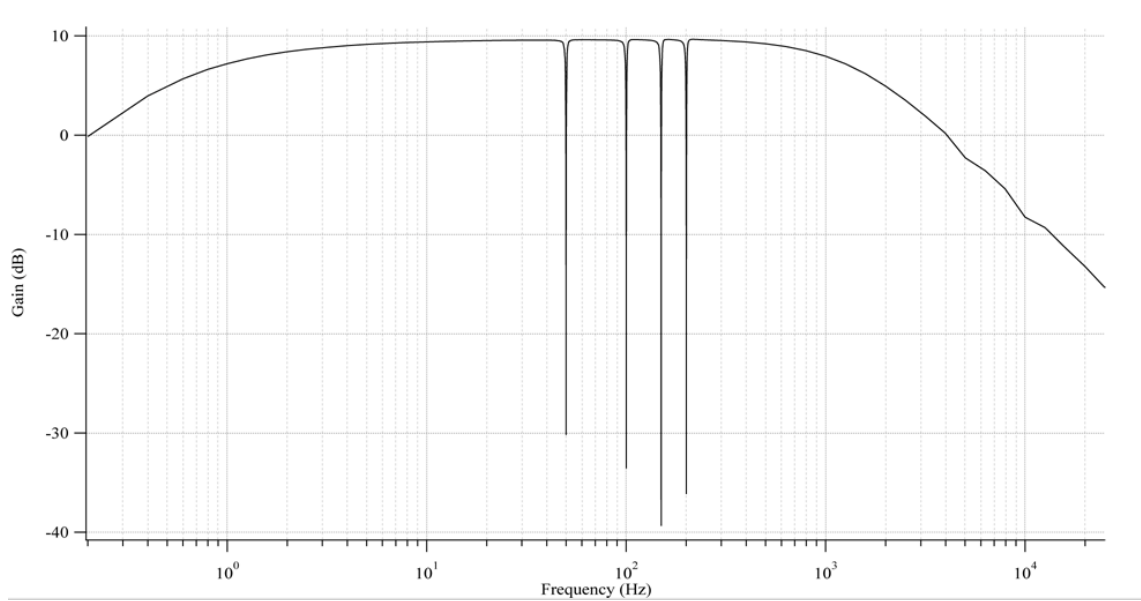


Figure 3.15: Frequency response of multiple notch noise immune sensor taken through 15cm air gap

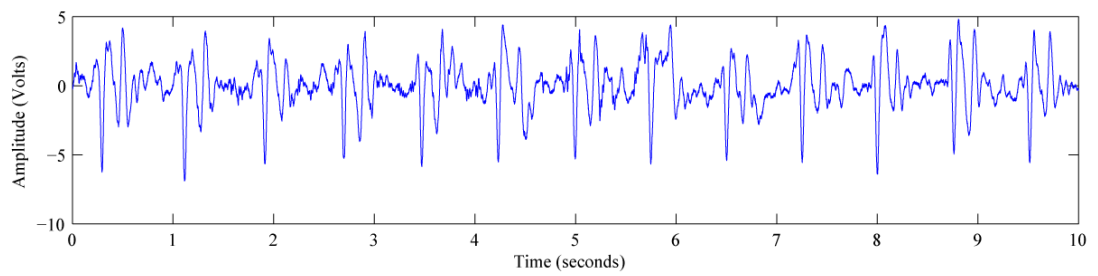


Figure 3.16: Human heart signal measured at a distance of 40 cm from the front of the body in a noisy unshielded environment. This is raw data with no signal averaging or digital signal processing applied.

## Chapter 4

# A Remote Cardiac Measurement

### 4.1 Introduction

With the performance of the EPS Sensors now more fully understood than ever before, a range of remote applications have become possible. These make use of the sensors in an open, remotely coupled configuration where an electrode is simply pointed at a signal source, with no well defined coupling capacitance in place. The input capacitance of the measurement then becomes dominated by the self capacitance of the sensor, and as such the measurement becomes more comparable to a measurement of electric field, as opposed to a capacitive measurement of a voltage source. In this chapter we present a sensor which incorporates the techniques described in chapter 3 and exploits the understanding gained from the work in chapter 2. This sensor is used to obtain a remote cardiac measurement, outside of a screened environment and through an air-gap of 40cm.

### 4.2 Remote Electrophysiological Signals

#### 4.2.1 Introduction

In 1843, Carlo Matteucci recorded electrical currents flowing in pigeon hearts for the first time. Later, in 1855, Albert von Kollicker and Heinrich Muller established that electrical

signals similar to these could be detected and shown to correspond to the beat of a frog's heart. By 1887, Austus Waller had recorded the first human electrocardiogram (ECG), and by 1900 William Einthoven had identified a set of distinctive waves and given them the names OPQRSTX. These letters, now referred to as a PQRS complex, are still used to describe the wave patterns observed in human ECG measurements[73, 2]. This work laid the foundation for modern electrocardiogram and bio-physiological measurement and monitoring techniques, and is discussed in many text books and summarized recently by Breathnach and Westphal[74].

Electric Potential Sensors have been previously demonstrated as being capable of detecting high quality Electro-physiological signals, including electrocardiogram, electroencephalogram, electromyogram and electro-oculogram based signals[19, 15, 75, 29, 76, 28]. In these cases, the use of an EPS based sensor, as compared with conventional methods, allows for the acquisition of medical quality signals without the need for gel based electrodes or skin preparation. The ability to measure some of these signals remotely would provide a host of additional benefits. Since electric fields average with distance from the source, it is unlikely that data of an equivalent quality could be collected remotely, however the ability simply to detect basic signs of life would prove extremely useful. Furthermore, if a heart rate can be detected, it becomes possible to make measurements such as Heart Rate Variability (HRV) simply and over significant periods of time, without inconveniencing the patient. Analysis of HRV has been developed as a technique over the previous twenty to thirty years and has been shown to have applications in the diagnosis of a range of conditions, both directly cardiac related[77] and other conditions such as diabetes [78].

The remote measurement of electrophysiological signals, such as this, has the potential to make a significant contribution to modern healthcare. As a result, techniques for measuring physiological characteristics and information remotely have become increasingly an area of interest and rapid development in recent years. The ability to record biologically significant information over long periods of time without discomfort to the patient, or in the patients own home, has clear benefits in terms of monitoring those with long term medical conditions or where medical complaints may only be detectable at infrequent points in time. Furthermore, the availability and low cost of modern sensors makes the pervasive use in all areas of daily life plausible. Examples of diverse applications include biometric identification, security, assisted living, healthcare monitoring at home as well as the monitoring of people carrying out safety critical tasks.

### 4.2.2 Methodology

An experiment was designed, using a modified ultra-high input impedance electric potential sensor configured to reject noise at 50Hz mains frequency, and harmonics thereof. These sensors are discussed in detail in Chapter 3. The remote detection of a cardiac signal was chosen to demonstrate the noise reduction techniques, through the use of a sensor as detailed in Chapter 3, resulting in the ability to detect very small electric field based signals in an open and unshielded environment. A cardiac signal is particularly useful as the signal is comparatively large for a body electrophysiological signal, and other techniques are available for acquiring related data which can be used for comparison with EPS data to establish the validity of the measurement.

Results have previously been reported, using an electric potential sensor, demonstrating the ability to detect and measure a cardiac signal in an electrically screened room[15] with detection possible at spacings of up to 1m between the surface of the body and the sensor. Here we provide evidence of the capability to reproduce some of these results in a working, open and unshielded laboratory. In this case, the sensor was located approximately 1.5m from a wall, and surrounded by mains operated equipment and cabling. Typically this would result in the saturation of the sensor with 50Hz and related harmonics, making signal acquisition impossible.

As shown in Figure 4.1, a chair was arranged with a sensor positioned behind it, at a separation distance of 10cm, such that the sensor was facing the back of the subject. A second sensor was then placed in front of the chair, at a distance of 40cm, with the sensor directed towards the chest of the subject. Data was processed in real time using Labview, in order to restrict the bandwidth of the sensors to a narrow 1 to 50Hz band. Furthermore, feedback was customized to ensure as high an order roll-off as possible at frequencies below 1Hz, in order to try and provide insensitivity to the very large low frequency signals caused by movement. In this case, the sensor was intended for obtaining cardiac related signals remotely, and therefore this movement immunity was important. With the exception of very basic low and high pass filtering, no further signal processing was required .

Data was collected using a National Instruments data acquisition card (NI-USB-6009)[70] at a sampling rate of 10 kSamples per second. Blocks of 1000 samples were collected,

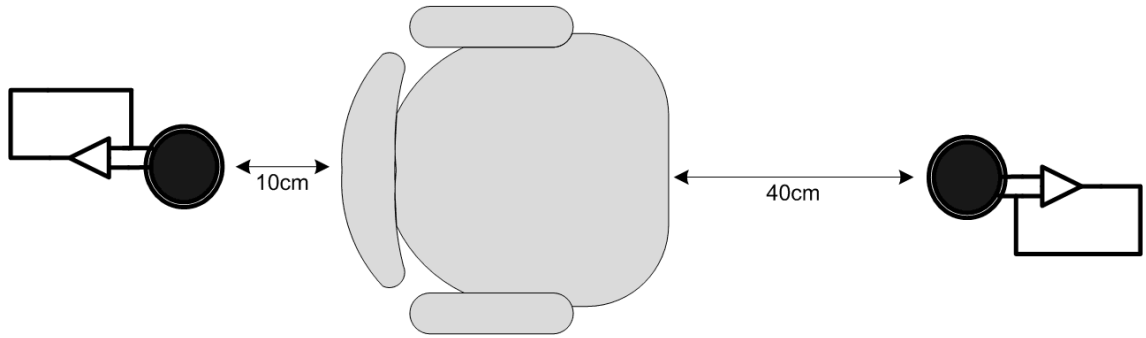


Figure 4.1: The experimental sensor arrangement

processed and visualized immediately, resulting in a real time display of the signal, updated at a rate of 10Hz.

### 4.2.3 Results

Data from the front facing and back facing sensors is presented here in Figures 4.2 and 4.3. In both cases the subject was able to hold their breath for the duration of the measurement, and some signal processing was applied to minimise movement signals. In this case, fourth order, Butterworth notch filters were applied in Labview with center frequencies at 50Hz and 100Hz. The signal was then band pass filtered to restrict the bandwidth to 1-50Hz. This 1Hz high pass filter had the effect of removing sensitivity to low frequency movement signals which occur as a result of breathing and other body movement. As a result there is no movement signal due to respiration visible in the data. The similarity between the front facing and back facing data is indicative of the fact that this signal is electrical in nature.

It was also possible, if the subject was to continue breathing while data was being collected, to obtain data containing both cardiac and respiration related signals as shown in figure 4.4. Since the time-scales over which these signals occur is quite different, this data could then be processed using Matlab, and two separated signals obtained. This was done using a high order low pass FIR filter with a cut off frequency of 1Hz. The result of this is shown in figure 4.5.

The data shown is generally consistent with the data obtained previously in screened room environments[15], but it is notable that it does not closely resemble a set of contact

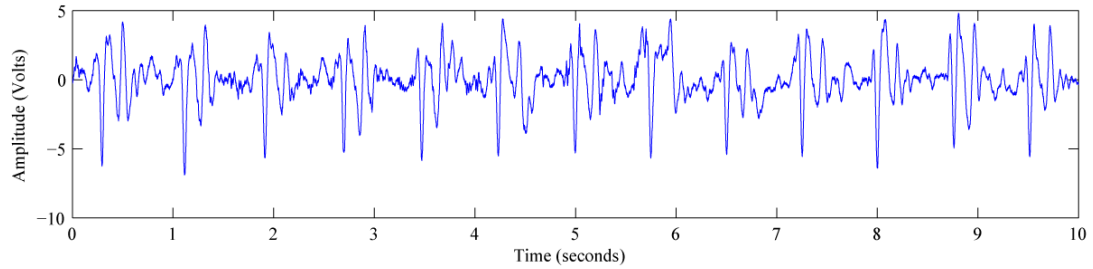


Figure 4.2: Data collected from the front of the subject with a 40cm air gap between the sensing electrode and the surface of the body. Data taken in an open unshielded environment, with the subject holding their breath for the duration of the measurement.

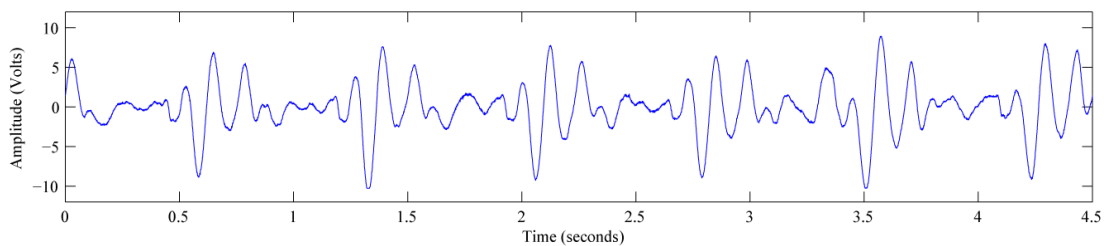


Figure 4.3: Data collected from the back of the subject with a 10cm air gap between the sensing electrode and the surface of the body. Data taken in an open unshielded environment, with the subject holding their breath for the duration of the measurement.

ECG data. Despite this, an argument can clearly be made that the measurement is, none the less, an electrocardiogram, since the signal is electrical in nature and representative of cardiac activity. The correlation between the signal obtained and the heartbeat was verified by measuring a signal using a pulse oximeter and comparing this data with remote ECG data obtained from the experimental sensors.

The temporal relationship between the data collected using these remote physiological sensors and a conventional contact ECG was very apparent, with the main peak in the data being coincident with the arterial pulse. The most probable explanation for the widening of the signal along the time axis is that the signal observed represents a combination of signals made up from both electrical and movement components. The combined respiration and cardiac data, showing cardiac data modulated on a respiration signal, provides supporting evidence for this theory.

### 4.3 Future work

A range of potential applications exist for this remote detection capability, and a number of possible routes forward for this research are clear. The ability to separate the movement and electrical signals would clearly expand the range of possible applications, and future work could include a study of the relative sensitivity of the sensor to these two signals, and seek to develop techniques for separating them. Modelling the effect of movement on the sensors would clearly provide information on this, and some modelling data is provided in the following chapter with this in mind. It may also be the case that this new technique opens up the possibility of a class of biometric measurement which contains both physiological and behavioural components, which may find applications in the fields of healthcare and security.

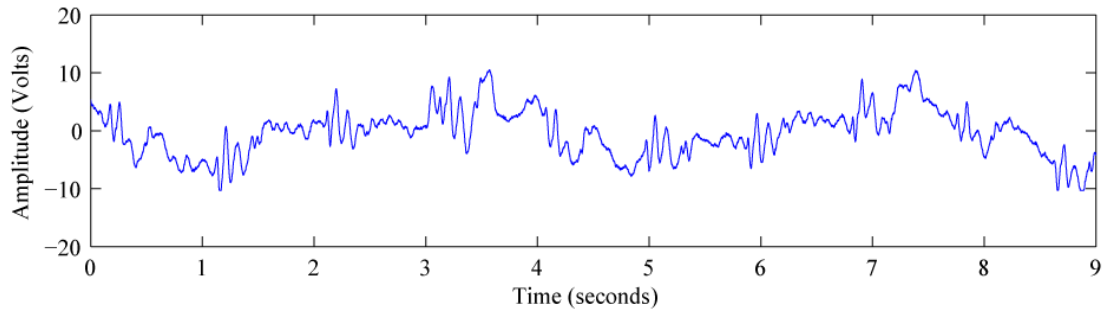


Figure 4.4: Raw data, with no analogue or digital signal processing applied, showing both the respiration and heart signal collected from the front sensor. Sensor positioned 40cm away from the front surface of the body.

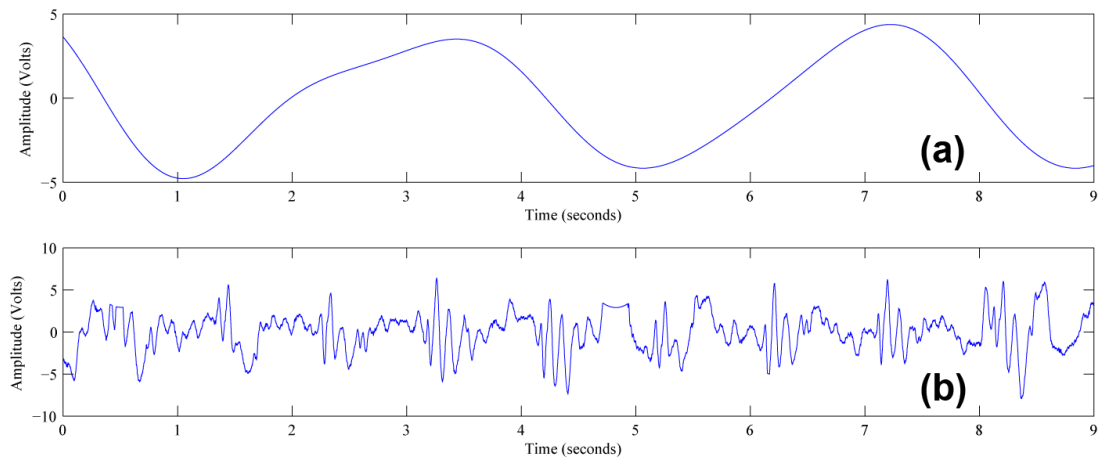


Figure 4.5: The result of applying a digital FIR filter technique to separate the low frequency respiration signal from the higher frequency cardiac signal. (a) 1Hz low pass filter applied to the data of Fig. 4.4 showing the signal due to respiration and (b) 1Hz high pass filter applied to the data of Fig. 4.4 revealing the cardiac component.

## Chapter 5

# Detecting electric field disturbances for passive through wall movement and proximity sensing

### 5.1 Introduction

Several possible mechanisms exist to explain the existence of changing electric field signals which occur as a result of movement. When a dielectric object is placed in a static electric field it will, over time, become polarised, such that its potential will rise to the potential at that point in the field. If this object then moves, a changing electric field will be generated. Since a static electric field, of the order of  $100Vm^{-1}$  exists between the ground and ionosphere[79], most objects will continuously become polarised when left in unscreened environments on the earth's surface. When moved, they will then generate a changing electric field which could be measured.

Additionally, a phenomena known as tribo-charging offers an alternative possible mechanism. This process, strongly linked to what is more commonly known as static electricity,

involves the polarisation of charge on an insulating material as a result of rubbing or contact between two dissimilar materials. As an object passes through air, it has the capability to acquire charge as a result of this tribo-charging process. Similarly, any contact between the object and other insulating materials leads to further charging effects. Tribo-charging, and other effects, result in people becoming charged as a result of touching floors, walls and objects as they move around[80]. As large potentials build up on an object, movement then leads to a changing electric field.

Yet another possible mechanism is apparent if an object is conducting, and in contact with the earth. The presence of an earthed body will distort the vertical potential gradient in the vicinity of the object. If a human body is modelled as a conductor, in contact with the earth's surface, the distortion to the ambient electric field of  $100V\text{m}^{-1}$  is significant. This is described in Feynman's famous lecture notes[81] and shown in Figure 5.1. As this earthed conductor moves around, variations in electric field are generated. Therefore, as a person approaches and then moves away from a sensor, variations in field can be detected.

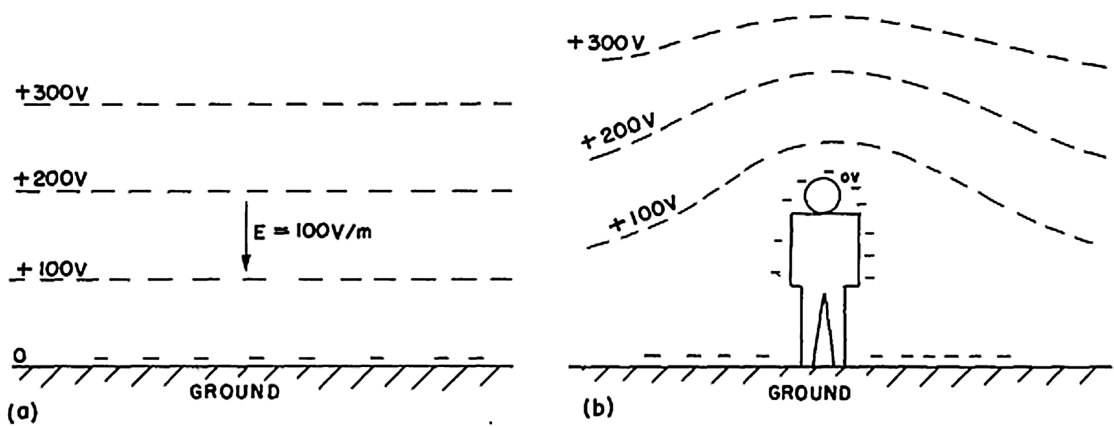


Figure 5.1: (a)The vertical potential distribution above the earth, (b)The disturbance to this potential distribution caused by a human body. Figure taken from The Feynman Lectures on Physics[79]

Any of the above mentioned mechanisms enable movement to be detected using an entirely passive technique, based only on this electric field variation. Furthermore, since all dielectric objects will become polarised in a charged atmosphere, substantial effort would need to be made to engineer a scenario in which movement did not result in electric field

disturbances. This detection technique only works well if the object is not obstructed by conducting materials, in common with the other technologies. However, it is unaffected by non-conducting obstructions or by conducting material which is suitably electrically isolated from earth. Most importantly, it is passive, providing a low power system which is potentially undetectable.

### 5.1.1 Method

With EP sensors operating in a remote mode, input capacitance is extremely significant, and dictates the sensitivity of the measurement. In order to detect large scale movements, an 8 element linear array of electrodes was constructed and mounted in a wooden frame. Screened and guarded co-axial cabling was used to connect the guard rings and electrode faces to a surface mount PCB positioned behind the centre of the array. The physical characteristics of the co-axial cabling were varied to ensure a balanced capacitance on each channel of the electrode, in an attempt to mitigate any variation in input capacitance that was likely to occur as a result of large differences in cable lengths at the front end of the sensors. This was achieved by varying the sizes of the internal conductors. A schematic of the array is shown in figure 5.2 and photographs in figures 5.3 and 5.4.

Signals are created as a direct result of movement, in front of the sensors, of large dielectric objects such as people. These signals can be very large when compared to ambient 50 Hz mains (line) noise and other electrical signals often detected by these sensors. While this has many benefits it means dynamic range, and appropriate levels of gain, must be given great consideration. A low level of gain (in this case a gain of two) was used in an attempt to prevent the sensors from saturating in the presence of large signals, and care was taken in the design to ensure the quality of the grounding on the board and ensure that output from one channel was suitably screened from other channels. In this way it was possible to maximize the dynamic range available.

The outputs from the sensors were connected to an 8 channel National Instruments USB 6009 data acquisition module[70], with the 5 V power supply being used to supply power to the sensors such that no additional supply was needed. 30 kSamples were taken from each

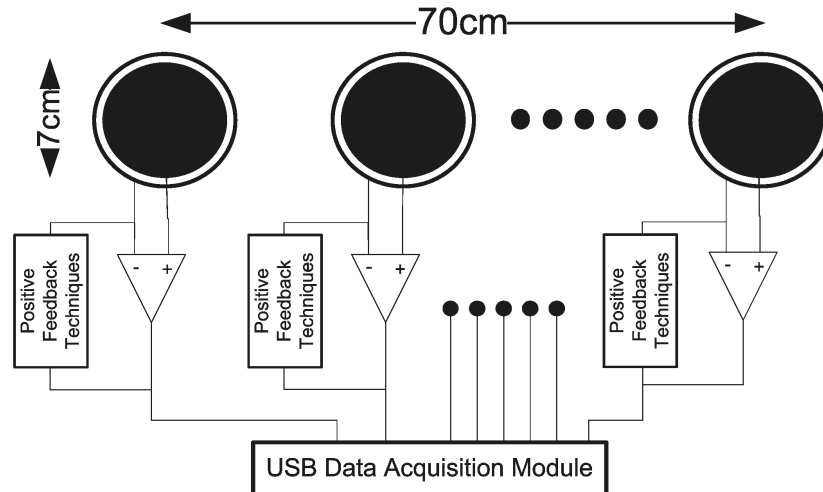


Figure 5.2: The 8 element sensor array - schematic

channel, at a sampling rate of 1 kSamples/s. These samples were then broken into blocks of 40 and an average DC value calculated. The effect of this operation was effectively to low pass filter the data at 25 Hz, giving a single value, per channel, every 25th of a second. This reduced the mains related 50 Hz noise, while leaving all the significant parts of the movement signal.

A pendulum was constructed, consisting of a 120 ml bottle of water, attached to a 2.6 m length of nylon fishing line, and swung in front of the sensor array, at a variety of spacings ranging from 100 mm to 700 mm. The data from all channels was collected in Labview and written to ASCII data files for processing and visualisation in Matlab. Labview code for this experiment is shown in Appendix A

A second experiment was then carried out, in order to explore the possibility of visualizing in real time the speed and direction of movement. To achieve this aim, data was collected, in 200 sample intervals at a sampling rate of 5 kSamples/s. These blocks were then averaged to find a DC average, again giving a 25 Hz low pass filtered signal. As compared with the previous experiment, this allowed the data to be filtered in real time, rather than collected in advance and then processed. A 1 by 8 element false colour image was generated for each sample, with colour being used to denote the amplitude of the signal. In this way, with very little signal processing, it was possible to gain a clear visual indication of both direction and speed of the object as it moved past the sensors.

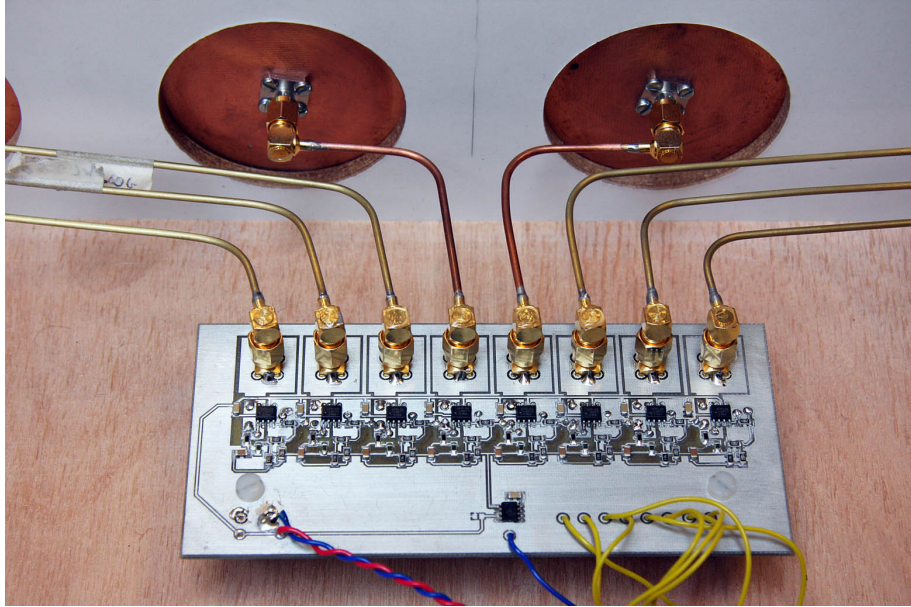


Figure 5.3: The 8 element sensor array - photo

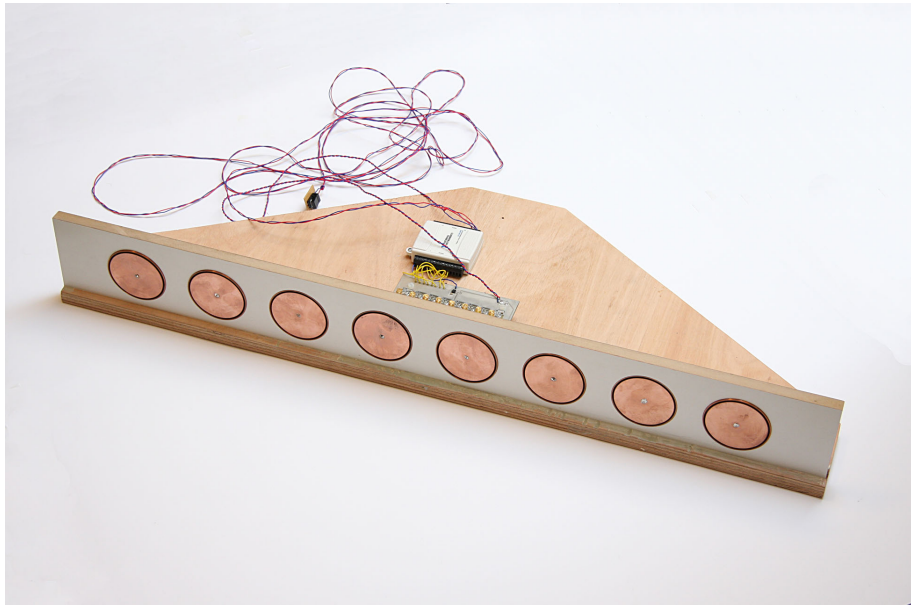


Figure 5.4: The 8 element electrode array

### 5.1.2 Experimental Results

In Chapter 4 the collection of remote electrophysiological data, including remote ECG, was discussed. With the sensitivity turned down however, these sensors have sufficiently high dynamic range that they become capable of detecting both very large, as well as small movements, at significant distances and close to the sensing electrode.

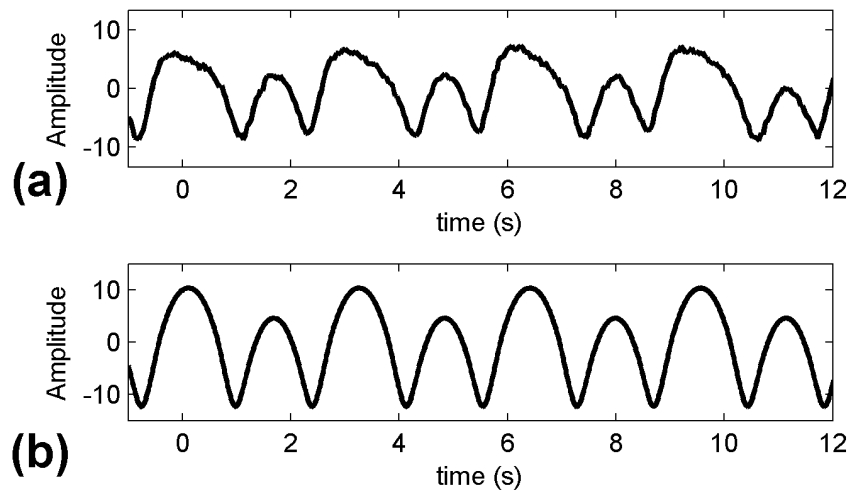


Figure 5.5: (a) - Experimental data from pendulum (b) - Theoretical data from finite element model

Figure 5.5 shows data collected from a single electrode in the array, placed 750 mm from a sample, and offset by about 300 mm from the centre of motion. The arrangement of sensor and sample is shown in Figure 5.6. The variation in the height of the peaks can be explained by the fact the sensor is significantly offset from the centre of motion, and therefore as the pendulum reverses direction the movement is asymmetric with respect to the sensor.

The data collected is then compared to data obtained from a Comsol Multiphysics model, developed by a colleague Dr Peter Stiffell, which uses finite element analysis to solve Laplace's equation for the field. This comparison is discussed in more detail in the next section, however a clear match is apparent. The experimental data is displayed in Figure 5.5(a), while the modelled data is visible in Figure 5.5(b). The general shape, and relative magnitudes of the peaks, can clearly be distinguished.

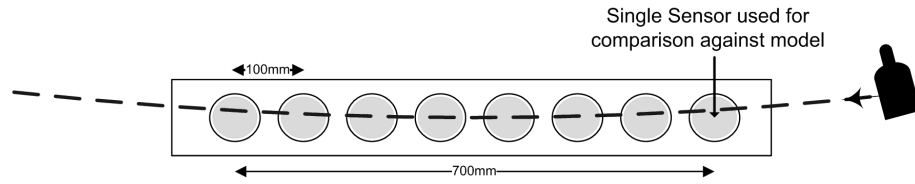


Figure 5.6: Arrangement of sensors and pendulum sample

The real time data visualisation of the data is also compelling. The movement of the bottle in a pendulous motion is clearly visible, with the approaching increase and corresponding decrease in signal amplitude as the bottle approached, passed, and then moved away from the sensor clearly visible in the false colour image. This data is shown pictorially in Figure 5.7 with a line showing motion of the pendulum as it passed in front of the array, superimposed on successive frames of data. Zero disturbance of the field is shown in white, while positive and negative disturbances are shown as an amplitude dependent grayscale.

A clearer, though less detailed, set of data was obtained by adopting an alternative approach for measuring position. The sensor with the largest amplitude signal was identified and the sample position defined as being at this point. The result of this process is shown in Figure 5.8. In this case, clearly information is being discarded. Any ability to infer position with any greater resolution than the spacing of the sensors is lost. In contrast, by comparing the amplitude of the outputs of the sensors, it could be possible to identify how close the sample was to two adjacent sensors and therefore improve resolution. Despite this, however, a simplified approach yields data which is easier to analyse.

Since the position and spacing of the sensors was known, a plot was then generated showing position against time. This is shown in Figure 5.9. As the pendulum is 2.60 m in length, the expected period can be approximately calculated as

$$2\pi\sqrt{\frac{\text{length}}{g}} = 2(3.14)\sqrt{\frac{2.60}{9.81}} = 3.23 \text{ seconds}$$

The value measured in the data is 3.24 seconds, demonstrating that tracking of position is possible.

Furthermore, it is possible to infer the velocity of the object using the data, since a single pass across the array can be seen to take 0.80 seconds and cover a distance of 70cm. This yields an estimated average velocity for this section of the swing, of  $\frac{0.70}{0.80} = 0.88\text{ms}^{-1}$

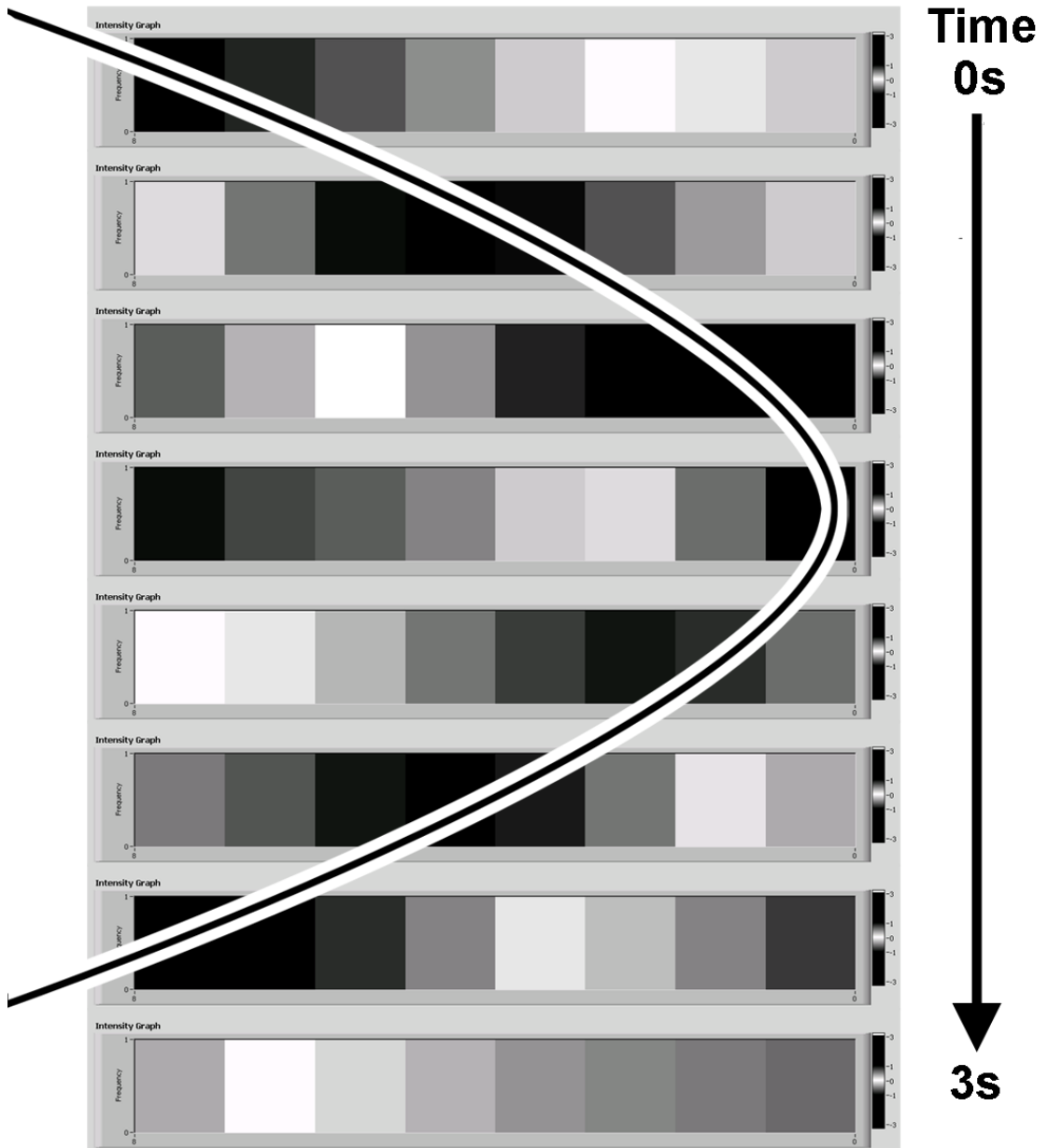


Figure 5.7: Frames of data from visualisation program arranged to show pendulous motion. Scale shown using white when no disturbance is present, and increasing grayscale for positive and negative disturbances.

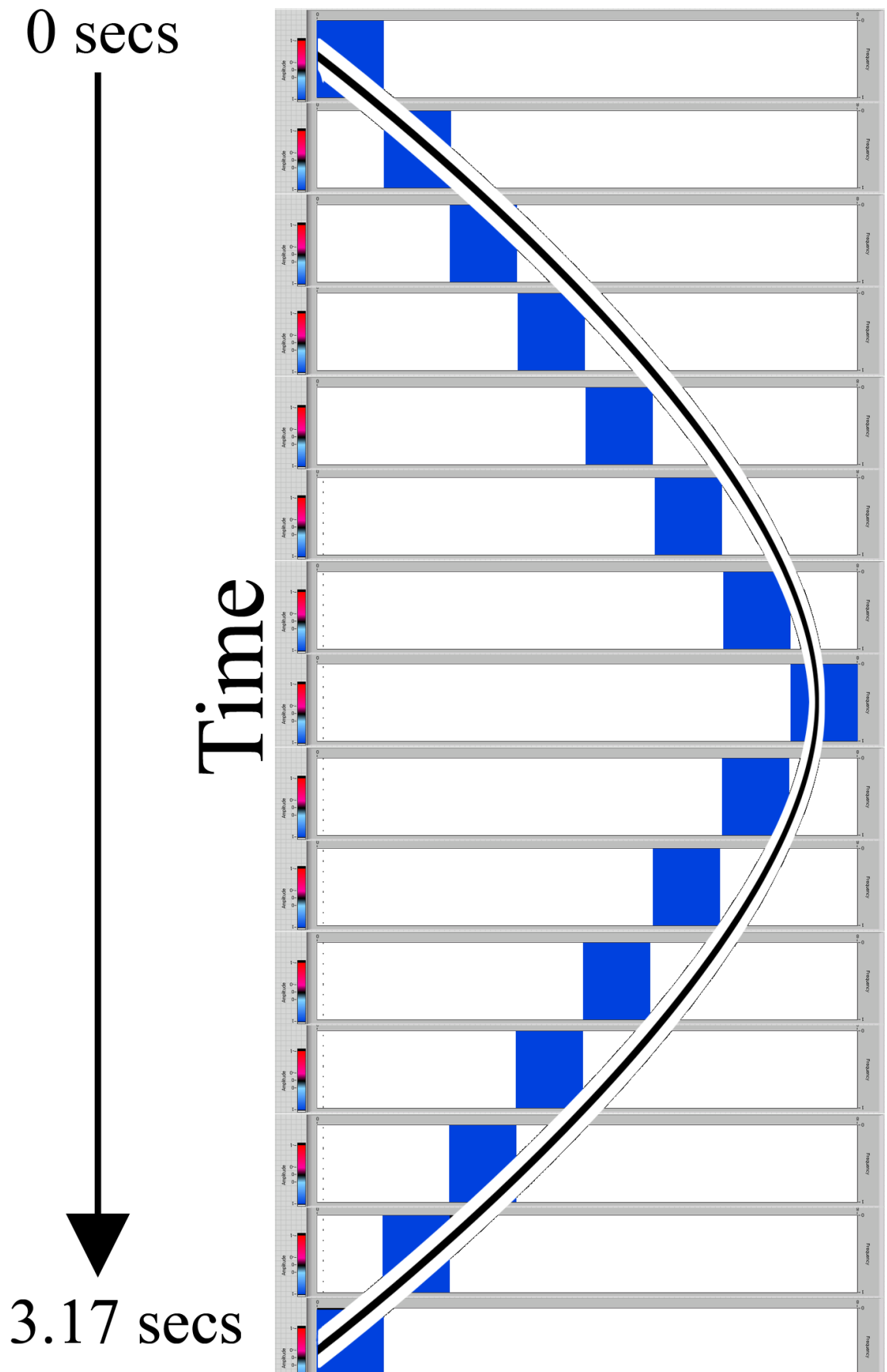


Figure 5.8: Motion visualised by selecting sensor with largest output signal

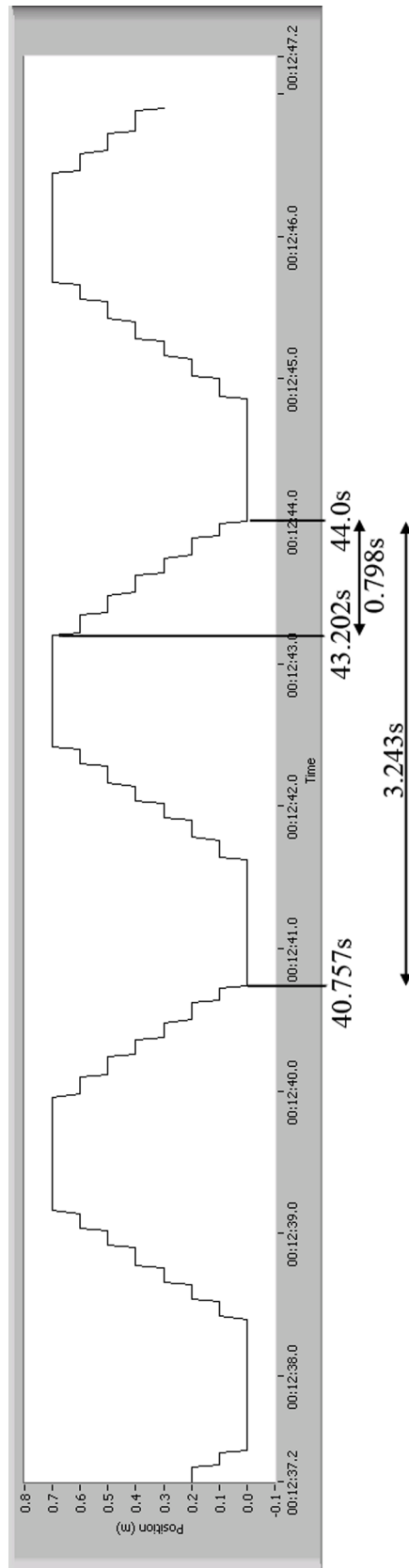


Figure 5.9: Plot of position against time calculated from sensor data

### 5.1.3 Simulation

A colleague, Dr Peter Stiffell, used Comsol Multiphysics[82], which is a unified physics simulation package for finite element analysis, to create a model of the experiment. Here, a moving mesh type model was defined, with a charge being allocated to a point object and the charged object being moved in a pendulous fashion past a sensing point, configured to be in a similar position to that of an element of the linear sensing array. A sensor was picked for modelling which was a significant distance from the centre of movement, in order to try and recreate the unusual shape of the signals obtained from this position. The simulation was carried out in a two dimensional plane, with all motion of the charge considered to be parallel to the sensing array.

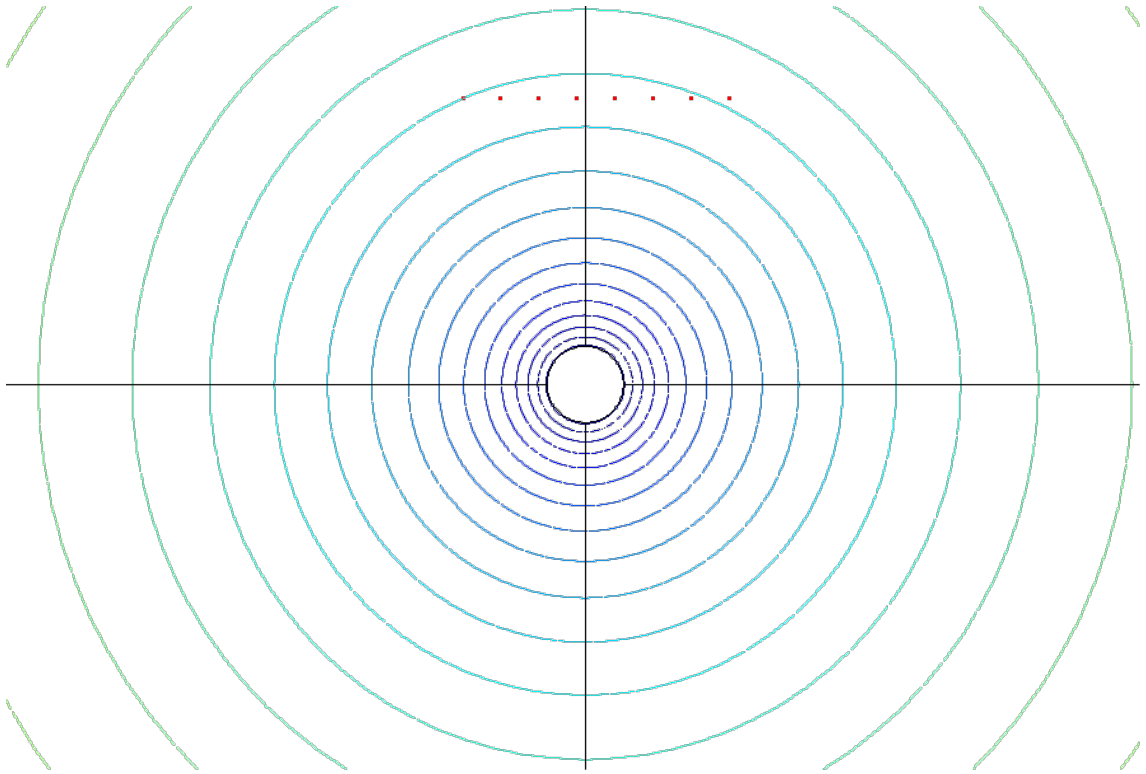


Figure 5.10: A finite element model showing equipotential lines induced by a field which occurs as a result of the presence of a charged object. The linear array of field measurement points is also shown.

The data from this model was then compared to the experimental data which is presented in this chapter. The arrangement of the model is shown in Figure 5.10 where the red dots

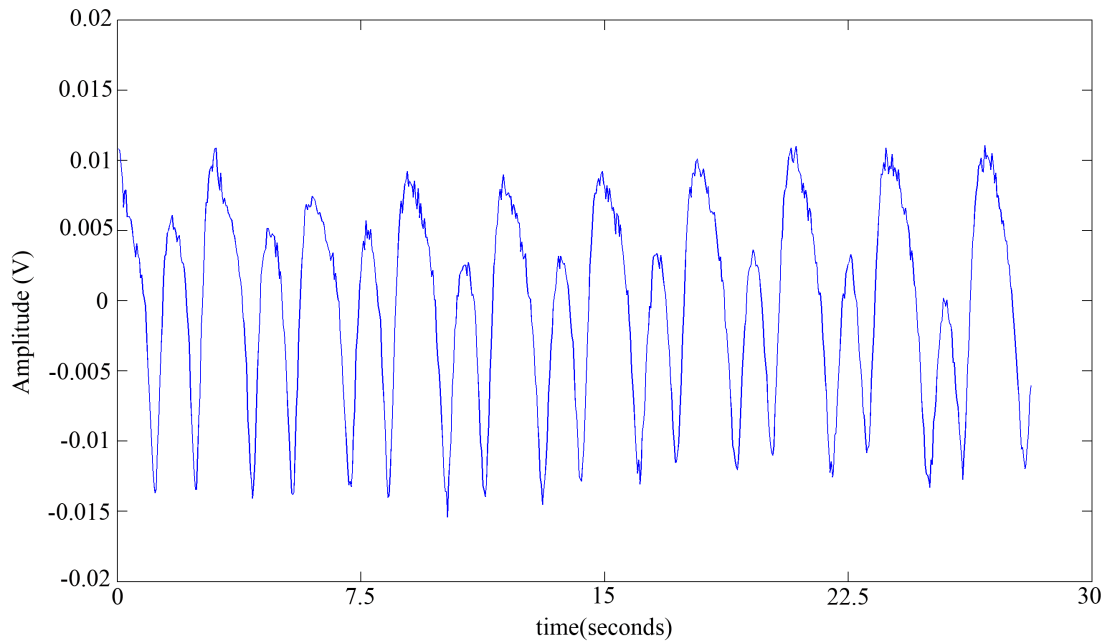


Figure 5.11: Data shown for sensor at one end of experimental linear array commencing after initial transients as a result of setting the pendulum in motion have died away. Amplitude is shown referred to voltage at the input of the sensor.

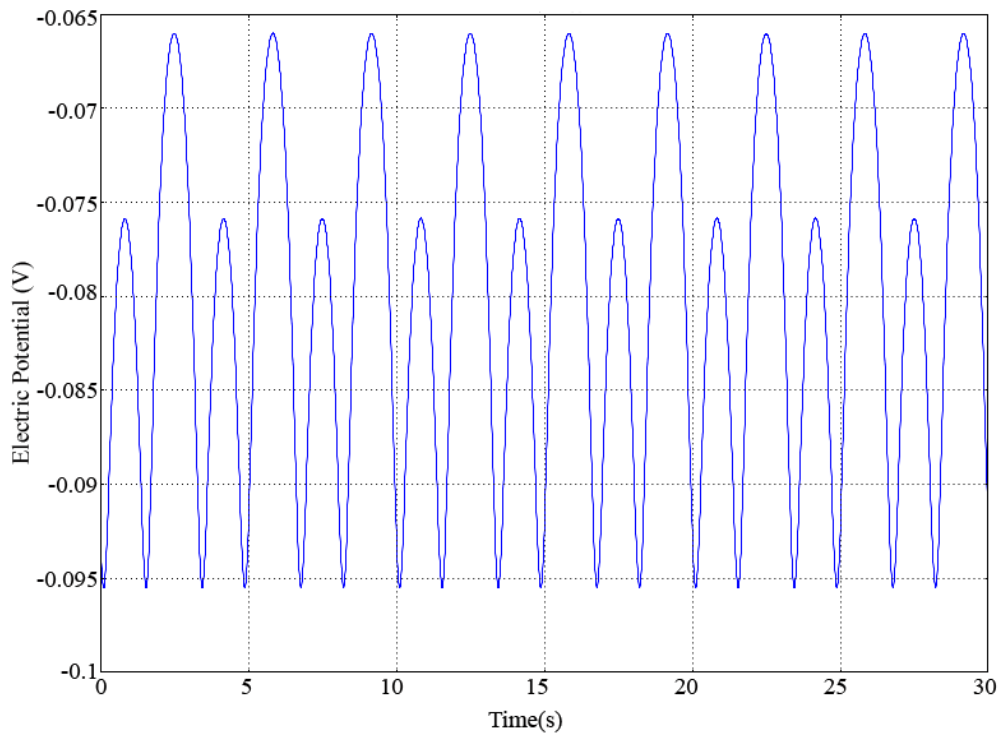


Figure 5.12: Data from simulation for measurement point positioned as for Fig.5.11

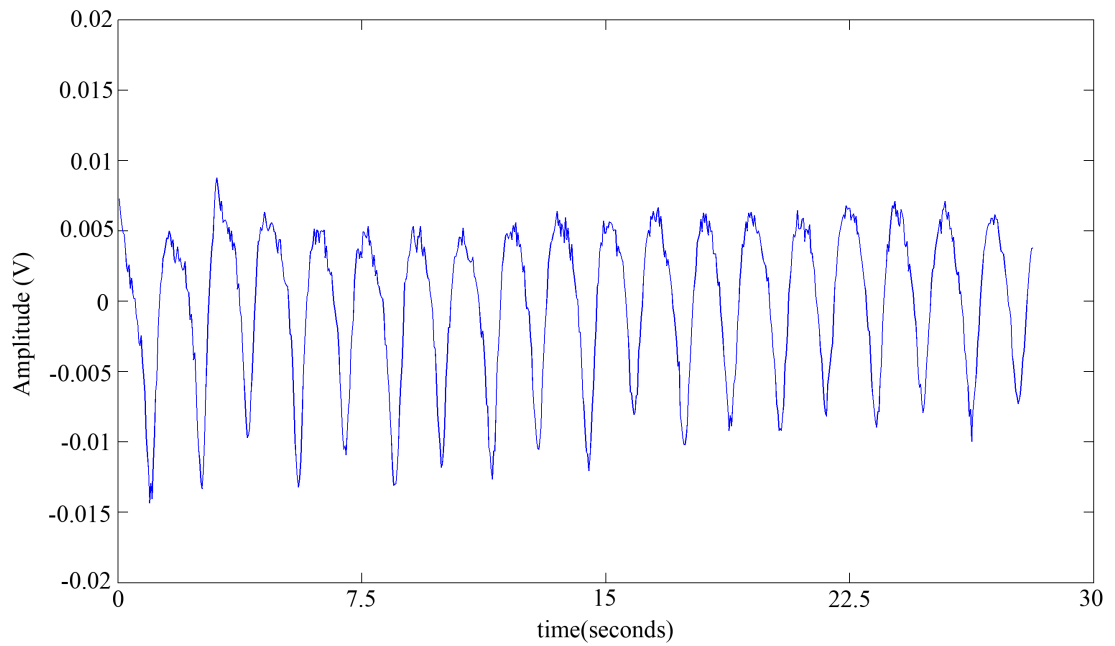


Figure 5.13: Data shown for sensor approximately in centre of experimental linear array commencing after initial transients as a result of setting the pendulum in motion have been allowed to die away. Amplitude is shown referred to voltage at the input of the sensor.

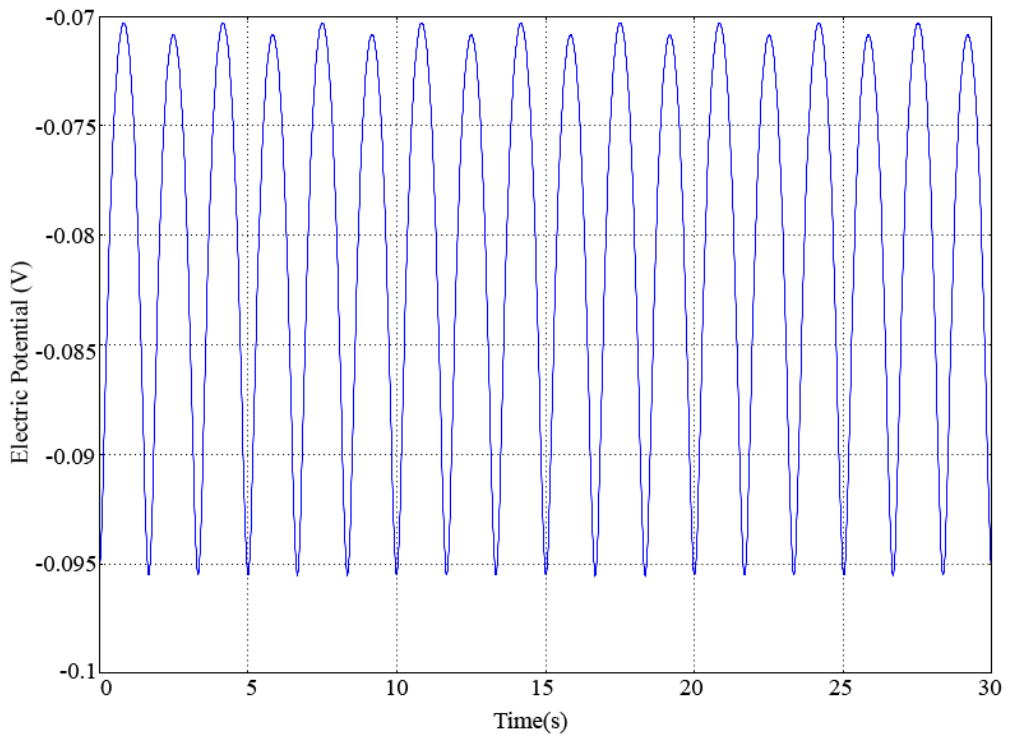


Figure 5.14: Data from simulation for point positioned as for Fig.5.13

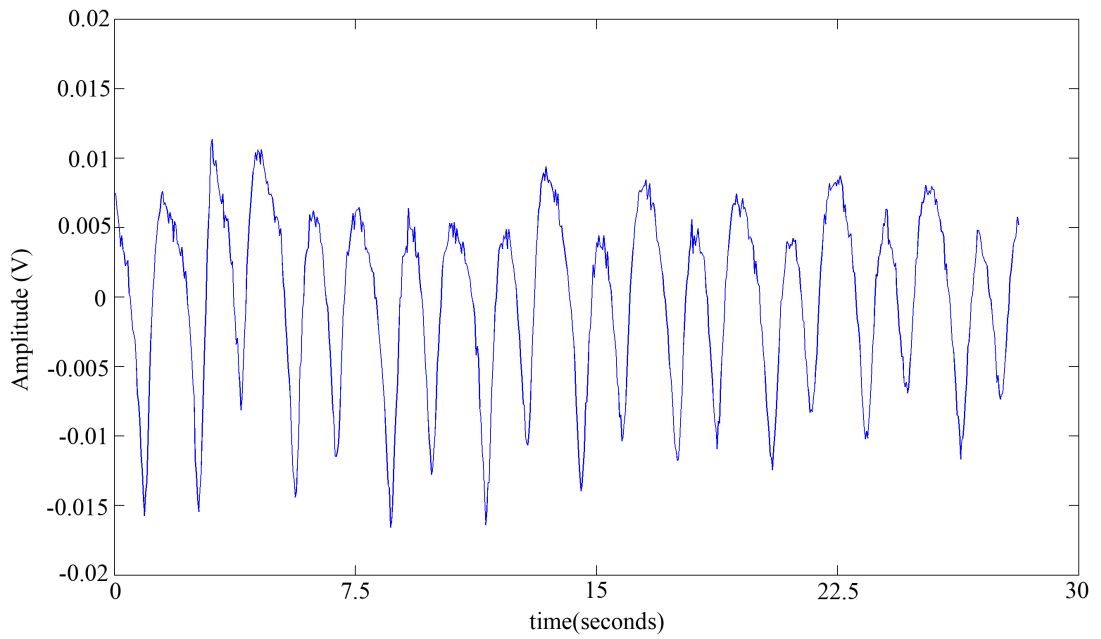


Figure 5.15: Data shown for sensor at opposite end of experimental linear array commencing after initial transients as a result of setting the pendulum in motion have been allowed to die away. Amplitude is shown referred to voltage at the input of the sensor.

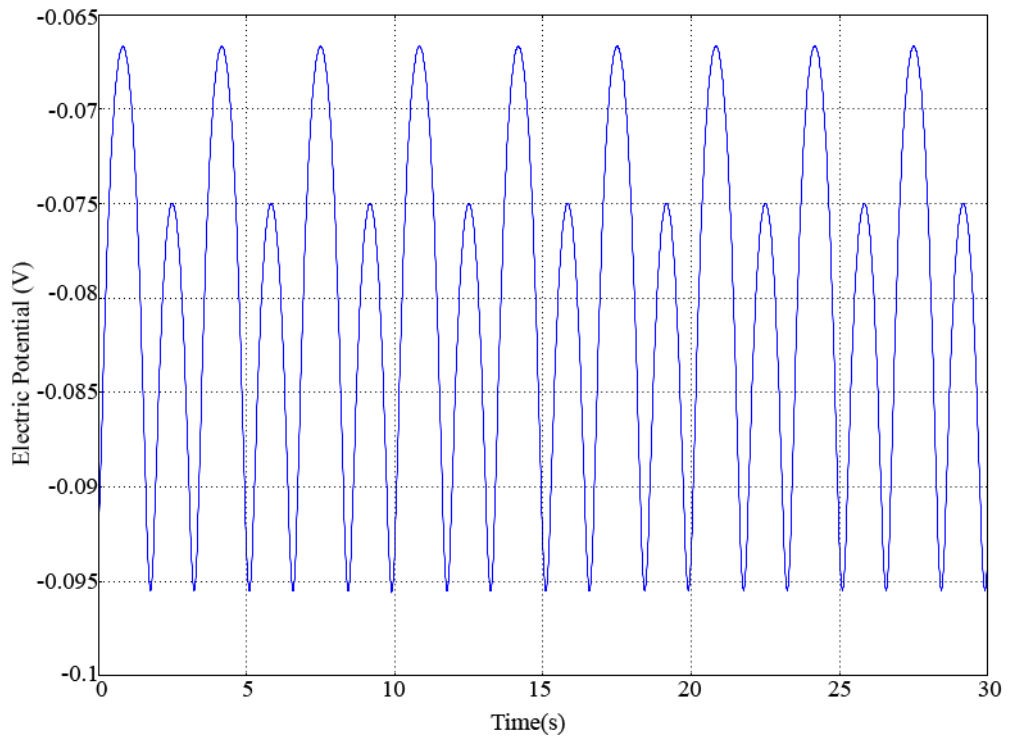


Figure 5.16: Data from simulation for point positioned as for Fig.5.15

depict the position of the measurement points, and equipotential lines are shown to depict the field originating from the point charge.

An electric potential induced by the field as the charged object moves back and forth in a pendulous movement in front of the array of measurement points can be plotted, using one adjustable parameter (the charge on the object). This simulation was then compared with data collected experimentally from the array. While significant noise is present in the experimental data, the functional form of the signal is reproduced. Figure 5.11 and Figure 5.12 show data for a sensor positioned at one end of the linear array, both experimentally and in simulation respectively. Here the matching of the form of the signals is apparent. A large variation in the height of alternate peaks can be clearly seen, and this is representative of the fact that the motion about this point is not symmetric, since the sensor is offset significantly from the centre of motion. Data from a more central sensor, shown in 5.13 and simulated in Figure 5.14, has a more even oscillation, and despite the presence of some noise in the experimental data, it can be observed that the form remains essentially the same. For further comparison, the sensor data collected from the other end of the array, shown in 5.15 when compared with simulation data in Figure 5.16 shows some variations from the simulation, and the presence of significant noise. However, within the later half of the data, the form shown in the simulated data can still essentially be seen in the experimental data.

The simulations presented are only for comparison with the experimental data. However, it is significant that it is possible to crudely reproduce the functional form of the experimental data in simulation, suggesting that the experimental data can be largely explained in the ways outlined in this chapter.

## **5.2 Further two-dimensional movement detection for gesture recognition and analysis**

### **5.2.1 Method**

A further experiment was carried out to explore the opportunities for inferring position and tracking movement within a two-dimensional space. Four EP sensors were constructed

with specifications which made them suitable for the remote detection of movement in an open environment. A low level of gain (in this case a gain of two) was used to reduce the probability of saturation in the presence of large signals and maximise the dynamic range available. The sensors were designed specifically to capture movement signals which have a typical frequency response of quasi-DC to  $\approx 10Hz$ . Circuit specifications were therefore chosen to enhance input resistance, irrespective of the impact on other input characteristics, and hence preserve as much usable low frequency bandwidth as possible. The low frequency roll-off was  $\approx 10mHz$ . The result was a set of sensors with settling times of the order of 100s of seconds, resulting in a quasi-DC response. It was expected that, since movements are relatively slow, this bandwidth would ensure movement signals were not differentiated by the sensor front end. Without this extended low frequency bandwidth, the component frequencies of the movement signal would have occurred within the roll off region of the sensor, resulting in a differentiated signal. This would have made comparison between simulation and experiment more difficult. The system behaved as a combined zero and first order system.

A small scale demonstration system was constructed using four sensors placed at the corners of a square area, of dimensions 0.5 m x 0.5 m. In this way, each opposed pair defined an axis, with the two axes perpendicular. This arrangement, with four sensors defining x and y axes, is shown in Figure 5.17.

The outputs from the sensors were connected to an 8 channel National Instruments USB 6009 data acquisition module[70] with the 5 V power supply being used to supply power to the sensors such that no additional supply was needed. Data was collected at 10 kSamples/sec for 40 ms, resulting in 400 samples. Basic digital signal processing included averaging these samples, which had the effect of low pass filtering the data. In particular, the sampling frequency and sample times were chosen to cancel line noise by averaging the 50 Hz across precisely 2 cycles and sampling for 40 ms. The same effect occurs for higher frequency harmonics of the line noise and the technique is analogous to using a simple comb filter.

The target object consisted of a 120 ml, 50 mm diameter bottle of water attached to a length of nylon line, chosen to be long enough to allow the assumption that the bottle was moving in the two-dimensional (2D) plane of the sensors. Measurements were preceded

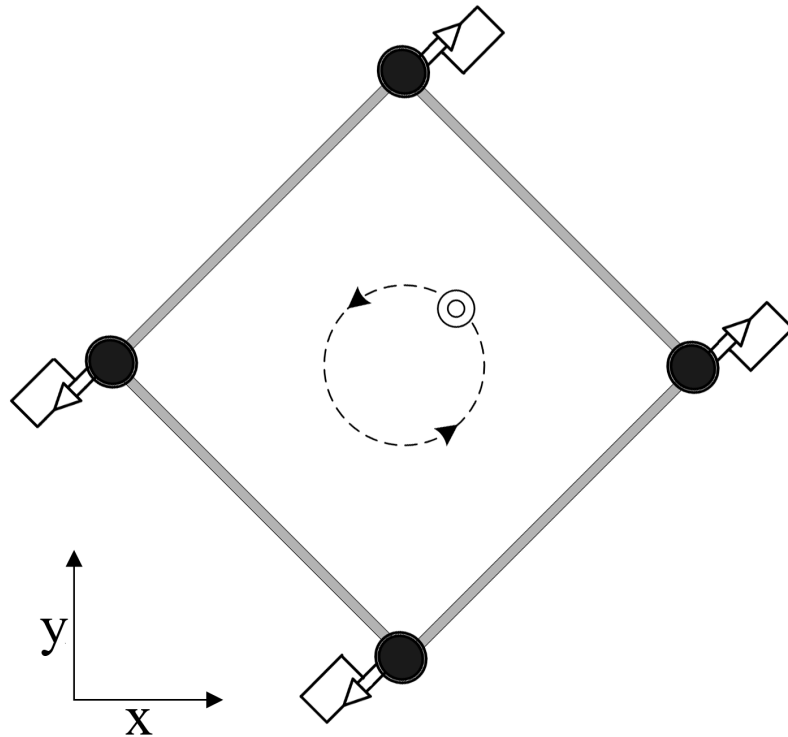


Figure 5.17: Arrangement for two-dimensional pendulum movement sensing experiment

by allowing the sensors to settle in the absence of the target. The bottle was then located in the centre of the plane and the offsets caused by the presence of a charged object in the detection field were recorded. These values were then used to define the zero point as the location at the centre of the two-dimensional space to which all other locations were referred. With the target allowed to move in the plane, differential measurements were made between each pair of sensors defining an axis. Three types of movement were investigated. Firstly, the target was swung in as straight a line as possible, oriented in the  $x$  direction. This was repeated for a line trajectory in the  $y$  direction. Finally, the target was swung in an approximately circular orbit in the  $x$ - $y$  plane.

The data from all channels was collected and processed in Labview. In these preliminary measurements, it was assumed that the output of the differential measurements was linearly related to the position of the target at a given time. This assumption is only adequate provided the excursions are small compared to the sensor spacing and taking place some distance from the sensor. In order for this to apply, the trajectories described above were limited to excursions of around  $1/3$  of the linear dimensions of the area.

The position was then shown in real-time using an intensity plot to define a dot within a two-dimensional plot. An algorithm was used to generate a matrix of data representing the position of the object. This involved first initializing a 200 by 200 array of zeros. The x and y positions were then found by taking a differential of the two sensors defining each axis, and multiplying by a factor designed to allow adjustment for different levels of sensor sensitivity. This value, which could be both positive or negative, was then offset by half the length of the array, with the intention of ensuring that the zero point in the array existed not at location zero, but at a location in the center of the data structure. The position was used to identify a corresponding position in the array, and the value at this position was changed to a 1. This technique is described in Matlab style pseudo-code in eqn 5.1. The VI used is detailed in Appendix A

```

1 array [0:500,0:500] = 0
  xpos = sensitivity*(sensor3-sensor1) + (sizeof(array),1)/2
  ypos = sensitivity*(sensor4-sensor2) + (sizeof(array),2)/2
  array(xpos,ypos) = 1

```

Listing 5.1: Matlab style pseudo-code describing differential position calculation equation

Experimental data was collected for small (compared to the detection area) linear movements parallel to each pair of sensors. Figures 5.18 and 5.19 show the real time outputs of the sensor array collected over 30 excursions of the target in the x and y directions respectively. The data confirms that the excursions were limited to around 1/3 of the area dimensions, as intended. It is clear from comparing Figures 5.18 and 5.19 that independent motion in the x and y directions is easily distinguished. In addition, Figure 5.18 shows that, where the movement is purely linear, there is minimal output from the pairs of sensors opposed to the direction of movement. In Figure 5.19 the data which indicates displacement in the opposed, x, direction is well reproduced over many trajectories and indicates that, in this case, the movement was not purely linear but comprised a small, 2D loop. This is not surprising, given the difficulty of restricting the movement of the freely swinging target to 1 dimension.

Finally, the target was moved in a nearly circular orbit and data was collected at random times during the movement. The output, in the form of an array, is shown in Figure 5.20,

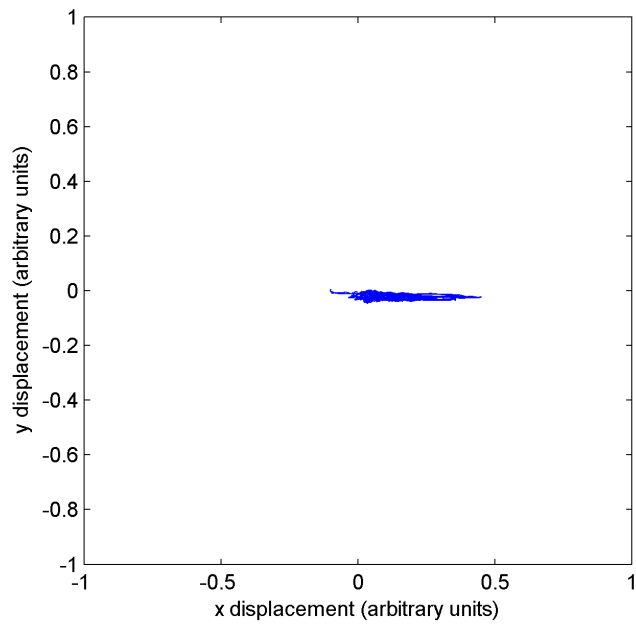


Figure 5.18: Data as a result of movement in x axis

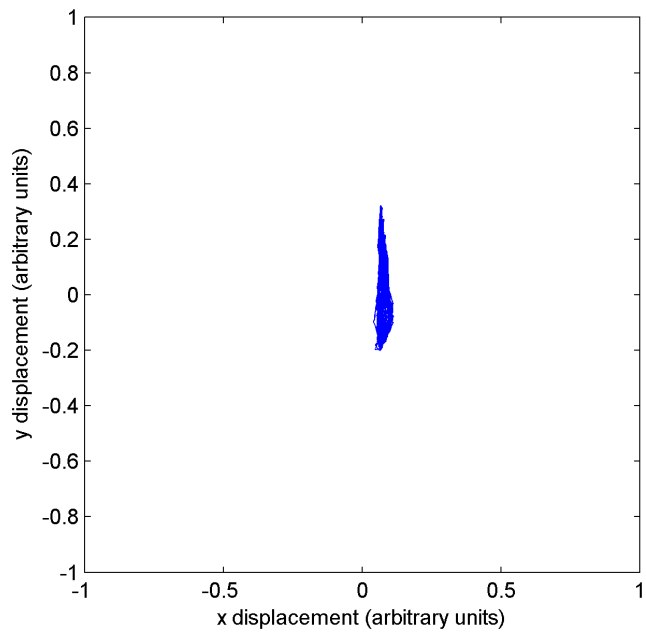


Figure 5.19: Data as a result of movement in y axis

along with a simple best fit trajectory. This is a very preliminary result and was limited by the need to keep target at an appreciable distance from all sensors at every point of its trajectory.

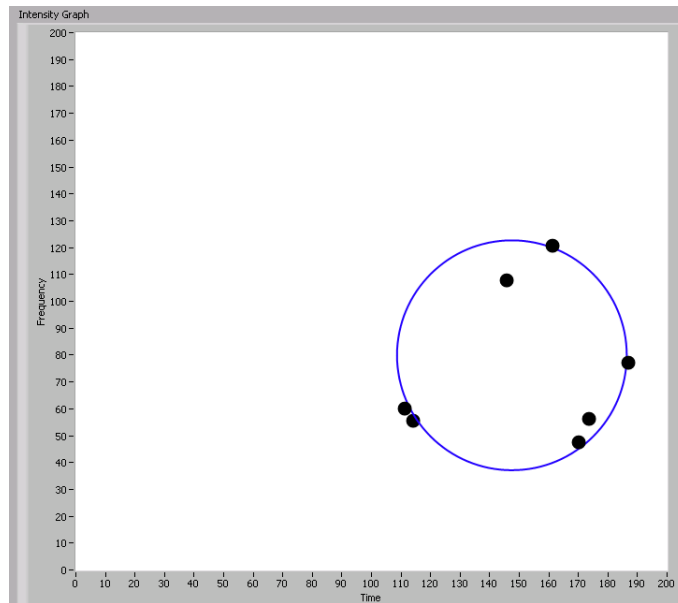


Figure 5.20: Data collected as a result of circular movement within XY sensor space

The experimental data of Figure 5.21 was compared against a COMSOL simulation, developed by Dr Peter Stiffell, of the time dependent position of a small charged sphere moving on a circular path within a 2D plane. The area was of dimensions 10 m x 10 m and the motion was determined from the voltages detected by four electric potential sensors located at the corners of the area. The finite element solutions of Laplace's equations were used to generate the voltages at the sensors for each point in time of the trajectory. A reverse calculation then used these simulated voltages to determine the proportional distance of the object between each orthogonal pair of sensors with time. In so doing, it was assumed that the field decreased in proportion to one over the distance of the source from each sensor. This  $\frac{1}{r}$  approximation is valid in the case of small amplitude excursions, when compared to the size of the sensing area. Triangulation between the pairs of sensors was then used to find the location of the source as predicted by the simulated voltages. By using sensor pairs to define the x and y axes, this triangulation becomes a solution of the intersection of two ellipses. For each point in time, a plot of the predicted location of the object was generated in order to construct a video of the full trajectory. Four frames of this are shown in Figure 5.21. The colour scale is arbitrary and indicates the likelihood of locating the object, with 1 equal to 100% likelihood.

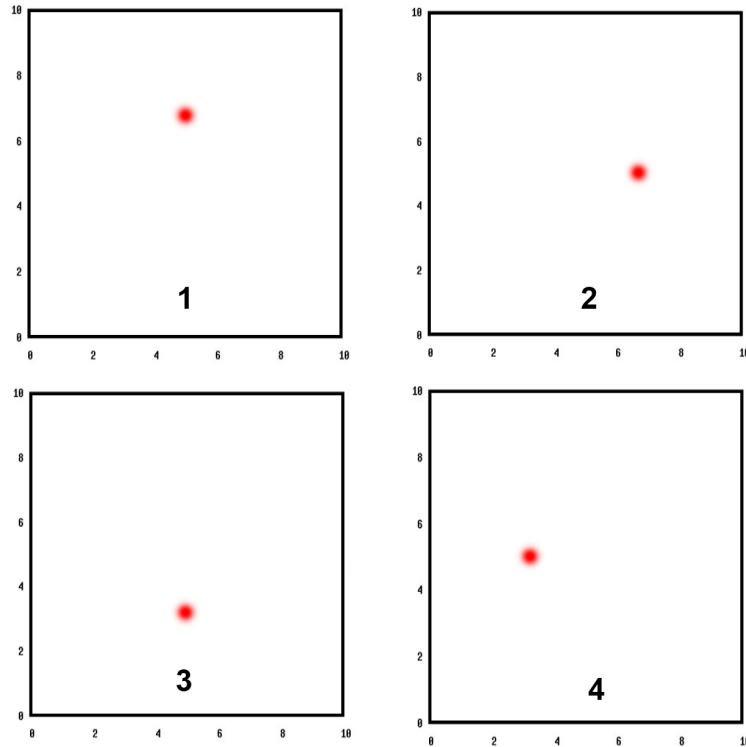


Figure 5.21: Result of simulation of positioning of charged object based on electric field detection. Red dot shows position of object as calculated in simulation.

It may be seen that this simple model for the way in which EP sensors can be used to track an object reproduces the trajectory of a moving charged object well. If real, as opposed to simulated, data is used with this model it would provide a straightforward method for extracting velocity of movement along with the trajectory.

### 5.2.2 Future work

Varying the arrangement of the sensors would provide an opportunity to look for very different types of signals. Possible future directions for this technology include arranging the sensors into the corners of a room (Figure 5.22). By comparing the relative amplitudes of a signal generated as a subject moved around a room, it would be possible to triangulate and track the position of a person moving around inside it.

Alternatively, by arranging for a grid of sensors to be constructed, as shown in Figure 5.23, it would be possible to reproduce the movement of a human hand. This would allow for detection of hand gestures, with potential applications in human machine interfaces.

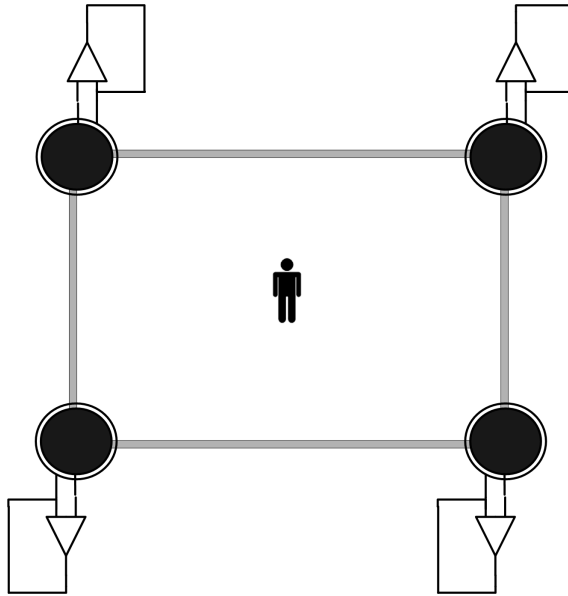


Figure 5.22: A possible arrangement of sensors, with corners being used and position of a person triangulated based on relative signal amplitudes

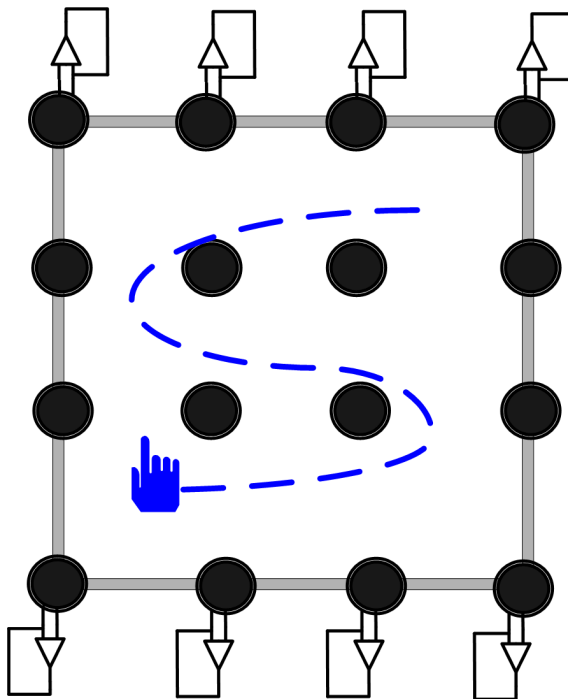


Figure 5.23: A grid arrangement of sensors for hand gesture detection

### 5.3 Conclusions

In this section we have demonstrated the ability to sense movement using a technique which is entirely passive, through sensing changes in the ambient electric field. We show that, with a sparse array of Electric Potential Sensors, it is possible to determine the position and trajectory of a single target with respect to the sensors located at the corners of a two dimensional plane. Extension to three dimensions would simply require an additional array to the orthogonal plane.

It is now necessary to develop a more sophisticated model of how the potential varies with distance of the source from any sensor in order to allow for larger excursions. The simulation would be used to verify the model by comparison with data from better defined trajectories.

A simulation of the experiment confirms that the trajectory of a single object can be determined from a simple analysis of the sensor signals. By using this model it becomes possible to extract velocity of movement, The drawback of this simple approach is that it is only able to track the motion of a single charged object or, more precisely, the motion of the "centre of charge" of all of the moving charged objects in the area defined by the sensor array. However, with the introduction of a small number of additional sensors, the area can be divided up into a sparse grid of detection zones. This provides the ability to determine when multiple objects are contributing to the total "centre of charge". Once the number of contributing elements is identified, the combined signal could be disaggregated into separate trajectories using methods such as blind source separation and frequency analysis.

This technique has been shown to yield movement signals, despite the presence of large walls and structures between the sensor and the sample, as long as the wall or structure is suitably isolated from, and does not form a good path to, earth[24]. This opens up the possibility of using a passive technique for the sensing of movement through-wall, with a variety of possible security applications. The measurement would be entirely undetectable, and therefore could be used in situations where radar based techniques were inappropriate.

Where a single individual is to be monitored, such as an elderly person in the home or the occupant of a detention cell, this system could be combined with remote life sign monitoring in a multi-modal sensor network to provide data on movement and state of health of at risk individuals. The technology is low power and easily integrated with wireless communication systems for remote data collection.

## Chapter 6

# Materials Characterisation

### 6.1 Introduction

The measurement and characterization of materials is an endeavour in which large amounts of effort have been expended. Knowledge of the structure and condition of materials is crucial in many manufacturing and industrial processes. Whether it be seeking to identify and locate internal fractures in an aircraft wing, looking for imperfections in a silicon wafer or attempting to align sapphire wafers for LED fabrication; materials measurement and testing is essential in enabling the production of goods and the provision of engineering services. Many techniques exist for measuring the physical properties and assessing the uniformity of a material, however the development of the Electric Potential Sensor creates an opportunity for a number of new and novel materials testing techniques.

In this chapter we show that charge distributions can be imaged, and that shapes drawn in charge on insulating materials with both a finger, or an earthed lead, can be clearly identified. The measurement is non invasive, such that no charge is added or removed to the sample as a result of the measurement, and entirely passive, with no excitation signal required. Instead the measurement involves making a DC measurement of static charge on a surface by moving the highly sensitive Electric Potential Sensors over the sample area to generate an AC signal which can be detected by the sensors. The technique is carried

out using a custom designed charge scanning instrument capable of imaging spatial charge distribution on insulating materials at a macroscopic scale.

The nature of the sensors involved allows measurement at resolutions limited only by the density of sensors that it is possible to fabricate. Furthermore if a CMOS process was employed, sensors at arbitrarily high densities, and therefore arbitrarily high resolutions, become plausible. Since the measurement is non-invasive, it is possible to measure and observe the decay of tribo-electrically generated charge, across time periods which vary between samples but are often in the order of many days.

## **6.2 Measurement of charge on insulating materials**

### **6.2.1 Introduction**

The EPS is capable of making an accurate measurement of spatial charge distribution, using a non-invasive technique. This measurement, based on a 16 element array of ultra-high impedance electric field sensors, is capable of producing both quantitative results for the total amount of surface charge present, as well as imaging the charge to produce plots representing spatial charge distribution. In this chapter we show the ability to calibrate the measurement against a conventional charge measurement which discharges the sample. Further to this, we show that our technique has no discharging effect on the sample and, as a result, it is possible to observe the discharging of insulating materials over periods of several days.

The generation of static charge on insulating materials, is a process that is still not well understood, and the exact cause of this effect remains the subject of scientific debate. A review of this area is given by Fuhrmann[61], and this background is discussed in more detail in chapter 1.

Surface-charge density on dielectric materials has, for some time, been classically measured using a dissectible capacitor[63] with this measurement being described in more detail by

Sessler[64]. The majority of industrial electrostatic processes involve controlled charging or discharging of particles and/or surfaces. A technique for measuring charge on particles is therefore useful, and traditionally a Faraday pail or Faraday cup is used[62]. When measuring charge on surfaces, a typical technique involves bringing a low impedance field meter close to a charged surface. If the field meter represents the only earthed object coupling to the surface charge, field lines will terminate on the electrode of the meter and a measurement can be obtained[65]. This clearly presents problems if more than one sensor is to be used simultaneously.

While a low impedance measurement is most often used to measure charge, there are examples of other high impedance measurements. A comprehensive review of electrostatic measurement instrumentation was published by Secker and Chubb[5] and includes examples of high impedance measurements of a similar style, such as Hughes and Secker[83]. In this chapter we report another approach to these measurement techniques, based on ultra high impedance sensors developed at Sussex, which create the possibility of arbitrarily high-resolution measurements. These could potentially be built using very high density arrays of sensors for real time imaging of charge distributions.

### 6.2.2 Overview of the charge scanner

A conventional flatbed scanner was disassembled, and the mechanical components combined with redesigned control electronics to allow Labview[70] control over the stepper motors mounted on the scanner head. Microprocessor code to control the motors and interface with Labview via the data acquisition card is given in Appendix B. The imaging sensor and related electronics were removed to allow mounting of an array of EPS sensors.

A linear array of sixteen ultra high input impedance electric potential sensors was constructed. Two PCBs, each containing eight channels, were assembled and attached to the sixteen electrode PCB. The electrodes each measured 6.5mm by 4.5mm, the exact arrangement is shown in Figure 6.1. The sensors use a combination of established high impedance techniques such as bootstrap and guarding, as well as a means of supplying the required DC bias current required by the amplifier to remain stable.

The two sets of sensors were connected to a multiplexer, to enable them to be read by an 8 channel National Instruments USB 6009[70] data acquisition module integrated into the scanner. The 16 element linear electrode was then mounted in the scanner and attached to the sensors. Guarding was applied to ensure maximum possible screening between channels and thus reduce the risk of cross channel leakage.

The total scanning area was 175mm wide and 230mm in length. The length was divided into 92 steps. A Labview Virtual Instrument (see Appendix A) was developed which stepped the scanner head, sampled all sixteen channels, waited a suitable period of time for the sensors to settle, then triggered another step to advance to the next position. By continuing with this step, sample, settle scheme across the entire surface it was possible to obtain a measurement which represented the derivative of the charge at each step. This data was therefore 16 elements wide, and 92 elements in length. In order to recover the charge distribution information it was necessary to then integrate the output data as given by equation 6.1

$$Q = C \int_{x_1}^{x_2} \frac{dV}{dx} dx \quad (6.1)$$

This equation holds providing the velocity of the sensor is kept consistent throughout the measurement. The integration was achieved in real-time for visualization using Labview, and also processed using an identical technique in Matlab for analysis and use in figures. In this way the charge distribution on the surface of the material could be displayed in real time. Raw data was logged and processed in Matlab to yield a 16x92 pixel image of the charge distribution.

The scanner, shown in Figure 6.2 was covered by an aluminium lid hinged at one end to screen against electrical noise as well as to ensure, where possible, that ambient air movements did not affect the presence of charge. No attempt was made to control temperature or humidity, and the scanner was operated in an open and busy laboratory in the presence of other equipment, ambient movement and temperature changes. In practice, this additional screening was only required for the longer experimental runs.

Samples of Mylar, PVC, Polyester, Acetate and Polythene were mounted in cardboard overhead transparency frames to form test slides. Samples were of varying thickness, as specified in Table 6.1. Two sets were built, one containing pure test materials and the other with flat copper discs, 30mm in diameter, attached to the underside centre of the slide with a small charging aperture cut in the sheet to allow charging of the conducting disc from the top. These discs were then charged to a known voltage of 1kV, whilst ensuring suitable safe practice guidelines were observed, and scanned using the scanner. The total charge over the area of the disc was summed to give an indication of the quantity of charge present on the disc. By measuring the total charge present on the disc using a conventional electrometer-based charge measurement it was possible to obtain a calibration factor that related the charge values obtained by the scanner to accepted SI units of charge.

Materials	Thickness of Sample	Charge after tribo-charging with earthed lead
Acetate	0.100mm	+8.91nC
Mylar	0.130mm	-0.528nC
Polyester	0.075mm	-0.251nC
Polythylene	0.025mm	-1.496nC
PVC	0.070mm	-13.2nC

Table 6.1: Samples and charge after tribo-charging

Each sample was charged, using the charging aperture, to 1kV, before being measured continuously to monitor the discharging of the disc. This data was then processed in

Matlab allowing the plotting of charge against time. These continuous measurements were taken every 3 minutes for between several hours and 8 days, with the length of measurement determined by the length of time required before the sample had discharged to a level below the resolution of the sensor.

The sample was then exposed to an ionizing blower, to ensure it was completely discharged, before being charged again to 1kV. Spot measurements were taken every few hours, in order to demonstrate that continuous measurement did not significantly affect the discharge time.

Samples without conductive discs were discharged using an ionizing blower, and then imaged to ensure they were fully discharged. The samples were then tribo-charged, using an earthed cable, before being scanned again to image the charge distribution as a result of tribo-charging.

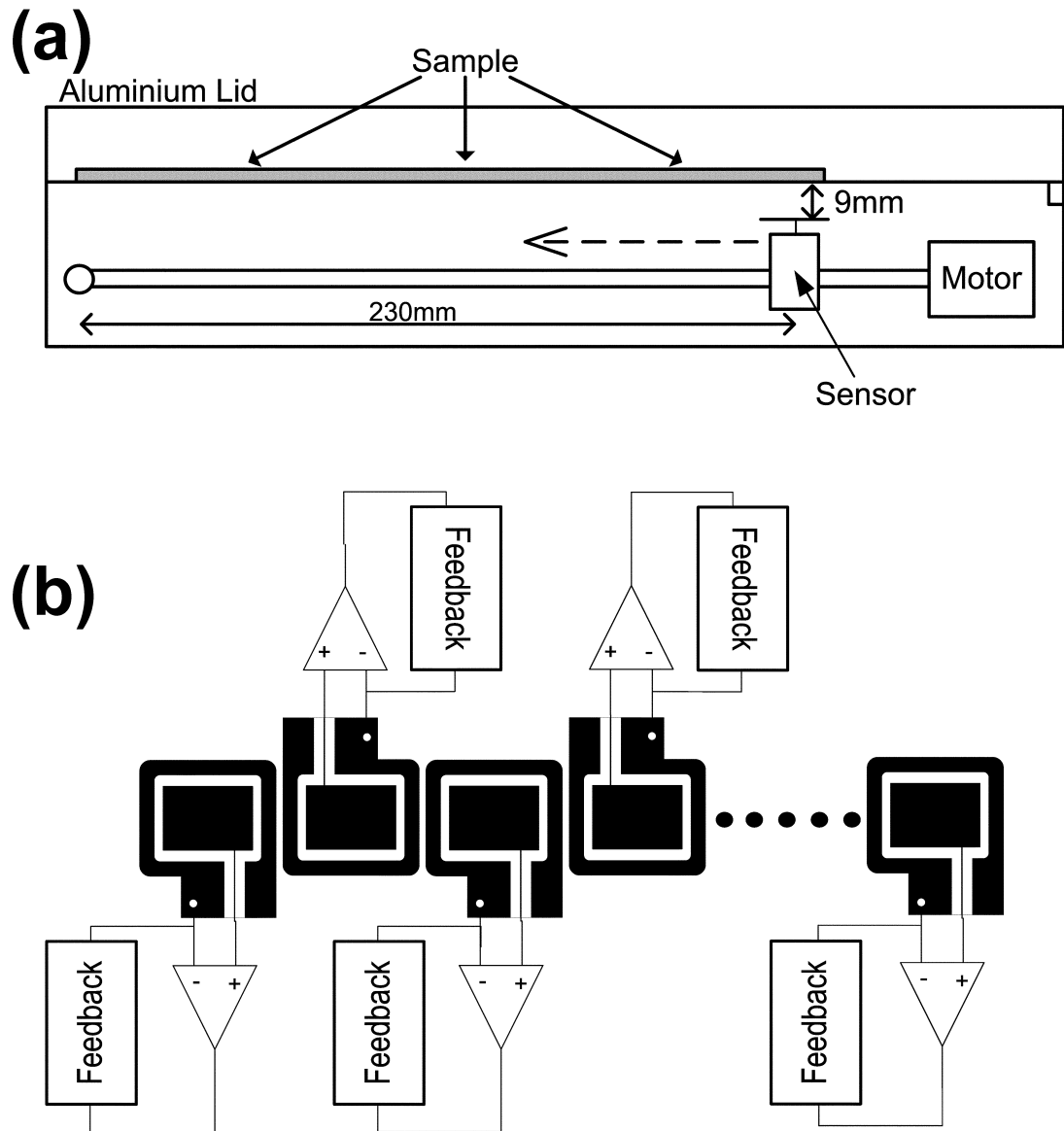


Figure 6.1: (a) Cross section of flatbed charge scanner instrument (b) Arrangement of electrode head with guarding shown for each electrode

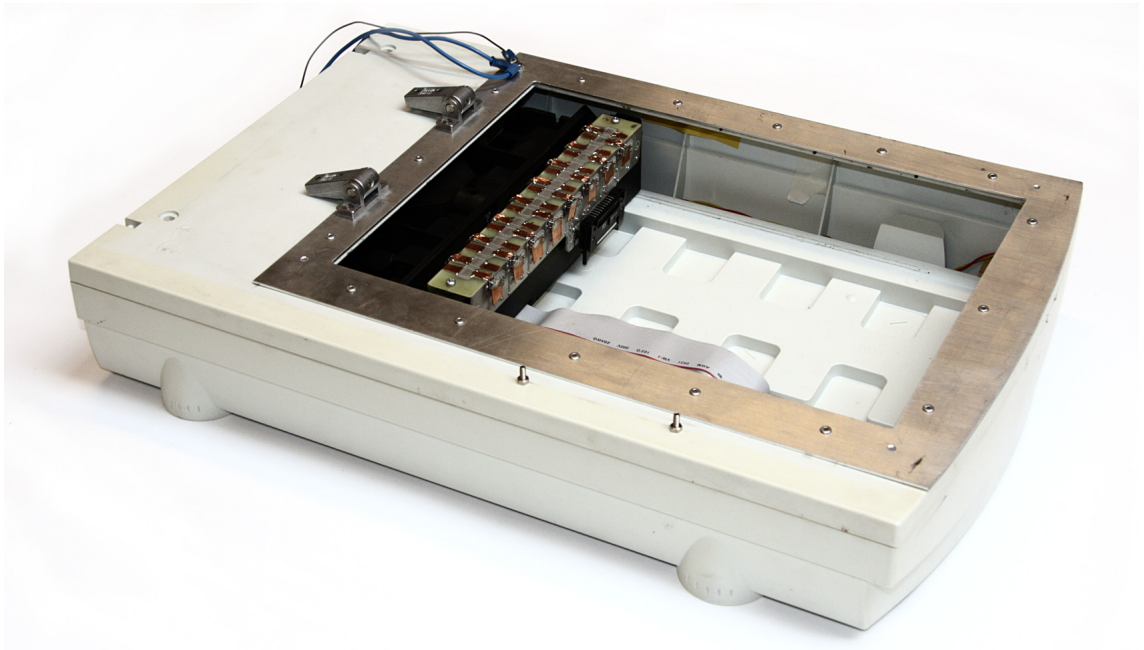


Figure 6.2: The charge scanner

### 6.2.3 Experimental Results

In order to demonstrate the non invasive nature of the measurement, a Mylar sample with a conducting charge island at its centre, as described in the previous section, was first charged using a 1kV voltage source, ensuring suitable safe practice guidelines were observed. By imaging the charge on the conductive disc continuously, with each scan taking 3 minutes to complete, it was possible to measure the discharge time over 8 days. This is shown in Figure 6.3. Units of charge, shown in nano coulombs on the y-axis, are established using a calibration technique described in Section 6.2.2 and verified with another calibration approach, described later in this chapter in Section 6.3.2. In this case, the spot data points have been normalized for the same initial charge, to compensate for errors in the charging process which make it difficult to reproduce the exact amount of initial charge prior to each measurement. Also plotted on Figure 6.3 are exponential decay curves fitted to both the continuous and non-continuous data sets. The correlation between the spot data points and continuous measurement, demonstrates that continuous measurement does not significantly affect discharge and that the measurement is truly non-invasive. It is clear from visual inspection that the decay shown in the spot data measurements is approximately equal to that in the continuous data, within the accuracy of the measurement. A measure of how closely the variance of the data may be explained by the fit can be calculated by squaring the residuals of the data, after the fit. This measure, known as R-Squared, yields values of 0.9775 and 0.9945 for the fits on the continuous and spot data points respectively, thus suggesting the fits accurately represent the data.

This continuous measurement was then repeated, for samples consisting of Mylar, Acetate and Polythene. This discharge data is presented as Figure 6.4. The discharge times involved are clearly very different for different materials, with Acetate having a substantially shorter (less than a day) discharge time, while Mylar and Polythene took approximately a week to reach the same level of discharge. From the polythene and Mylar data there are what appears to be erroneous fluctuations which become particularly significant after  $2 \times 10^5$  seconds once the charge has fallen to a significantly low level. These sinusoidal fluctuations roughly correspond to a diurnal cycle, and it is suggested that these fluctuations occur as a result of the uncontrolled temperature and humidity conditions under which the measurement took place. The fact that the acetate discharge data, shown enlarged as the inset in Figure 6.4, took place over a much shorter period of

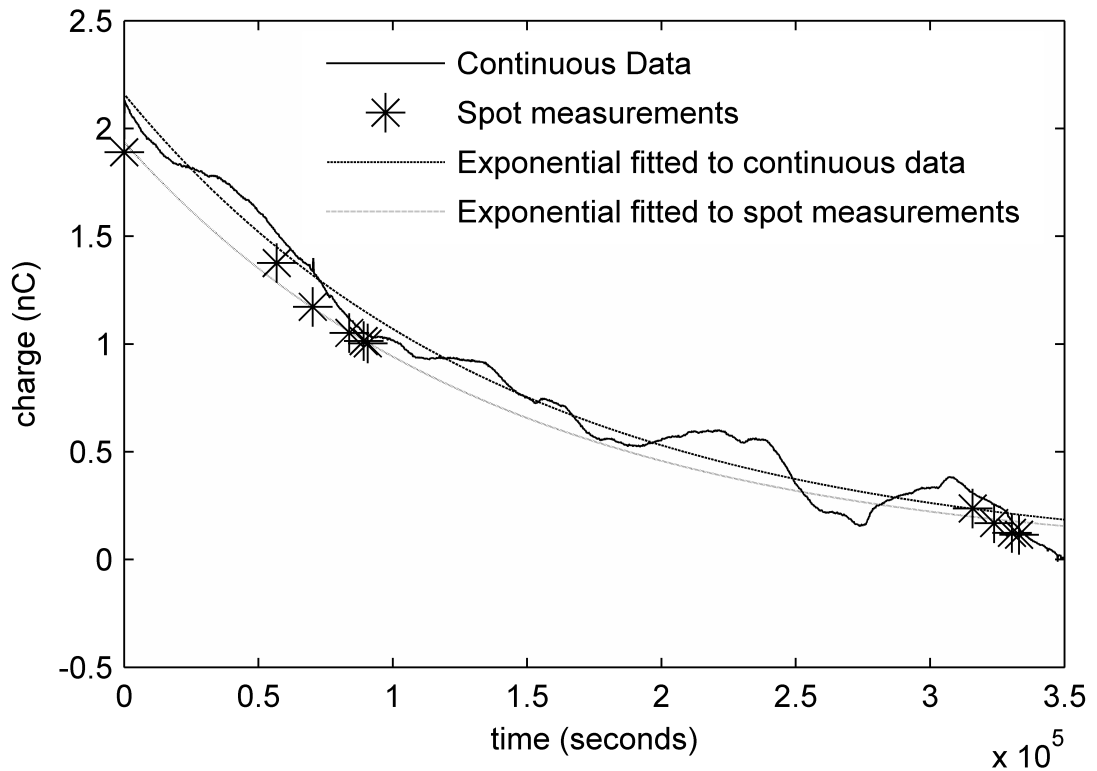


Figure 6.3: Discharge of Mylar sheet over 8 days, with spot measurements compared against continuously measured data and overlaid with exponential fits to data

time and is notably free from these fluctuations would appear to support this hypothesis.

The charge distribution images for Mylar, over an 8 day period, are shown pictorially in figure 6.5. By visualizing the data in this way, it is possible to make observations about the nature of the discharge process. It appears, in this case, that as the charge decays there is no visible spreading of the charge, as perhaps might have been expected.

Samples without a charging island were then used to observe tribo-charging effects. Having discharged a sheet of Mylar, a letter in the shape of a 'Q' was drawn on it with an earthed cable. This was then imaged and the data integrated in Matlab to calculate charge spatial density, since the measurement yields the derivative of the charge. The result is presented here in Figure 6.6, with Figure 6.6a showing the raw integrated data and Figure 6.6b showing data visualized after a piecewise bilinear interpolation has been applied in Matlab. The Q, drawn originally on the surface of the material, is clearly visible.

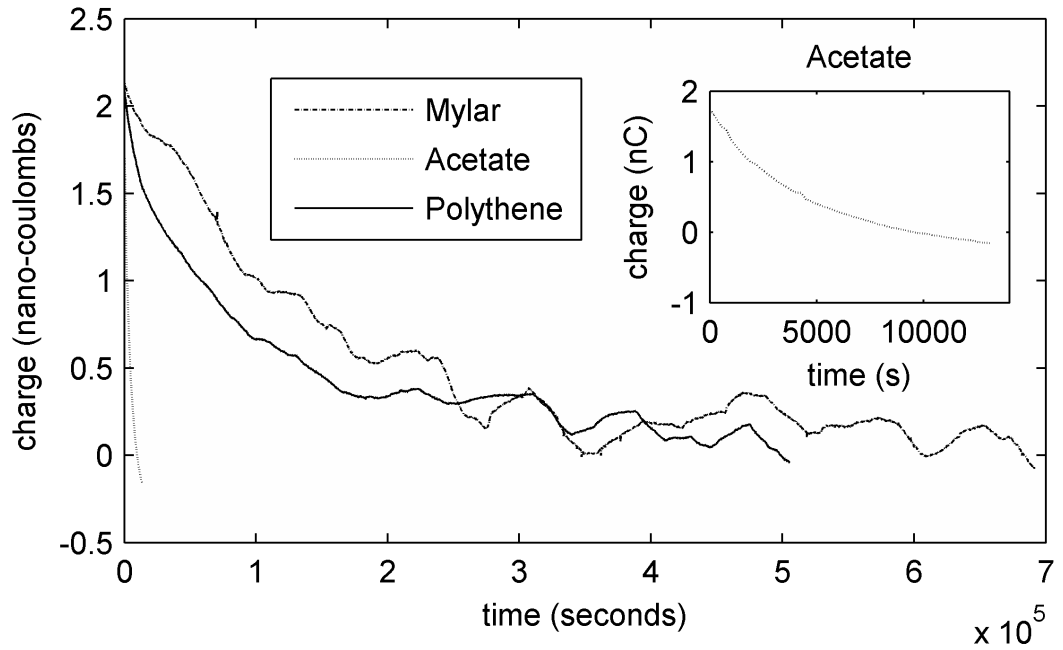


Figure 6.4: Charge decay of Mylar, Acetate and Polythene samples. Inset shows charge decay on acetate rescaled to improve visibility

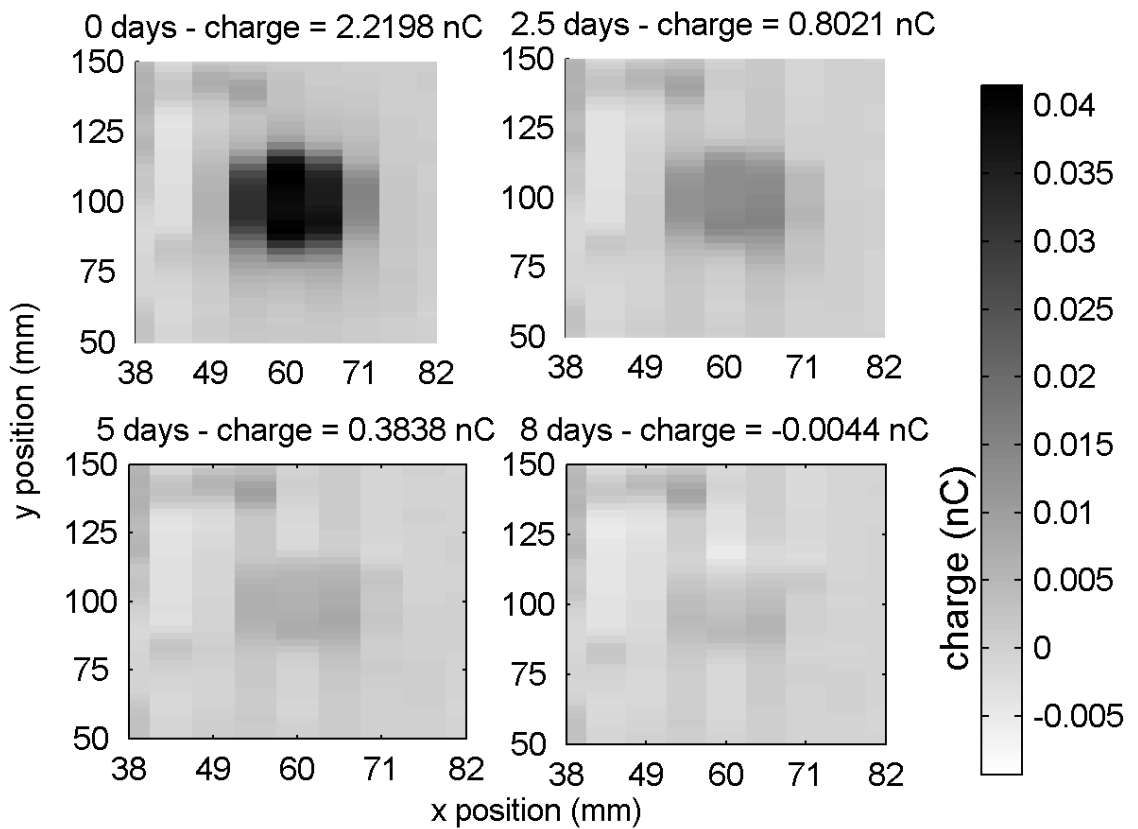


Figure 6.5: Discharge of charged island on Mylar sheet over 8 days

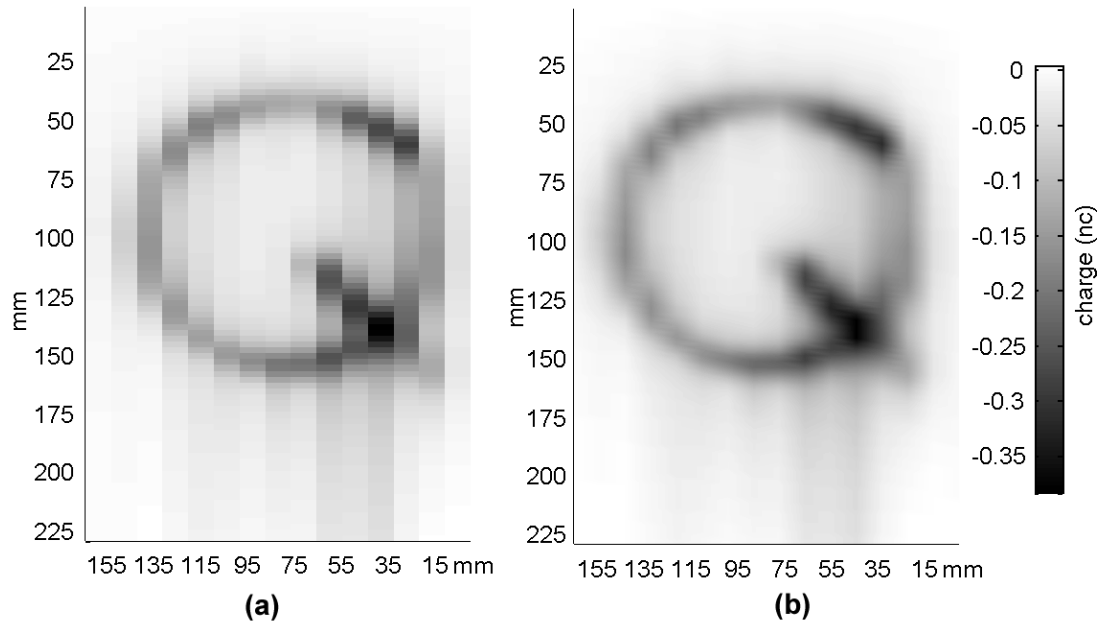


Figure 6.6: Image of a Q shape charge distribution on PVC (a)raw integrated data (b)data interpolated and smoothed using Matlab

This measurement was repeated for samples of Acetate, Mylar, Polyester, Polythene and PVC. Both an earthed cable and a human finger were used to draw a single circle of approximately the same size onto each of these surfaces. The total integrated charge resulting from a scan of the surface in each case is shown in Table 6.1

Having shown that non invasive measurements are possible, and that therefore the discharging process can be observed, it was possible to collect data showing shapes drawn with a finger or earthed lead on insulating materials, such as the Q described in earlier in this section, discharge over time. The discharge of a letter Q on a sheet of Acetate over 8 hours is shown pictorially in Figure 6.7

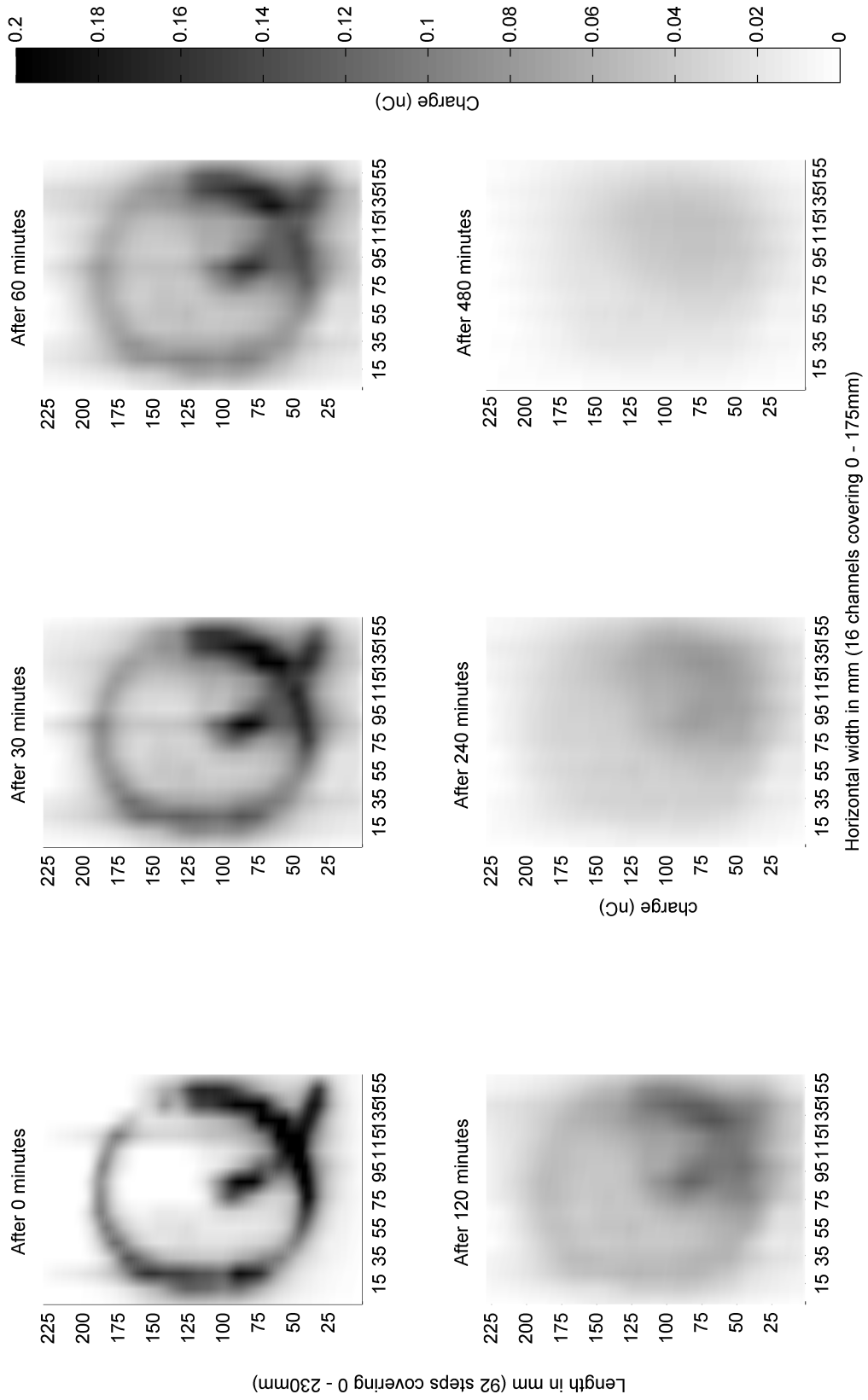


Figure 6.7: Image of a Q shape charge distribution on acetate, shown discharging over an 8 hour period

## 6.3 Measuring tribo-charging phenomena

### 6.3.1 Introduction

In this section we extend the measurements taken on samples of Mylar, Kapton and PTFE sheet, in which we image the spatial charge distribution on these sheets which occurs as a result of tribo-charging, by an earthed lead and by a human finger. These measurements are then compared with several published tribo-electric series[66], and by comparing measurements taken on samples of varying material and thickness, we show that it is possible to make fully quantitative measurements of the tribo-electrically generated charge density and therefore to establish a quantitative tribo-electric series. This opens up the possibility of absolute, rather than simply relative, positioning of materials within a tribo-electric series using a repeatable and calibrated measurement technique.

### 6.3.2 Overview of the experiment

A set of material samples were obtained, consisting of well specified sheets of Mylar, Kapton and PTFE. Mylar samples, of varying thickness, were also obtained. Material dimensions are shown in Table 6.2. These samples were again mounted in cardboard overhead transparency frames to ensure they remained rigid during measurement and to avoid handling.

Table 6.2: Sample materials and dimensions

Material	Dimensions
PTFE	230mm x 175mm x 0.050mm
Kapton	230mm x 175mm x 0.050mm
Mylar	230mm x 175mm x 0.050mm
Mylar	230mm x 175mm x 0.023mm
Mylar	230mm x 175mm x 0.125mm
PVC	230mm x 175mm x 0.100mm
Acetate	230mm x 175mm x 0.070mm

A commercial charge measuring electrometer[84] was connected such that the reference was common (ground), and the input of the electrometer was connected to a standard 3.5mm plug. The sample was mounted in the scanner and the lead was positioned within a short reach, before being zeroed. The lead was then drawn across the sheet, and as charge was deposited or removed from the surface of the sample, this was indicated on the electrometer. The sample was then scanned and the total amount of charge indicated by the electrometer used as a calibration factor to allow the measurements made by the scanner to be given in absolute terms (i.e. total charge in nanocoulombs). This value was found to be stable over time, when measured at several points over a period of several days. It was also found to be consistent irrespective of the material sample used.

A carbon fibre brush was attached to the arm of the scanner in such a way that it would brush over a sample of material as the scanner made a measurement. The brush was 40mm wide, and attached to the head of the scanner arm in such a way that it would be pulled over approximately 60% of the sheet as the scanner head processed across the scanning area. Labview control software was then written which scanned each sample twice. Samples were first discharged, by placing them in front of an ionizing blower for several minutes. The scanner then passed the sensors across the sample, as described above, measuring the discharged state. In the process of this, the brush passed behind the scanner head, performing a repeatable tribo-charging process on the sample. The scanner then scanned a second time, this time measuring the quantity of charge added to the sample by the brush. This process was repeated several times to establish the repeatability of the charging process.

### **6.3.3 Quantitative tribocharging results**

By measuring the discharged state of each sample, then taking a measurement of the charge deposited using the carbon-fibre brush charging method it was possible to obtain a very reliable and repeatable quantity of tribo-electric charging. Once these charged samples are scanned, the section charged by the brush is clearly visible, and the image resulting from one such scan is shown in Figure 6.8.

The charge was then summed over the full area of the sheet to give an indication of the total charge on the sheet. A measure of the error which arises from a combination of the

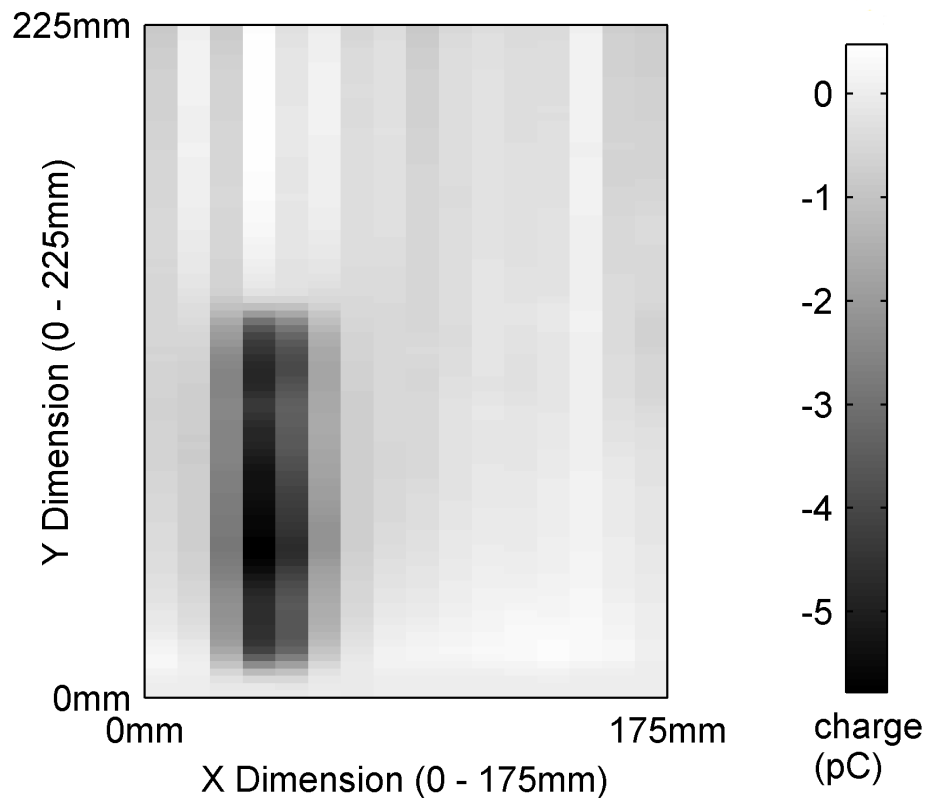


Figure 6.8: A Mylar sample imaged after being charged by the carbon fibre brush within the scanner

measurement and charging process, calculated by dividing the standard deviation of the values to establish a variation, or error, percentage was calculated. This, as well as the charging data, is shown in Table 6.3.

Having measured the amount of charge typically deposited using a repeatable standard measure of tribo-generated charge, the samples were then compared to several previously published triboelectric series[66] in an attempt to compare our quantitative measurement of susceptibility to triboelectric charging processes with previous results

Table 6.4 lists the materials tested in the order that they appear on conventional triboelectric series, along with data from the tribocharging test experiment. This demonstrates that the results discussed in this section mirror the relative positions of these materials on published series. Furthermore they clearly indicate that it is possible to give a quantitative indication of charging and position within the series.

Table 6.3: Measurements of total charge deposited using standardized tribo-charging process

Material	Thickness	Charge	Variation in measured charge
PTFE	50um	-20.0nC	
PTFE	50um	-18.9nC	
PTFE	50um	-18.3nC	+/- 4.5%
Kapton	50um	-13.3nC	
Kapton	50um	-11.46nC	
Kapton	50um	-12.0nC	+/- 7.2%
Mylar	50um	-1.44nC	
Mylar	50um	-1.317nC	
Mylar	50um	-1.36nC	+/- 4.5%
Mylar	23um	-0.70nC	
Mylar	23um	-0.77nC	
Mylar	23um	-0.82nC	+/- 7.9%
Mylar	125um	-1.09nC	
Mylar	125um	-0.9nC	
Mylar	125um	-1.08nC	+/- 10.45%
PVC	100um	-9.6nC	
PVC	100um	-8.6nC	
PVC	100um	-8.9nC	+/- 5.68%
Acetate	70um	+14.99nC	
Acetate	70um	+12.86nC	
Acetate	70um	+13.22nC	+/- 8.33%

Table 6.4: Materials tested, in order they appear on other tribo-electric series (positive to negative charging) and charge as measured by the charge imaging scanner

Material	Mean charge after tribocharging
Acetate	+13.69 nC
Polyethylene terephthalate/Mylar	-1.37 nC
Polyvinylidene Chloride/PVC	-9.03 nC
Kapton	-12.25 nC
PTFE/Teflon	-19.06 nC

## 6.4 Conclusions

In this chapter we have demonstrated the ability to image the spatial distribution of static charge on insulating materials. We have shown that it is possible to observe the very slow discharge of an island of charge within these materials and to reproduce shapes and images drawn onto a surface using charge deposited through tribocharging. In addition by comparing continuous and sparse data sets we have demonstrated the technique to be truly non-invasive and to have no measurable effect on the decay time. The measurement could be improved if it was operated in an environment where temperature and humidity could be strictly controlled and this is a consideration for further development.

If further safeguards were taken to ensure reliable results, notably ensuring temperature and humidity were strictly controlled, and possibly making use of a vacuum in which to carry out the charging and measurements, these techniques could allow for a fully quantitative tribo electric series to be developed. In comparison to previous studies, which often require multiple charging events in the order of 400 contacts to establish a reliable and measurable quantity of charge, we have shown repeatable and measurable results can be obtained using only a single charging event.

It appears that the variation in charging of Mylar with different levels of thickness might be explained by the somewhat unknown nature of the tribo-charging technique. In this experiment, thicker materials result in a larger force being applied vertically downwards counter to the brush as it moves across the surface, while very thin materials, such as the 23m Mylar, tend to be significantly displaced by the brush and therefore charge less. A better arrangement might involve the samples being mounted against a rigid insulating material to ensure they were not displaced by the brush, in order to ensure charging was more consistent across various thickness of material.

The input impedance of the sensor is sufficiently high that smaller electrodes could be used to study these processes at the micron scale, and this is discussed in chapter 7. Alternatively, with a higher density array of sensors it would also be possible to image at substantially higher resolutions and build up a far more detailed picture. If a two

dimensional array could be constructed, it may be possible to observe tribo-charging, and discharging in real time, with the potential for fast video images of charge and discharge events. In this case, while the array elements are somewhat large, we have shown that arrays of this type are possible with these sensors, and that it would be possible to fabricate them at much higher densities.

This charge spatial distribution imaging instrument provides a real possibility for the development of a method of measuring, in a quantifiable way, both the magnitude and spatial distribution of charge on a variety of materials. In addition to a range of industrial applications this could enable substantial further study of tribo-electric charging effects. The non invasive nature of the measurement, made in such a way that it does not discharge the sample, enables the measurement of discharge processes within these materials, with further scope for improving the understanding of these phenomena.

## Chapter 7

# High resolution material surface measurement system

### 7.1 Introduction

The need to characterize and study materials, as well as analyse them for potential changes or faults which are not visible on the surface, creates a requirement for imaging and measurement techniques and instrumentation. In Chapter 6 a charge scanning instrument was discussed which imaged spatial charge distribution on insulating materials at a macroscopic scale. In contrast, this chapter describes an electric field microscopy instrument. The measurement made in chapter 6 was entirely passive, with sensors passed over a surface and a signal occurring as a result of moving the sensors through a static electric field which occurred as a result of static charge on the material. In contrast, the measurement described here is an active one.

Scientists and engineers, who are interested in the properties of a material at the micrometre and nanometre scales, have the choice of a wide range of techniques and approaches to the imaging of materials and their properties. Many of these techniques are either traditional optical microscopy methods, or techniques based on the principles of atomic force microscopy (AFM). These AFM approaches require separation distances

between sensor and sample of the order of several angstroms, and so while offering ultra high resolution measurements of surface and material properties, are often not suitable for measurements over areas greater than a few square millimetres.

In this chapter an alternative technique is described, where a capacitively coupled EP sensor is used to measure a signal proportional to the surface topography of the material. An AC signal is applied to the conducting sample, and the resulting field detected using an EPS. This sensor is then stepped, in a raster scan, across the sample area. At each point the amplitude of the field is measured, where this amplitude varies with the coupling capacitance between sensor probe and sample surface. As the probe to sample separation distance varies, this capacitance varies, resulting in an image of the surface of the sample. The sensitivity of these sensors means that extremely small probes, in the order of microns, can be used. However, in contrast to the methods described above, this technique can be applied at a range of scales from  $1\ \mu\text{m}$  to several metres.

## 7.2 Methodology

An XY table was used, with stepper motors used to drive lead screws to which a carriage was attached. This allowed for control of the carriage in both the x and y directions, with a high degree of precision. The stepper motors used were capable of a minimum linear step size of  $6\ \mu\text{m}$ . A sensor was mounted on the moveable carriage, with a  $25\ \mu\text{m}$  diameter electrode attached to the sensor electronics. The electrode consisted of a co-axial structure, with a thin  $25\ \mu\text{m}$  sense wire, surrounded by two guarded plates. The probe was secured inside a block of high resistance epoxy resin to ensure it was protected against breakage if it was to collide with the surface of the sample. The sensor electronics were mounted inside a guarded box, very close to the electrode and attached vertically above it. A 1kHz reference signal was generated with an external signal generator configured to generate a sine wave at a frequency within the bandwidth of the sensors. This reference signal was applied to the conducting sample. The arrangement of the experiment is shown in Figure 7.1.

Control electronics were designed and built to allow the instrument to be controlled by a computer running Labview. A microprocessor was used to control two high power stepper

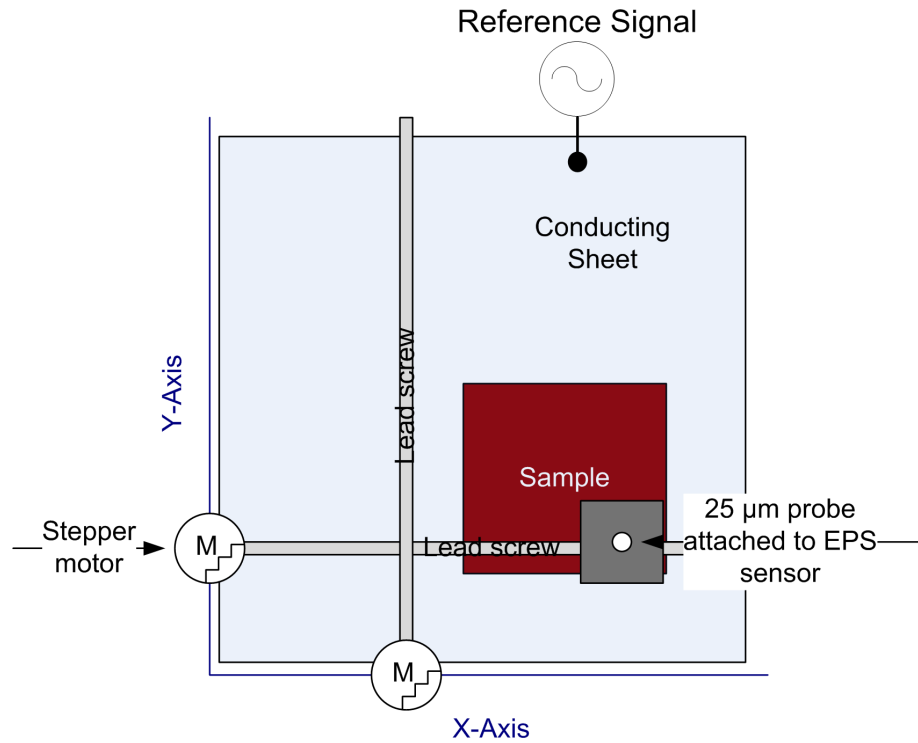


Figure 7.1: XY Electric Potential Topography System

motor controller ICs. Signals on the inputs of the motor controller selected the direction of movement, type of step (half or full), and configured the controller. A clock pulse was used to trigger a step, which in turn drove stepper motors attached to lead screws in order to move the sensor carriage. Micro-switches were attached to the carriage to act as limit switches in x and y directions. These were connected to inputs on the microcontroller.

Assembler code was written (see Appendix B) to interface between the digital IO signals generated by Labview on the outputs of the USB acquisition card, and the stepper motor controller. The microcontroller detected a trigger pulse and control signals generated in Labview, and in turn triggered the stepper motor controllers to step the motors bidirectionally in x or y directions, or to return the carriage quickly to the zero point, activating the limit switches. The microcontroller was able to trigger full or half steps, either singularly or in sets of 10. This gave the option of steps of  $6\mu m$ ,  $12\mu m$ ,  $60\mu m$  or  $120\mu m$ . An LCD display was interfaced to provide control and debugging information as needed, and library routines developed to control the complex timing signals required to control the display. This was configured to indicate when communication with Labview was occurring, and in the event of movement, in which direction it occurred. The system described is shown pictorially in Figure 7.2

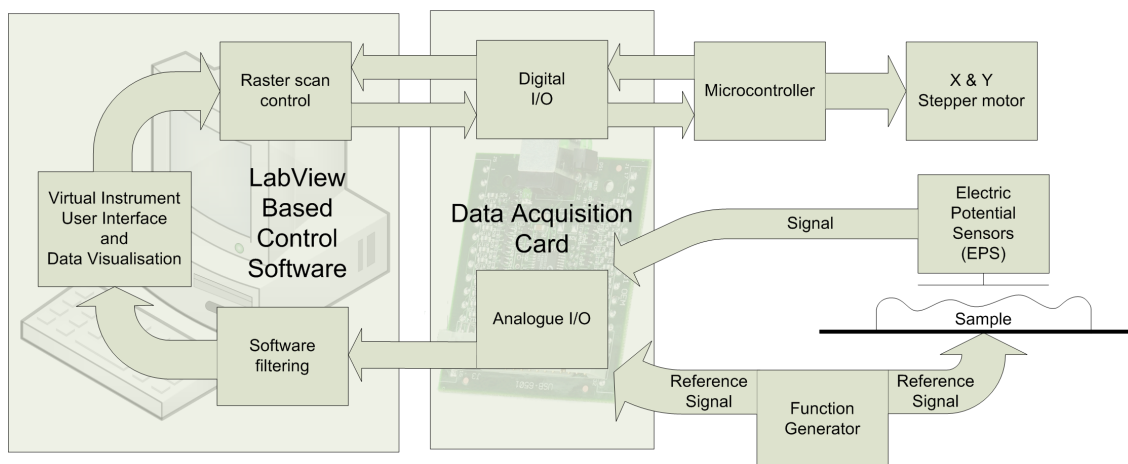


Figure 7.2: XY System Overview

A  $25\ \mu\text{m}$  diameter electrode was attached to an EP sensor, and a sample placed between a conducting electrode and the sensor. A reference signal was applied to the conducting sample, and the magnitude of the signal appearing on the output of the sensor measured using a National Instruments USB data acquisition card. The height of the sensor was kept constant, and adjusted with a vertical screw thread, sprung to ensure it did not slip over time. As with the charge scanning instrument in Chapter 6 the separation distance between the sample and the sensor was required to be of the order of the step size and probe size to ensure none of these factors limited the resolution. In this experiment, clearly, the  $25\ \mu\text{m}$  electrode made the very smallest steps unnecessary. A separation distance of  $25\ \mu\text{m}$  was used to match the electrode diameter.

The Labview routine used to collect data, comprised a one directional raster scan across the surface of the sample, made up of a series of steps in the x direction, each one followed by a measurement, and continuing in this way until the end of a line. At this point the y direction was stepped, the scanner head returned to a zero position in the x direction and the process repeated until a selected x by y area had been scanned. After each step, data was acquired in Labview, filtered in software to remove noise and displayed on the screen. Each step and data reading took 50ms to complete. Data files were generated and saved for later analysis and post processing using Matlab. The maximum scan area was 300mm by 300mm.

### 7.3 Results

A standard sample used for roughness calibration was chosen to demonstrate the potential of this type of measurement for surface topography measurements. In this case, a metal sample, cut using a  $125\mu\text{m}$  vertical mill was placed on the scanner, and data collected. A section of the sample, measuring 6mm by 3mm was measured using the scanner. The sample was then carefully photographed to provide an optical comparison for the data. This data is shown in Figure 7.3

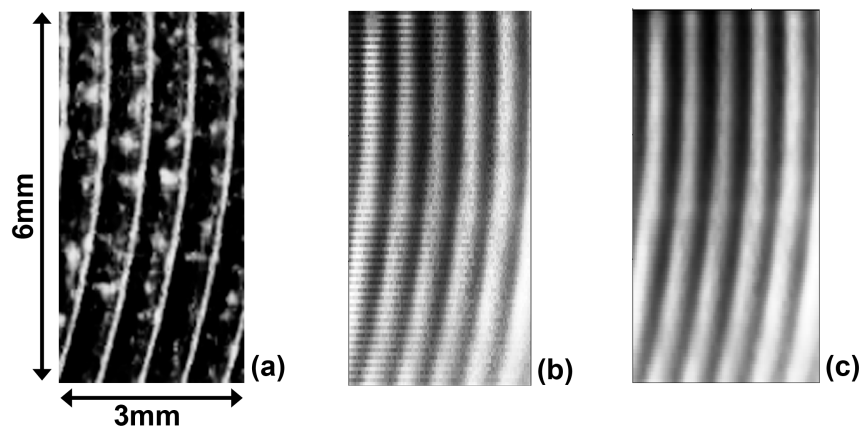


Figure 7.3: XY Data compared with photograph. (a) Optical image, (b) raw data from scanner, (c) data after post processing/smoothing

It is clear from the images that the data gives an indication of surface topography of this metal sample. The milled pattern can clearly be identified in the data (Figure 7.3 (b) and (c) as being the same as that in the optical image (a). The data was also rendered as a three dimensional image to provide a 3D view of the topology of the surface. The result of this technique is shown in Figure 7.4

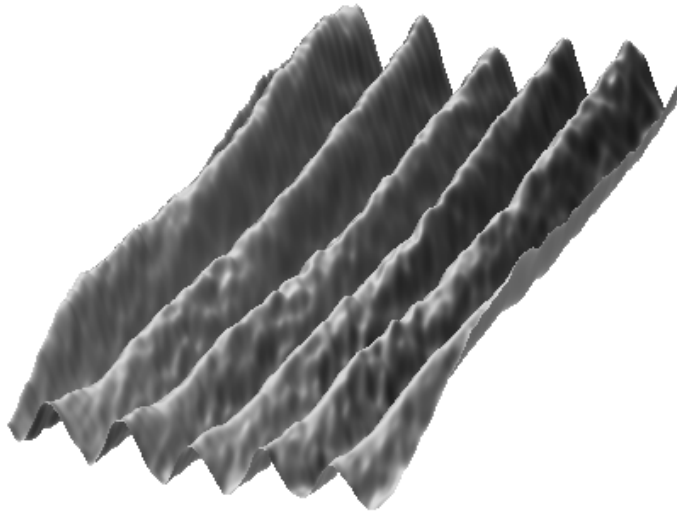


Figure 7.4: Three dimensional rendering of the data collected by the XY scanner

## 7.4 Conclusions and future work

The data shown here demonstrates the potential of this type of measurement for micron, and potentially sub-micron, scale measurements of material properties. Since the measurement being made is dependent on the capacitance between the conducting surface supplying the reference signal and the sensor electrode, additional materials measurement approaches are conceivable. One might involve placing an insulating sample between the sensor and a conducting plate. With a reference signal applied to the plate, variations, faults or defects in the insulating material would result in variations in dielectric constant and therefore coupling capacitance. In this way, it would be expected that defects within the material, which could not be seen on an optical image, would also be clearly visible in data from this scanner system. This opens up the possibility of a wide range of material testing and fault finding applications. Many other possible applications exist for this type of measurement. The ability to take measurements first on a large scale, identify areas of interest, then change the tip or step size and take a much higher resolution scan of a small subsection of the sample has great promise. This provides a clear advantage over the alternative material characterization techniques based on atomic force microscopy which

were described in chapter 1. While those techniques demonstrate remarkable sensitivity, they are useful only at nanometre scales. In contrast, these EPS based techniques are scalable.

Other possible applications include the characterization and fault detection of carbon composite samples. This is a technique which is currently difficult using existing techniques, and new ones are needed. If the surface topology of a sample was known, or a technique could be found for separating signal variations caused by surface topology, it would become possible to identify hidden faults in these materials, with potential applications for a range of carbon composite manufacturing and safety testing related areas.

The XY scanner could also be configured to carry out higher resolution measurements of charge spatial distribution, in much the same way as the charge scanner described in Chapter 6. While these scans would take substantially longer, they would allow for far higher resolution scans and the imaging of far smaller charge distributions. This greater resolution could also allow measurements on biological systems, with the potential for investigating charge and potential imaging of biological cells and systems.

A  $4\mu\text{m}$  diameter electrode is currently being fabricated, and this, combined with methods for reducing the vertical distance between the sample and the sensor, will allow for higher resolution measurements. An accurate Z axis control is also planned, with feedback used to allow scans which maintain a constant height above the sample, irrespective of any surface roughness or irregularities. This again would aid in the diagnosis of internal faults in material samples.

## Chapter 8

# Conclusions

In this thesis we have presented a range of techniques and designs with the purpose both of extending the range of applications to which it was possible to apply the electric potential sensor, as well as improving the performance of these sensors in existing application areas. In particular, we have applied these techniques to a range of remote sensing applications where the presence of significant amounts of screening from electrical noise and interference was either impossible, impractical or undesirable.

In Chapter two, data was presented which had been collected for the purpose of understanding more clearly the constraints on the capabilities of the sensors and the limits of the positive feedback techniques being used to enhance their performance. By mapping the phase space established by the use of bootstrapping and neutralisation, and comparing this data with simulated data obtained from a Spice computer model, a number of significant new conclusions could be drawn. When applying neutralisation, a positive feedback signal is applied through a capacitor to the input in order to cancel out input capacitance of the sensor. In comparison, a guarding technique involves a signal fed back through the capacitance which exists between the guarding structure and the input. In this way, it is possible to identify that in many cases neutralisation and guarding represented essentially the same technique. This made it possible to substantially simplify sensor designs without affecting performance.

Furthermore, it became clear that despite reducing the effective input capacitance using feedback techniques from the output of the sensor, it was not possible to gain the same improvement in signal to noise that might be expected as a result of this improvement in input characteristics, unless a noiseless signal source could be used to provide this feedback signal. As a result, in many cases, the use of neutralisation provided no further benefit over increasing the gain of the sensor.

In many remote applications, the most significant noise sources are those external to the sensor. These large signals, occurring as a result of electrical interference or movement, are often orders of magnitude larger than the signal of interest. Since increased gain also has the effect of increasing the magnitude of these signals, it is often the case that the reduced dynamic range poses a more serious issue than those potentially overcome by the use of positive feedback techniques. If the positive feedback techniques used to enhance sensitivity, could be used selectively to enhance sensitivity at frequencies of interest, or reduce sensitivity to known noise sources, the potential exists to substantially increase dynamic range without compromising sensitivity.

The data discussed in Chapter two resulted in a greater understanding of the performance of EPS sensors in remote applications. This enabled a number of experiments to be attempted, as detailed in chapters four to seven, which would not have been possible, or would at least have been substantially more difficult, had these techniques not been so fully understood. Principally, we found that while positive feedback techniques can have the beneficial effect of allowing customization of the frequency response to reduce noise at frequencies which are not of interest; for remote applications, where the most significant noise source is external to the sensor, these should be avoided in order to maximise dynamic range.

Chapter three presented some experimental sensor designs which explored the potential of a new technique intended to allow the construction of signal specific sensors. It was intended that these techniques would result in sensors that could be configured to have sensitivity only to particular signals of interest, or to be insensitive to particularly problematic noise sources. A sensor that would respond only to a particular mix of harmonics would allow the detection of very small signals of interest, such as those produced in many electro-physiological measurements, even in the presence of very large

noise and interference signals. By using tunable filters to control feedback in the sensor, it was possible to achieve this effect and accept only specific frequency components at the front end. However, the primary limitation of this technique was extremely long settling times for high-Q versions of the circuit. This, combined with greatly increased circuit complexity and unavoidable additional noise as a result of using digitally tunable filters, made this approach practical only in very specific circumstances, and only where a signal was continuous. Since many of the intended remote applications of this sensor were electro-physiological, and many of these signals consist of complex pseudo-periodic signals, a different approach was developed.

A sensor that was insensitive to large, well defined noise and interference signals, such as those arising from proximity to an electrical mains operated device, would also provide potential benefits for operating sensors in remote environments. This effectively represented the dual of the approach described above. Frequency selective feedback was used to suppress the largest frequency components of a 50 Hz mains interference signal, leading to rejection of the order of 95 dB. Furthermore, unlike post processing approaches, this allowed the acquisition of a signal even in the presence of noise that would previously have driven the sensor into saturation. This approach was shown to be useful in open, noisy environments. In both versions of the tuned sensors, remote programming of the frequency selective feedback was incorporated.

In addition, it was determined that in cases where the detected signal was relatively large, and since a reduction in gain did not lead to a reduction in signal to noise ratio, sensors could be prevented from saturating simply by using a much lower gain front end. In these cases, post processing could then be used to remove noise signals before amplifying the remaining signal.

Chapter four described an application of the tunable noise insensitive sensors, in the form of an experiment to measure a cardiac based signal remotely through an air gap of 40cm. This was demonstrated outside of a screened room, in a busy laboratory environment and in the presence of a range of electrical mains operated equipment. This was made possible by a combination of the noise reduction techniques discussed in Chapter three, but also as a result of the improved understanding of sensor performance and characteristics which arose from the work described in Chapter two. The data presented was shown

to be consistent with previously published results obtained within a screened room, and coincident with cardiac data collected using a pulse oximeter.

This improved understanding was then further applied in Chapter five, in which a movement sensing and position tracking experiment was described. EPS sensors were demonstrated detecting presence and tracking movement, both in a linear array in one axis and to a limited extent in two dimensions. Unlike many alternative motion tracking techniques, the fact that this novel approach is not optical means it could be applied to track and locate objects through walls, structures and surfaces. As a completely passive technique, there is no requirement for objects to be attached to a transmitter or irradiated with any kind of signal source. As a result there exists substantial applications in the fields of human computer interfacing and security, which could not be addressed using current techniques. Preliminary finite element calculations are presented for comparison with experimental data, and used to show agreement between theory and measured results for a linear movement sensing array.

In Chapter six, a novel charge measurement system based on electric potential sensors was described. The instrument presented was capable of imaging the spatial distribution of charge on insulating materials. Applying our improved understanding of the sensor input characteristics made it possible to design a sixteen element sensor array within a relatively confined space. The scanner was demonstrated monitoring, without affecting, the decay rate of charge on a range of insulating materials, as well as producing images showing the spatial distribution of complex shapes and images of charge which have been 'drawn' onto the surface by tribo-charging. Unlike many alternative measurement techniques, our technique is non invasive and is shown to have no measurable effect on decay time. Furthermore, the possibility of characterizing materials based on their ability to acquire charge through contact electrification could allow a quantitative tribo-electric series to be established. Since the limitation on the spatial resolution of the measurement is the density to which it is possible to fabricate an array, very high resolutions would be possible and real time imaging of charging processes becomes conceivable if a two-dimensional array were to be constructed.

Finally, in Chapter seven, the design and construction of a high-resolution, materials characterisation system was described. While only very early results from this system

were discussed in this thesis, the sensor was shown working with sensitivities that enabled it to work at the micron scale, without needing to operate inside a heavily screened enclosure. The improved ability of these sensors to make field measurements with very small micron scale electrodes was demonstrated, and was achieved as a result of the greater understanding of sensor input characteristics, which has come about in part from the experiments discussed in previous chapters. There are clearly many future possible directions for materials measurements with this instrument, notably a charge scanning mode measurement which would allow much higher resolution measurements of the same nature as those discussed in Chapter six.

In this thesis, a range of Electric Potential Sensor applications outside of screened environments and which did not require physical contact between sensor and signal source have been demonstrated. These advances have been enabled by the development of a combination of new techniques and a greater understanding of the sensors and their characteristics and performance. It is shown that, in principle, these sensors could potentially find future applications within the fields of human computer interfacing, defence and security, health monitoring, materials measurement and industrial manufacturing.

## References

- [1] R. S. Kirby, *Engineering in history*. New York ; London :: McGraw-Hill, 1956., includes bibliographies. Cited on 1
- [2] S. Grimnes and O. G. Martinsen, *Bioimpedance and bioelectricity basics*, 2nd ed. London :: Academic,, 2008., previous ed.: 2000. [Online]. Available: <http://www.engineeringvillage.com/controller/servlet/OpenURL?genre=book&isbn=9780123740045> Cited on 1, 59
- [3] J. C. Maxwell, “A dynamical theory of the electromagnetic field,” *Philosophical Transactions of the Royal Society of London*, vol. 155, pp. 459–512, 1865. [Online]. Available: <http://rstl.royalsocietypublishing.org/content/155/459.short> Cited on 1
- [4] T. R. Foord, “Measurement of the distribution of surface electric charge by use of a capacitive probe,” *Journal of Physics E: Scientific Instruments*, vol. 2, no. 5, pp. 411–413, 1969. [Online]. Available: <http://stacks.iop.org/0022-3735/2/411> Cited on 3
- [5] P. E. Secker and J. N. Chubb, “Instrumentation for electrostatic measurements,” *Journal of Electrostatics*, vol. 16, no. 1, pp. 1 – 19, 1984. [Online]. Available: <http://www.sciencedirect.com/science/article/B6V02-47X7G7W-BG/2/fe3fe4052f5f6ebc2b660aaed9e52ded> Cited on 6, 91
- [6] D. P. Hammond, “A rotating vane electrometer of high sensitivity,” *Journal of Physics E: Scientific Instruments*, vol. 4, no. 2, pp. 97–98, 1971. [Online]. Available: <http://stacks.iop.org/0022-3735/4/97> Cited on 6
- [7] V. I. Struminsky, “Vibrating-wire transducers for electrostatic measurements,” *Journal of Electrostatics*, vol. 54, no. 3-4, pp. 301 – 310, 2002. [Online]. Available: <http://www.sciencedirect.com/science/article/B6V02-4555PDN-8/2/33faec4855b5ed34f45fd8001eee9284> Cited on 6

- [8] A. Kumada, Y. Shimizu, M. Chiba, and K. Hidaka, "Pockels surface potential probe and surface charge density measurement," *Journal of Electrostatics*, vol. 58, no. 1-2, pp. 45 – 58, 2003. [Online]. Available: <http://www.sciencedirect.com/science/article/B6V02-47C49KJ-1/2/5e2c79c43ae4c586408ba1f47b69bbcd> Cited on 7
- [9] K. Koo and G. Sigel, "An electric field sensor utilizing a piezoelectric polyvinylidene fluoride (pvf2) film in a single-mode fiber interferometer," *Quantum Electronics, IEEE Journal of*, vol. 18, no. 4, pp. 670–675, Apr 1982. Cited on 7
- [10] S. T. Vohra, F. Bucholtz, and A. D. Kersey, "Fiber-optic dc and low-frequency electric-field sensor," *Opt. Lett.*, vol. 16, no. 18, pp. 1445–1447, 1991. [Online]. Available: <http://ol.osa.org/abstract.cfm?URI=ol-16-18-1445> Cited on 7
- [11] R. J. Prance, T. D. Clark, H. Prance, and A. Clippingdale, "Non-contact vlsi imaging using a scanning electric potential microscope," *Measurement Science and Technology*, vol. 9, no. 8, p. 1229, 1998. [Online]. Available: <http://stacks.iop.org/0957-0233/9/i=8/a=014> Cited on 7
- [12] A. J. Clippingdale, R. J. Prance, T. D. Clark, and C. Watkins, "Ultrahigh impedance capacitively coupled heart imaging array," *Review of Scientific Instruments*, vol. 65, no. 1, pp. 269–270, 1994. [Online]. Available: <http://link.aip.org/link/?RSI/65/269/1> Cited on 7, 10
- [13] A. J. Clippingdale, R. J. Prance, T. D. Clark, and F. Brouers, "Non-invasive dielectric measurements with the scanning potential microscope," *Journal of Physics D: Applied Physics*, vol. 27, no. 11, p. 2426, 1994. [Online]. Available: <http://stacks.iop.org/0022-3727/27/i=11/a=026> Cited on 7, 10
- [14] R. J. Prance, S. T. Beardsmore-Rust, P. Watson, C. J. Harland, and H. Prance, "Remote detection of human electrophysiological signals using electric potential sensors," *Applied Physics Letters*, vol. 93, no. 3, p. 033906, 2008. [Online]. Available: <http://link.aip.org/link/?APL/93/033906/1> Cited on 8
- [15] C. J. Harland, T. D. Clark, and R. J. Prance, "Electric potential probes - new directions in the remote sensing of the human body," *Measurement Science and Technology*, vol. 13, no. 2, pp. 163–169, 2002. [Online]. Available: <http://stacks.iop.org/0957-0233/13/163> Cited on 8, 10, 37, 50, 59, 60, 61
- [16] R. J. Prance and A. Aydin, "Acquisition of a nuclear magnetic resonance signal using an electric field detection technique," *Applied Physics Letters*, vol. 91, no. 4, p.

- 044103, 2007. [Online]. Available: <http://link.aip.org/link/?APL/91/044103/1> Cited on 8, 10
- [17] W. Gebrial, R. J. Prance, C. J. Harland, P. B. Stiffell, H. Prance, and T. D. Clark, “Non-contact imaging of carbon composite structures using electric potential (displacement current) sensors,” *Measurement Science and Technology*, vol. 17, no. 6, pp. 1470–1476, 2006. [Online]. Available: <http://stacks.iop.org/0957-0233/17/1470> Cited on 8, 10
- [18] W. Gebrial, R. J. Prance, T. D. Clark, C. J. Harland, H. Prance, and M. Everitt, “Noninvasive imaging of signals in digital circuits,” *Review of Scientific Instruments*, vol. 73, no. 3, pp. 1293–1298, 2002. [Online]. Available: <http://link.aip.org/link/?RSI/73/1293/1> Cited on 8, 10
- [19] R. J. Prance, A. Debray, T. D. Clark, H. Prance, M. Nock, C. J. Harland, and A. J. Clippingdale, “An ultra-low-noise electrical-potential probe for human-body scanning,” *Measurement Science and Technology*, vol. 11, no. 3, pp. 291–297, 2000. [Online]. Available: <http://stacks.iop.org/0957-0233/11/291> Cited on 8, 10, 59
- [20] H. Rowe, “Extremely low frequency (elf) communication to submarines,” *Communications, IEEE Transactions on*, vol. 22, no. 4, pp. 371–385, Apr 1974. Cited on 9
- [21] R. Barr, D. L. Jones, and C. J. Rodger, “Elf and vlf radio waves,” *Journal of Atmospheric and Solar-Terrestrial Physics*, vol. 62, no. 17-18, pp. 1689 – 1718, 2000. [Online]. Available: <http://www.sciencedirect.com/science/article/B6VHB-41S4Y5X-D/2/d13f21a282101fd6abf9ac76465124c2> Cited on 9
- [22] M. H. Repacholi and B. Greenebaum, “Interaction of static and extremely low frequency electric and magnetic fields with living systems: Health effects and research needs,” *Bioelectromagnetics*, vol. 20, no. 3, pp. 133–160, 1999. [Online]. Available: [http://dx.doi.org/10.1002/\(SICI\)1521-186X\(1999\)20:3<133::AID-BEM1>3.0.CO;2-O](http://dx.doi.org/10.1002/(SICI)1521-186X(1999)20:3<133::AID-BEM1>3.0.CO;2-O) Cited on 10
- [23] J. Bastian, “Electrosensory organisms,” *Physics Today*, vol. 47, pp. 30–37, Feb. 1994. Cited on 10
- [24] S. Beardsmore-Rust, P. Watson, P. B. Stiffell, R. J. Prance, C. J. Harland, and H. Prance, “Detecting electric field disturbances for passive through-wall movement and proximity sensing,” *Smart Biomedical and Physiological*

- Sensor Technology VI*, vol. 7313, no. 1, p. 73130P, 2009. [Online]. Available: <http://link.aip.org/link/?PSI/7313/73130P/1> Cited on 10, 87
- [25] S. T. Beardsmore-Rust, R. J. Prance, A. Aydin, H. Prance, C. J. Harland, and P. B. Stiffell, "Signal specific electric potential sensors for operation in noisy environments," *Journal of Physics: Conference Series*, vol. 178, p. 012011 (6pp), 2009. [Online]. Available: <http://stacks.iop.org/1742-6596/178/012011> Cited on 10
- [26] S. T. Beardsmore-Rust, P. Watson, R. J. Prance, C. J. Harland, and H. Prance, "Quantitative measurement of tribo-electric charging phenomena of dielectric materials," *Proc. ESA Annual Meeting on Electrostatics 2009*, vol. Session 5, p. 1, 2009. Cited on 10
- [27] S. T. Beardsmore-Rust, P. Watson, R. Prance, C. J. Harland, and H. Prance, "Imaging of charge spatial density on insulating materials," *Measurement Science and Technology*, vol. 20, no. 9, p. 095711 (6pp), 2009. [Online]. Available: <http://stacks.iop.org/0957-0233/20/095711> Cited on 10
- [28] C. J. Harland, T. D. Clark, and R. J. Prance, "Applications of electric potential (displacement current) sensors in human body electrophysiology," in *3rd World Congress on industrial process tomography Banff Canada*, 2003. Cited on 10, 59
- [29] C. J. Harland, T. D. Clark, and R. Prance, "High resolution ambulatory electrocardiographic monitoring using wrist mounted electric," *Measurement Science and Technology*, vol. 14, no. 7, pp. 923–928, 2003. [Online]. Available: <http://stacks.iop.org/0957-0233/14/923> Cited on 10, 59
- [30] W. Gebrial, R. J. Prance, C. J. Harland, and T. D. Clark, "Noninvasive imaging using an array of electric potential sensors," *Review of Scientific Instruments*, vol. 77, no. 6, p. 063708, 2006. [Online]. Available: <http://link.aip.org/link/?RSI/77/063708/1> Cited on 10
- [31] W. Gebrial, R. J. Prance, C. J. Harland, C. Antrobus, and T. D. Clark, "The propagation delay of electrical signals in saline using electric potential sensors," *Journal of Physics D: Applied Physics*, vol. 40, no. 1, pp. 31–35, 2007. [Online]. Available: <http://stacks.iop.org/0022-3727/40/31> Cited on 10
- [32] E. J. Baranoski, "Through-wall imaging: Historical perspective and future directions," *Journal of the Franklin Institute*, vol. 345, no. 6,

- pp. 556 – 569, 2008, advances in Indoor Radar Imaging. [Online]. Available: <http://www.sciencedirect.com/science/article/B6V04-4RW43B8-1/2/124873f5c4326b95738c23c54fdd0717> Cited on 10
- [33] S. Borek, “An overview of through the wall surveillance for homeland security,” *Applied Imagery and Pattern Recognition Workshop, 2005. Proceedings. 34th*, vol. 1, pp. 6 pp.–47, Dec. 2005. Cited on 10
- [34] R. P. Post and H. M. Sasaki, “Remote video surveillance systems,” E. M. Carapezza, Ed., vol. 7333, no. 1. SPIE, 2009, p. 73330C. [Online]. Available: <http://link.aip.org/link/?PSI/7333/73330C/1> Cited on 11
- [35] H. Ruser, K. Wenzl, and C. Kargel, “Detection and tracking of humans with a sparse network of lidar sensors,” S. Mott, J. F. Buford, G. Jakobson, and M. J. Mendenhall, Eds., vol. 7352, no. 1. SPIE, 2009, p. 73520A. [Online]. Available: <http://link.aip.org/link/?PSI/7352/73520A/1> Cited on 11
- [36] J. K. Aggarwal and Q. Cai, “Human motion analysis: a review,” *Computer Vision and Image Understanding*, vol. 73, no. 3, pp. 428 – 440, 1999. [Online]. Available: <http://www.sciencedirect.com/science/article/B6WCX-45N4KFX-11/2/b6f072bae12852ac170f35bdc2d31e92> Cited on 11
- [37] V. Pavlovic, R. Sharma, and T. Huang, “Visual interpretation of hand gestures for human-computer interaction: a review,” *Pattern Analysis and Machine Intelligence, IEEE Transactions on*, vol. 19, no. 7, pp. 677–695, Jul 1997. Cited on 11
- [38] A. Bobick and J. Davis, “The recognition of human movement using temporal templates,” *Pattern Analysis and Machine Intelligence, IEEE Transactions on*, vol. 23, no. 3, pp. 257–267, Mar 2001. Cited on 11
- [39] A. Wilson and A. Bobick, “Parametric hidden markov models for gesture recognition,” *Pattern Analysis and Machine Intelligence, IEEE Transactions on*, vol. 21, no. 9, pp. 884–900, Sep 1999. Cited on 11
- [40] L. S. Theremin and O. Petrishev, “The design of a musical instrument based on cathode relays,” *Leonardo Music Journal*, vol. 6, pp. 49–50, 1996. [Online]. Available: <http://www.jstor.org/stable/1513305> Cited on 11
- [41] T. G. Zimmerman, J. R. Smith, J. A. Paradiso, D. Allport, and N. Gershenfeld, “Applying electric field sensing to human-computer interfaces,” in *CHI '95*:

*Proceedings of the SIGCHI conference on Human factors in computing systems*. New York, NY, USA: ACM Press/Addison-Wesley Publishing Co., 1995, pp. 280–287.

Cited on 11

- [42] J. A. Paradiso and N. Gershenfeld, “Musical applications of electric field sensing,” *Computer Music Journal*, vol. 21, no. 2, pp. 69–89, 1997. [Online]. Available: <http://www.jstor.org/stable/3681109> Cited on 11
- [43] J. R. Smith, “Field mice: Extracting hand geometry from electric field..” *IBM Systems Journal*, vol. 35, no. 3/4, p. 587, 1996. [Online]. Available: <http://search.ebscohost.com/login.aspx?direct=true&db=buh&AN=9708226277&site=ehost-live> Cited on 11
- [44] I. Freescale Semiconductor, “Mc33794 (electric field imaging device),” 2006, technical Data. [Online]. Available: [http://www.freescale.com/files/analog/doc/data\\_sheet/MC33794.pdf](http://www.freescale.com/files/analog/doc/data_sheet/MC33794.pdf) Cited on 11
- [45] M. Ltd, *Semiconductor Devices Data Book - Microwave transistors, diodes and subassemblies*, M. Ltd, Ed. Mullard Ltd, 1982, vol. Book 1, no. Part 5. Cited on 12
- [46] S. Banerjee, F. Steenkeste, P. Couturier, M. Debray, and A. Franco, “Telesurveillance of elderly patients by use of passive infra-red sensors in a ‘smart’ room,” *J Telemed Telecare*, vol. 9, no. 1, pp. 23–29, 2003. [Online]. Available: <http://jtt.rsmjournals.com/cgi/content/abstract/9/1/23> Cited on 12
- [47] S. Nag, M. A. Barnes, T. Payment, and G. Holladay, “Ultrawideband through-wall radar for detecting the motion of people in real time,” *Radar Sensor Technology and Data Visualization*, vol. 4744, no. 1, pp. 48–57, 2002. [Online]. Available: <http://link.aip.org/link/?PSI/4744/48/1> Cited on 12
- [48] S. Nag, H. Fluhler, and M. Barnes, “Preliminary interferometric images of moving targets obtained using a time-modulated ultra-wide band through-wall penetration radar,” *Radar Conference, 2001. Proceedings of the 2001 IEEE*, vol. 1, pp. 64–69, 2001. Cited on 12
- [49] A. Jain, “Technology: Biometric recognition,” *Nature*, vol. 449, no. 7158, pp. 38–40, 2007. Cited on 13

- [50] A. Watson, "Biometrics: Easy to steal, hard to regain identity," *Nature*, vol. 449, no. 7162, pp. 535–, 2007. Cited on 13
- [51] G. Lawton, "Biometrics: A new era in security," *Computer*, vol. 31, no. 8, pp. 16–18, Aug 1998. Cited on 13
- [52] N. K. Ratha, J. H. Connell, and R. M. Bolle, "Enhancing security and privacy in biometrics-based authentication systems." *IBM Systems Journal*, vol. 40, no. 3, pp. 614 –, 2001. [Online]. Available: <http://search.ebscohost.com/login.aspx?direct=true&db=buh&AN=5081427&site=ehost-live> Cited on 13
- [53] A. Jain, L. Hong, and S. Pankanti, "Biometric identification." *Communications of the ACM*, vol. 43, no. 2, pp. 90 – 98, 2000. [Online]. Available: <http://search.ebscohost.com/login.aspx?direct=true&db=buh&AN=11888174&site=ehost-live> Cited on 13
- [54] N. J. Grabham and N. M. White, "Validation of keypad user identity using a novel biometric technique," *Journal of Physics: Conference Series*, vol. 76, p. 012023 (6pp), 2007. [Online]. Available: <http://stacks.iop.org/1742-6596/76/012023> Cited on 13
- [55] U. Morbiducci, L. Scalise, M. De Melis, and M. Grigioni, "Optical vibrocardiography: a novel tool for the optical monitoring of cardiac activity," *Annals of Biomedical Engineering*, vol. 35, no. 1, pp. 45–58, Jan. 2007. [Online]. Available: <http://dx.doi.org/10.1007/s10439-006-9202-9> Cited on 14
- [56] T. Matsui, I. Arai, S. Gotoh, H. Hattori, B. Takase, M. Kikuchi, and M. Ishihara, "A novel apparatus for non-contact measurement of heart rate variability: a system to prevent secondary exposure of medical personnel to toxic materials under biochemical hazard conditions, in monitoring sepsis or in predicting multiple organ dysfunction syndrome," *Biomedicine & Pharmacotherapy*, vol. 59, no. Supplement 1, pp. S188 – S191, 2005, proceedings of the 5th International Symposium Workshop on Circadian Rhythms and Clinical Chronotherapy. [Online]. Available: <http://www.sciencedirect.com/science/article/B6VKN-4HGTNB0-12/2/27bdde96cca7a3b16fca33432e750501> Cited on 14
- [57] G. Binnig, H. Rohrer, C. Gerber, and E. Weibel, "Surface studies by scanning tunneling microscopy," *Phys. Rev. Lett.*, vol. 49, no. 1, pp. 57–61, Jul 1982. Cited on 14, 15

- [58] A. Majumdar, “Scanning thermal microscopy,” *Annual Review of Materials Science*, vol. 29, no. 1, pp. 505–585, 1999. [Online]. Available: <http://arjournals.annualreviews.org/doi/abs/10.1146/annurev.matsci.29.1.505> Cited on 15
- [59] J. R. Matey and J. Blanc, “Scanning capacitance microscopy,” *Journal of Applied Physics*, vol. 57, no. 5, pp. 1437–1444, 1985. [Online]. Available: <http://link.aip.org/link/?JAP/57/1437/1> Cited on 15
- [60] P. Henry, “The role of asymmetric rubbing in the generation of static electricity,” *Applied Physics Letters*, vol. 4, pp. S31–S36, 1953. Cited on 16
- [61] J. Fuhrmann, “Contact electrification of dielectric solids,” *Journal of Electrostatics*, vol. 4, no. 2, pp. 109 – 118, 1978. [Online]. Available: <http://www.sciencedirect.com/science/article/B6V02-47X7FJ0-36/2/20c1c7b94db450dff6775f6c71f90f6d> Cited on 16, 90
- [62] B. Gross, G. M. Sessler, and J. E. West, “Charge dynamics for electron-irradiated polymer-foil electrets,” *Journal of Applied Physics*, vol. 45, no. 7, pp. 2841–2851, 1974. [Online]. Available: <http://link.aip.org/link/?JAP/45/2841/1> Cited on 16, 91
- [63] B. Gross, “Experiments on electrets,” *Phys. Rev.*, vol. 66, no. 1-2, pp. 26–28, Jul 1944. Cited on 16, 90
- [64] G. M. Sessler and M. G. Broadhurst, *Electrets*, 3rd ed., ser. The Laplacian Press series on electrostatics. Morgan Hill, Calif. :: Laplacian Press., c1998., vol. Vol.1, previous ed. published as 1 v. : Berlin : Springer, 1987. Cited on 16, 91
- [65] D. M. Taylor and P. E. Secker, *Industrial electrostatics : fundamentals and measurements*, ser. Electronic & electrical engineering research studies. 13 Electrostatics and electrostatic applications series ;. Taunton, Somerset, England :: Research Studies Press, c1994., includes bibliographical references and indexes. Cited on 16, 91
- [66] A. F. Diaz and R. M. Felix-Navarro, “A semi-quantitative tribo-electric series for polymeric materials: the influence of chemical structure and properties,” *Journal of Electrostatics*, vol. 62, no. 4, pp. 277 – 290, 2004. [Online]. Available: <http://www.sciencedirect.com/science/article/B6V02-4CS8J93-1/2/d373ed322d60fa531322ecc0bc1d3b59> Cited on 16, 102, 104

- [67] J. G. Graeme, *Applications of operational amplifiers : third-generation techniques*, ser. The BB electronics series. New York ; London :: McGraw-Hill., 1973., includes index. Cited on 19, 20
- [68] J. F. Keithley, *Low level measurements : precision DC current, voltage and resistance measurements.*, 5th ed. Berkshire :: Keithley Instruments Inc., 1998, first published: 1972. Cited on 20
- [69] *AD5290 Compact +30 V / 15 V 256-Position Digital Potentiometer*, Analog Devices, Norwood MA 02062. Cited on 22
- [70] H. National Instruments Corp. (UK) Ltd and U. N. Road, Berkshire RG14 5SJ, 2008. [Online]. Available: <http://www.ni.com> Cited on 22, 60, 67, 80, 92
- [71] N. Semiconductor, *LMF100 Switched Capacitor Filter Datasheet*, 2900 Semiconductor Drive P.O. Box 58090 Santa Clara, California, 1999. Cited on 40, 41, 44
- [72] R. J. Prance, S. Beardsmore-Rust, H. Prance, C. J. Harland, and P. B. Stiffell, “Adaptive electric potential sensors for smart signal acquisition and processing,” *Journal of Physics: Conference Series*, vol. 76, p. 012025 (5pp), 2007. [Online]. Available: <http://stacks.iop.org/1742-6596/76/012025> Cited on 45
- [73] O. S. Narula, *His bundle electrocardiography and clinical electrophysiology*. Philadelphia :: F. A. Davis Co., 1975, includes bibliographical references and index. Cited on 59
- [74] C. S. Breathnach and W. Westphal, “Early detectors of the heart’s electrical activity,” *Pacing and Clinical Electrophysiology*, vol. 29, no. 4, pp. 422–424, 2006. [Online]. Available: <http://dx.doi.org/10.1111/j.1540-8159.2006.00363.x> Cited on 59
- [75] C. J. Harland, T. D. Clark, and R. J. Prance, “Remote detection of human electroencephalograms using ultrahigh input impedance electric potential sensors,” *Applied Physics Letters*, vol. 81, no. 17, pp. 3284–3286, 2002. [Online]. Available: <http://link.aip.org/link/?APL/81/3284/1> Cited on 59
- [76] H. Prance, P. Watson, R. Prance, C. Harland, S. Beardsmore-Rust, and A. Aydin, “High spatial resolution, dry-electrode surface emg aquisition system,” in *Proceedings of AAATE 2009*, 2009, pp. pp 109–113. Cited on 59
- [77] M. Malik, J. T. Bigger, A. J. Camm, R. E. Kleiger, A. Malliani, A. J. Moss, and P. J. Schwartz, “Heart rate variability: Standards of measurement, physiological

- interpretation, and clinical use,” *Eur Heart J*, vol. 17, no. 3, pp. 354–381, 1996. [Online]. Available: <http://eurheartj.oxfordjournals.org> Cited on 59
- [78] S. C. Malpas and T. J. Maling, “Heart-rate variability and cardiac autonomic function in diabetes.” *Diabetes*, vol. 39, no. 10, pp. 1177–1181, 1990. [Online]. Available: <http://diabetes.diabetesjournals.org/content/39/10/1177.abstract> Cited on 59
- [79] J. A. Chalmers, *Atmospheric electricity*, 2nd ed., ser. International series of monographs in natural philosophy ; v. 11. Oxford :: Pergamon Press,, 1967, bibliography: p. 451-499. Cited on 65
- [80] T. Ficker, “Charging by walking,” *Journal of Physics D: Applied Physics*, vol. 39, no. 2, p. 410, 2006. [Online]. Available: <http://stacks.iop.org/0022-3727/39/i=2/a=025> Cited on 66
- [81] R. Feynman, R. B. Leighton, and M. Sands, *The Feynman lectures on physics*. San Francisco :: Pearson/Addison-Wesley, 1963, originally published: 1963-1965. Cited on 66
- [82] *COMSOL Multiphysics*, COMSOL, Stockholm, 2008. [Online]. Available: <http://www.comsol.com> Cited on 75
- [83] K. A. Hughes and P. E. Secker, “A two-dimensional charge scanning instrument for flat insulating sheet,” *Journal of Physics E: Scientific Instruments*, vol. 4, no. 5, pp. 362–365, 1971. [Online]. Available: <http://stacks.iop.org/0022-3735/4/362> Cited on 91
- [84] *610C Solid State Electrometer*, Keithley Instruments, Cleveland, Ohio. Cited on 103

## Appendix A

### Labview VIs

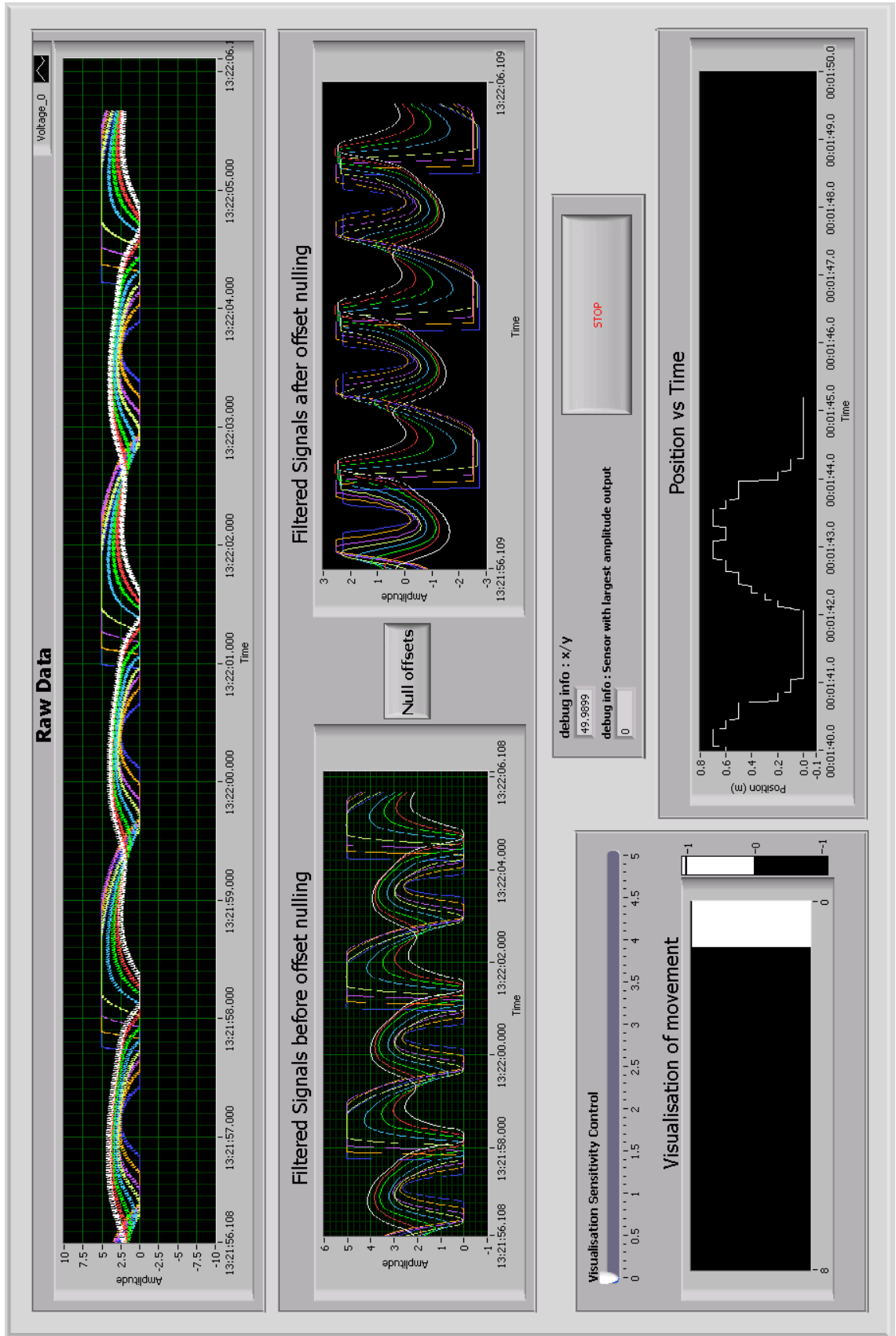


Figure A.1: Pendulum Movement Experiment Front Panel

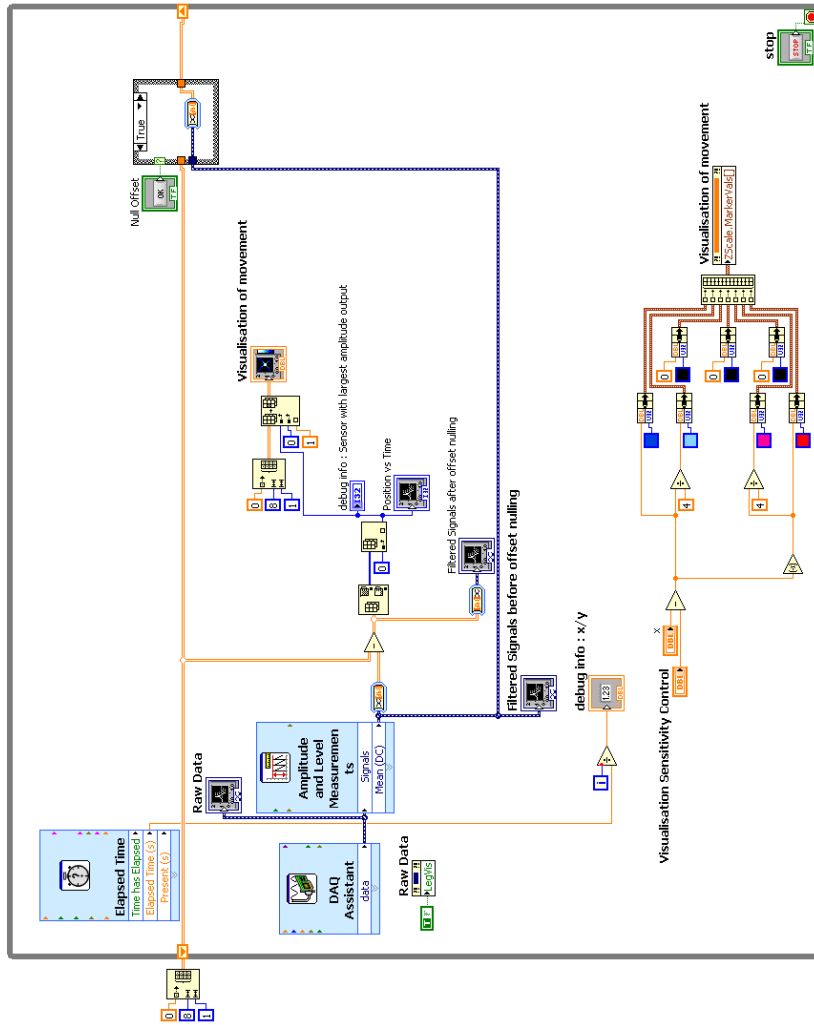


Figure A.2: Pendulum Movement Experiment Block Diagram

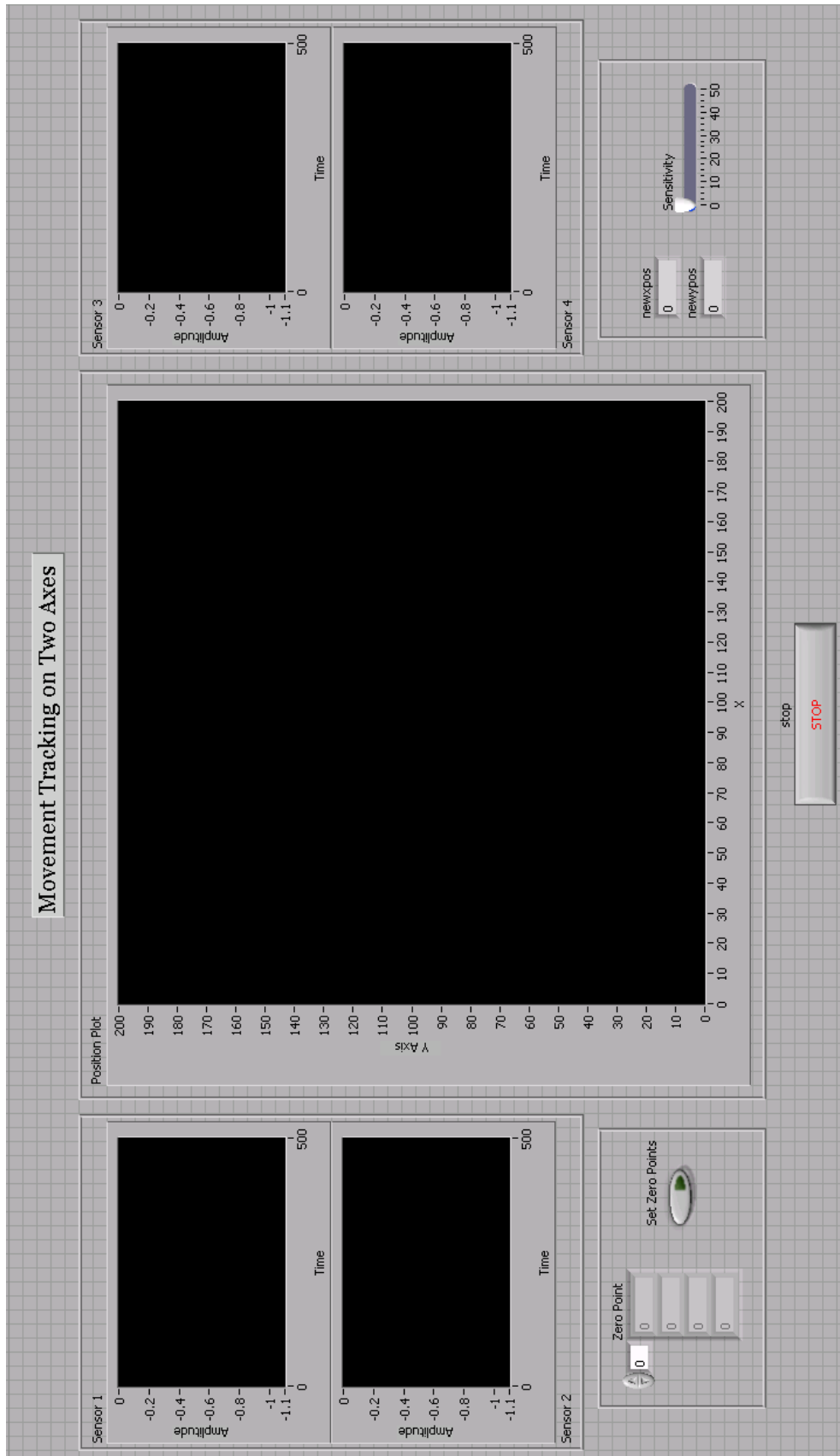


Figure A.3: 2D Movement Experiment Front Panel

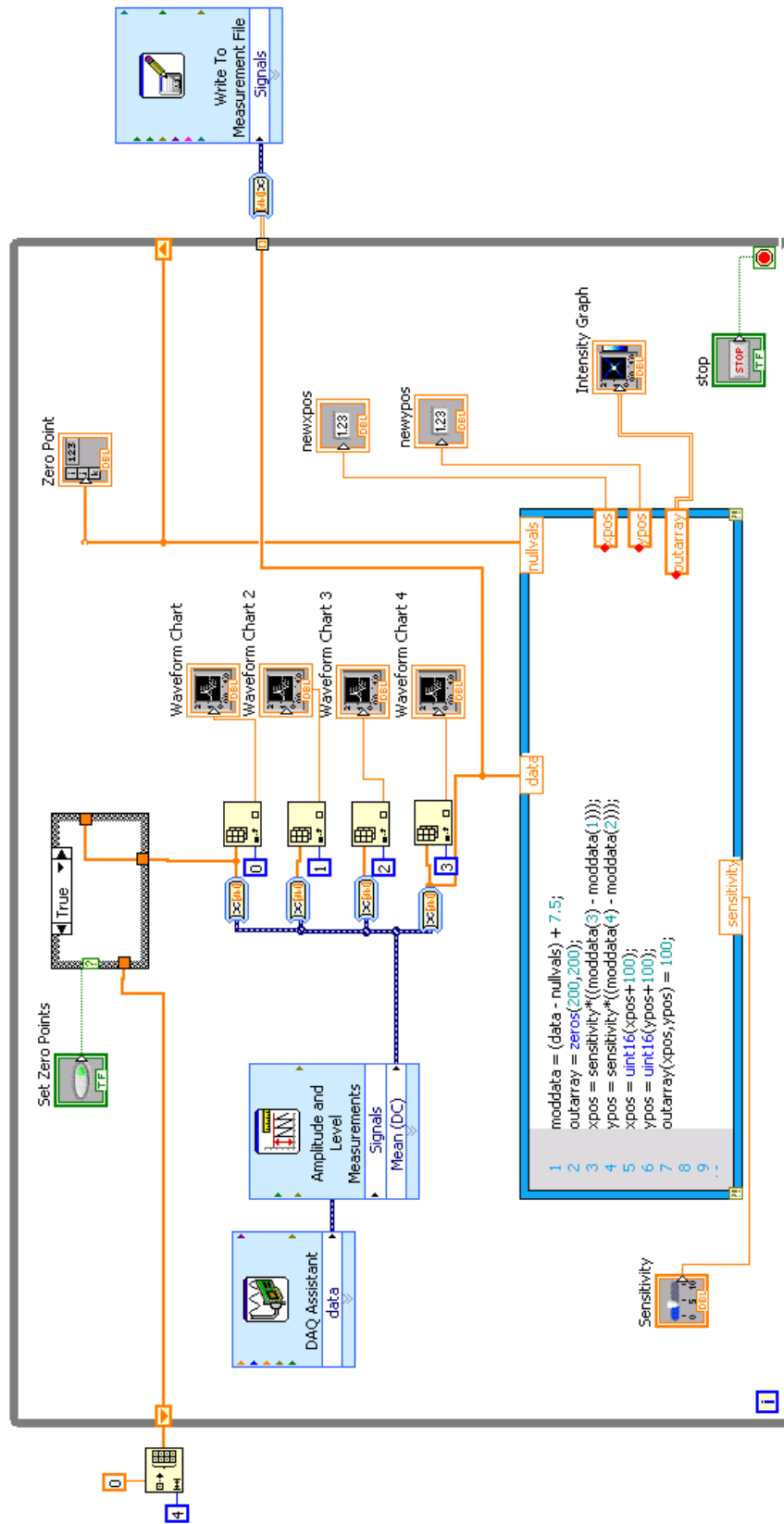


Figure A.4: 2D Movement Experiment Block Diagram

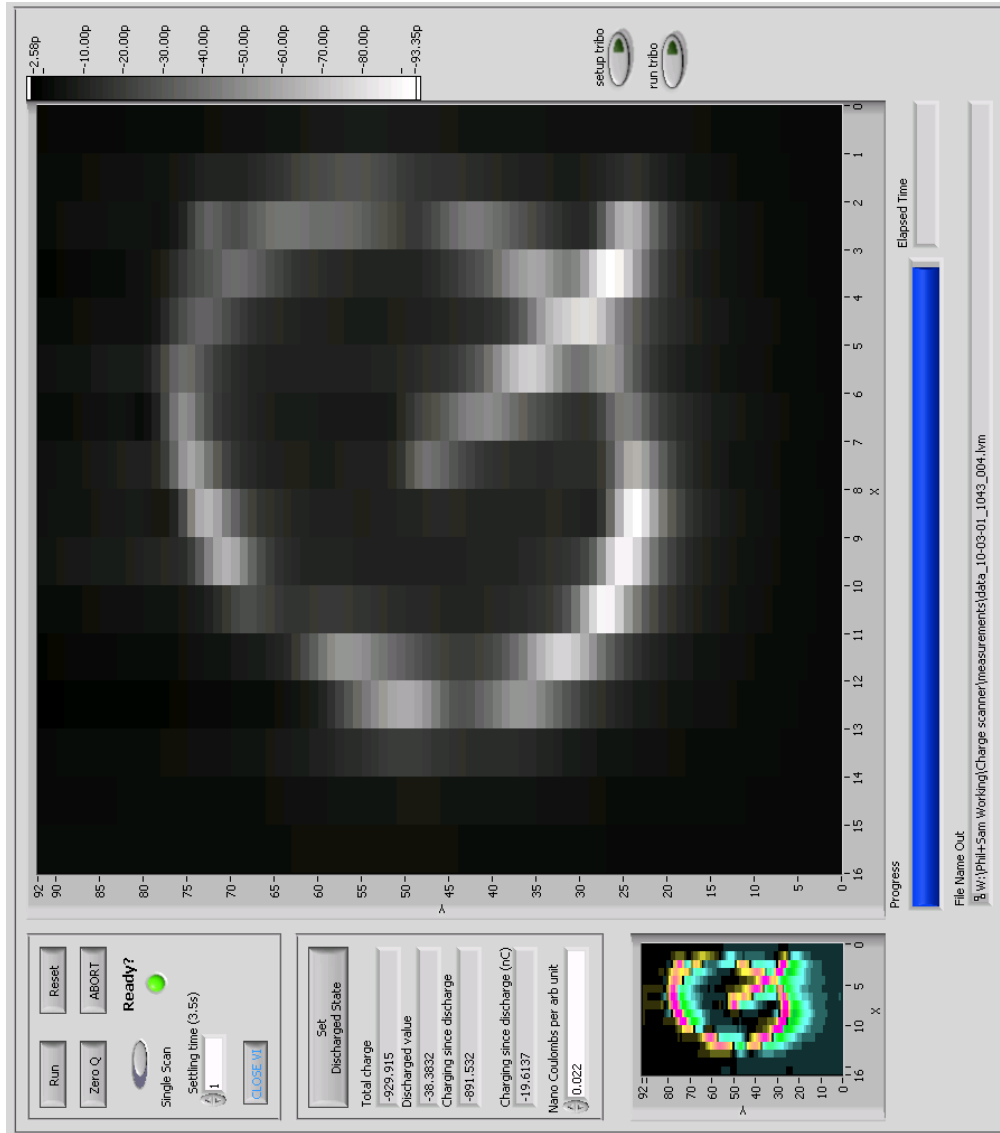


Figure A.5: The Charge Scanner Virtual Instrument Front Panel

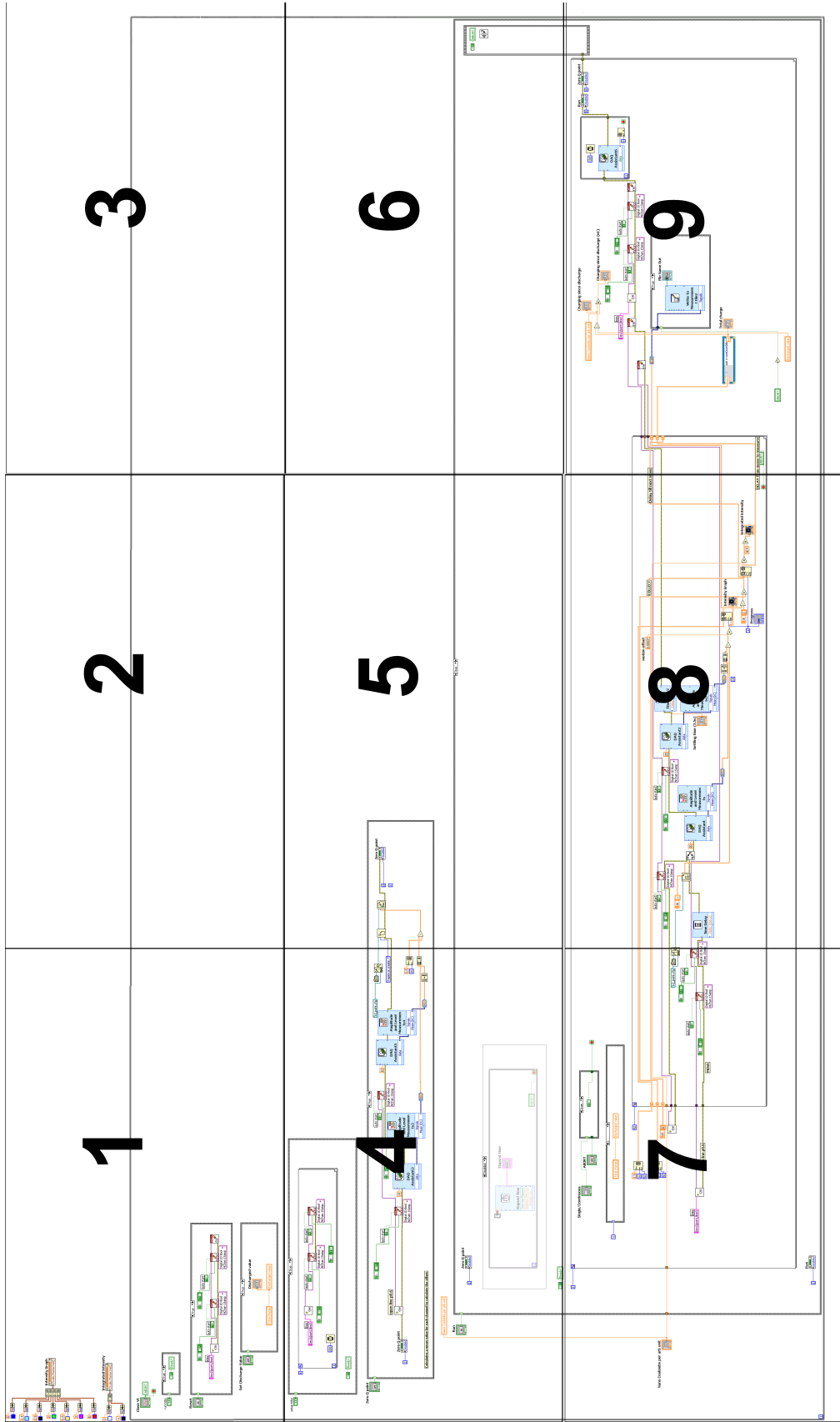


Figure A.6: The Charge Scanner Virtual Instrument

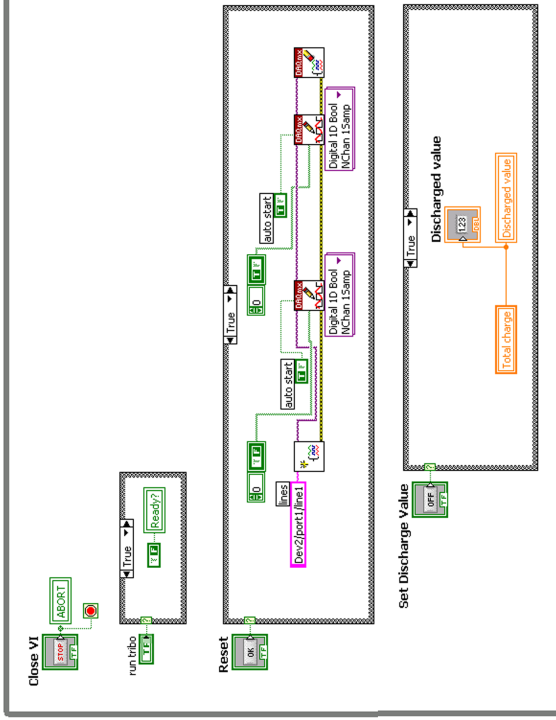
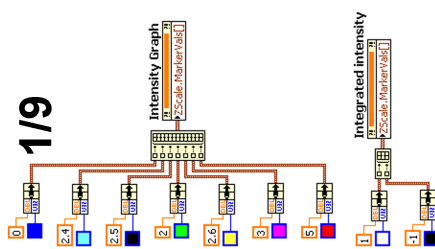


Figure A.7: The Charge Scanner Virtual Instrument - detail 1 of 9



Figure A.8: The Charge Scanner Virtual Instrument - detail 2 of 9



Figure A.9: The Charge Scanner Virtual Instrument - detail 3 of 9

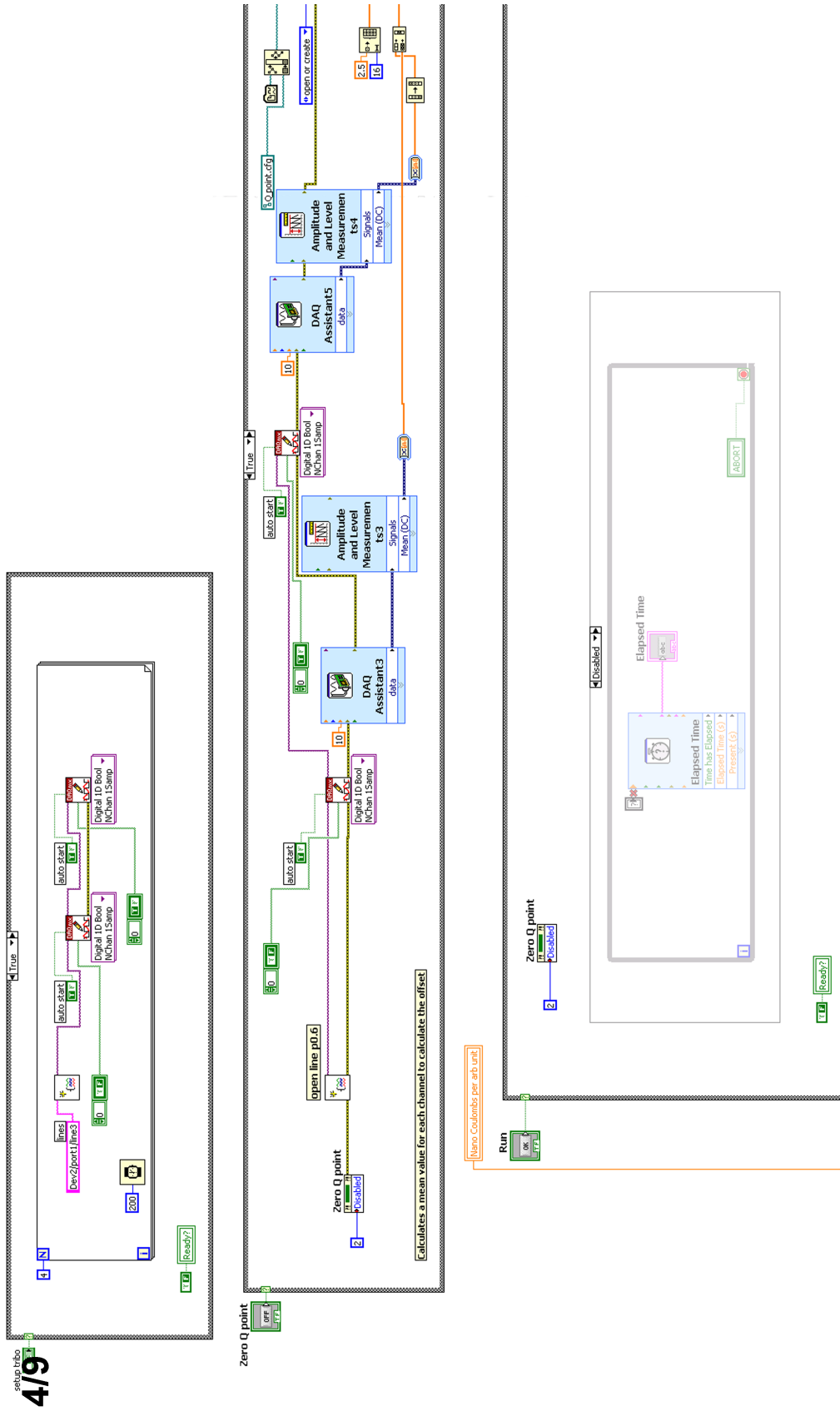


Figure A.10: The Charge Scanner Virtual Instrument - detail 4 of 9

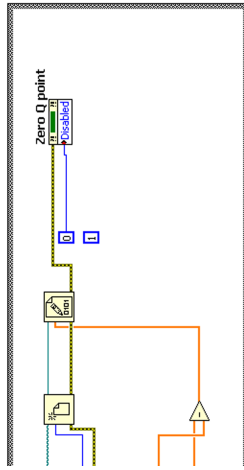


Figure A.11: The Charge Scanner Virtual Instrument - detail 5 of 9

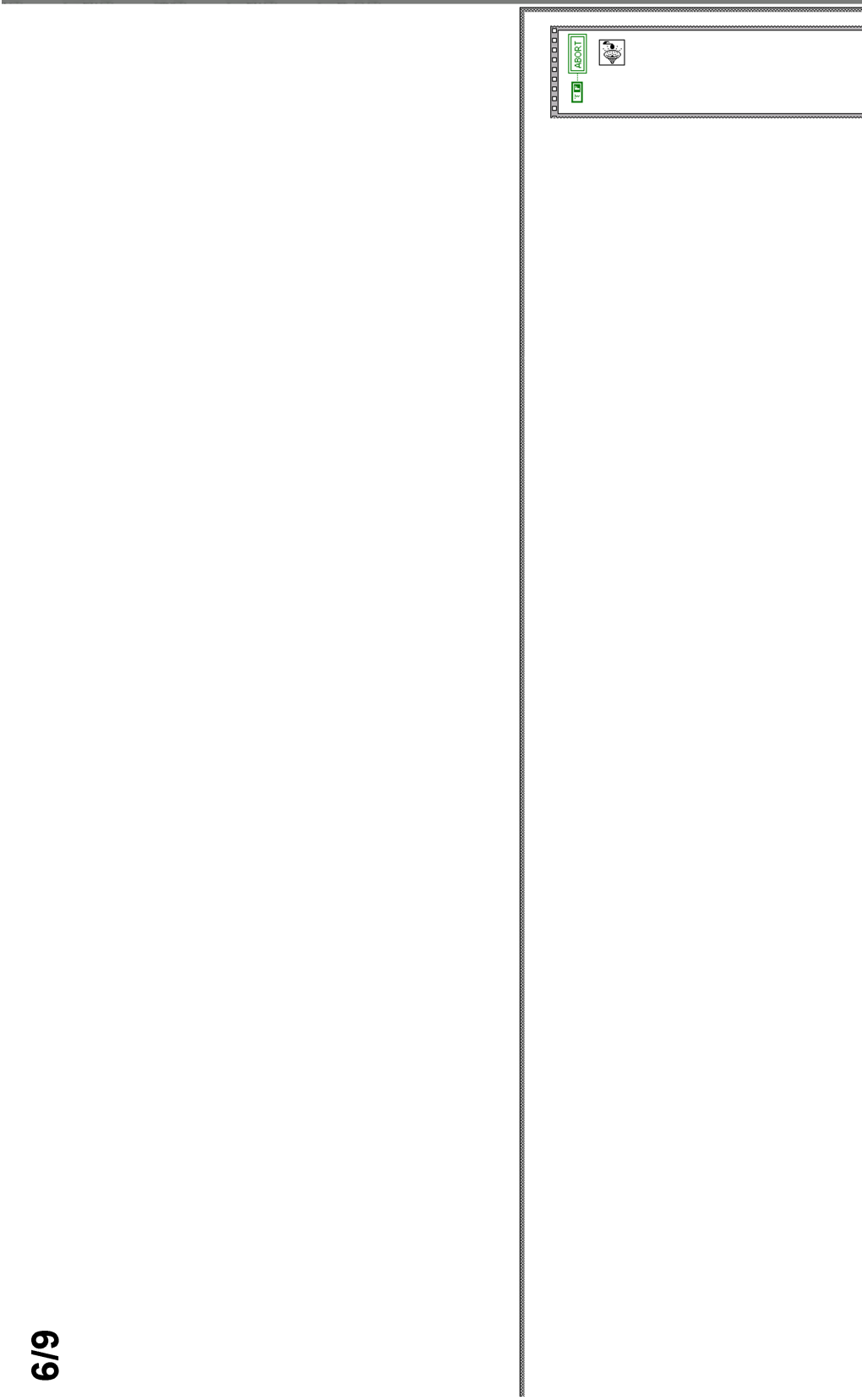


Figure A.12: The Charge Scanner Virtual Instrument - detail 6 of 9



8/9

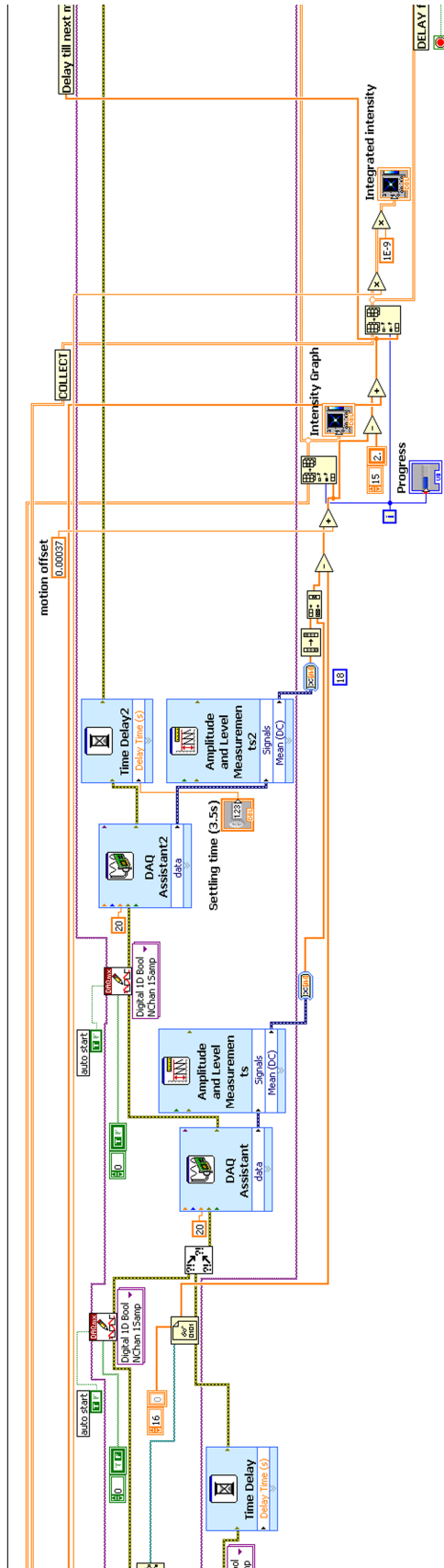


Figure A.14: The Charge Scanner Virtual Instrument - detail 8 of 9



## Appendix B

# Microprocessor Assembler Code

```

D:\SAMPIC\XY scanner\xyvarspeed.ASM

        list      p=PIC16F877
        include   <P16F877.INC>
        _CONFIG _CP_OFF & _WDT_OFF & _BODEN_OFF & _PWRTE_ON & _HS_OSC & _WRT_ENABLE_ON &
        _LVP_OFF & _DEBUG_OFF & _CPD_OFF

;*****
; XY controller software
; Sam Beardsmore-Rust using modified LCD libraries also by SBR
; Ensure RC5 and RC2 are kept high for full steps
;
; Enable left/right with RD1
; Enable up/down with RD2
;
; RC0 = left switch
; RC1 = right switch
;*****
; 4 BIT LCD interface with PIC
; only port B is implemented
; Includes subroutines for driving standard LCD display
; RB7-RB4 = DB7-DB4 ; RB3=E ; RB2=RW ; RB1=RS
;
; Released 21st August
; Copyright Sam Beardsmore-Rust
;*****

;declaration
BIT_E EQU 3
BIT_RW EQU 2
BIT_RS EQU 1

        cblock 0x20
            TEMP
            TEMP2
            V_DLY
            V_DLY1
            V_DLY2
            V_DLY3
            V_DLY4
            V_DLY20MHZ
            SCROLL_COUNTER
            DIGITSTATE
            DIGIT100S ; this holds the 100s from VALUE
            DIGIT10S ; this holds the 10s from VALUE
            DIGIT1S ; this holds the 1s from VALUE
            VALUE ; this will hold the hex value
            SCREEN_OFFSET
            W2
            CHECKW
            SPEEDLOOP
            EGGCOUNTER1
            EGGCOUNTER2
            CLOCKWASHIGH
            ZEROWASHIGH
            PREVPORTA
        endc

        org 0x0000
; STARTUP code
        GOTO START
        nop
        nop
        nop

ISR
        GOTO INT

        org 0x005 ;start of program at
        goto START

INT
        RETFIE ; blank ISR (Interrupt Service Routine)

; Tables that follow are for use by various LCD related routines. it is essential they remain at
; the start of memory space
; as any overlapping into subsequent pages of memory will cause serious problems and almost
; certainly result in crashes

```

Figure B.1: XY Scanner Motor Control and LCD Display code - 1 of 15

```

D:\SAMPIC\XY_scanner\xyvarspeed.ASM

; and death. Ignore this warning at your peril.]

NUMTABLE
    ADDWF PCL,1
    RETLW '0'
    RETLW '1'
    RETLW '2'
    RETLW '3'
    RETLW '4'
    RETLW '5'
    RETLW '6'
    RETLW '7'
    RETLW '8'
    RETLW '9'
NUMTABLE_END
    RETLW 0x00

DIGIT_100_TABLE
    ADDWF PCL,1
    RETLW 0x00
    RETLW D'100'
    RETLW D'200'
DIGIT_100_TABLE_END
    RETLW 0x00

DIGIT_10_TABLE
    ADDWF PCL,1
    RETLW 0x00
    RETLW D'10'
    RETLW D'20'
    RETLW D'30'
    RETLW D'40'
    RETLW D'50'
    RETLW D'60'
    RETLW D'70'
    RETLW D'80'
    RETLW D'90'
DIGIT_10_TABLE_END
    RETLW 0x00

; tables end, initialisation code begins.]

START
; initialize PIC - sets up inputs and registers, modify this routine to suit your requirements
    CALL INITPIC
; initialize LCD - This should not require modifying, but read data sheet for Samsung KS0070B LCD
controller or similar for more information
    CALL INITLCD

; initialise some registers to zero
    MOVLW 0x00
    MOVWF DIGITSTATE
    MOVWF SCREEN_OFFSET

; disable interrupts as they are not required for these library functions. You may want to enable
this for some projects.]
    BCF INTCON,GIE

; main function
MAIN
    CALL STATUSIS
;    CALL VERYLONGDELAY
    BSF PORTD,2 ; Enable motor controllers ( added as of 16th of jan 2009)
    BSF PORTD,1
    BSF PORTA,0;
    MOVLW 0x40
    CALL VLONGDELAY
    CALL OK

;TEST
;    MOVLW 0xFF
;    XORWF PORTA,1
;    CALL SHORTDLY
;    CALL CLEARSCREEN
;    MOVLW 'C'
;    CALL LCDWRITE
;    MOVLW '1'

```

Figure B.2: XY Scanner Motor Control and LCD Display code - 2 of 15

D:\SAMPIC\XY\_scanner\xyvarspeed.ASM

```

;      CALL    LCDWRITE
;      GOTO    TEST

;      MOVLW   'A'
;      CALL    LCDWRITE
;      BTFSC   PORTA,5
;      CALL    CLOCKMOVE
;      MOVLW   'B'
;      CALL    LCDWRITE
;      BTFSC   PORTA,2
;      GOTO    ZEROMOVE
;      MOVLW   'C'
;      CALL    LCDWRITE
;      BTFSC   TMR1H,7
;      GOTO    TIMER1
;      MOVLW   'E'
;      CALL    LCDWRITE
;      BTFSC   PORTE,0
;      GOTO    FULL
;      GOTO    HALF
MLOOP

      CALL    CHECKCLOCKPULSE
      CALL    CHECKZEROPULSE

      BTFSC   TMR1H,7
      GOTO    TIMER1

      BTFSC   PORTE,0
      GOTO    FULL
      GOTO    HALF
      GOTO    MLOOP

CHECKCLOCKPULSE
      BTFSC   PORTA,5      ; Check clock pin
      BSF    CLOCKWASHIGH,0 ; If it's high, set clock was high bit
      BTFSC   CLOCKWASHIGH,0 ; check clockwashigh bit
      GOTO    JCLOCKWASHIGH ; and if it was high, go to clockwashigh
      GOTO    JCLOCKWASLOW

JCLOCKWASHIGH
      BTFSC   PORTA,5      ; check state of port now
      RETURN            ; Clock is still high, so do nothing
      BCF    CLOCKWASHIGH,0 ; if it's now low, clear clockwashigh bit
      CALL    CLOCKMOVE    ; and go to clockmove
      RETURN            ; then return to main loop

JCLOCKWASLOW
      RETURN            ; if it is high, and was high, do nothing.

CHECKZEROPULSE
      BTFSC   PORTA,2      ; Check clock pin
      BSF    ZEROWASHIGH,0 ; If it's high, set clock was high bit
      BTFSC   ZEROWASHIGH,0 ; check clockwashigh bit
      GOTO    JZEROWASHIGH ; and if it was high, go to clockwashigh
      GOTO    JZEROWASLOW

JZEROWASHIGH
      BTFSC   PORTA,2      ; check state of port now
      RETURN            ; Clock is still high, so do nothing
      BCF    ZEROWASHIGH,0 ; if it's now low, clear clockwashigh bit
      CALL    ZEROMOVE    ; and go to clockmove
      RETURN            ; then return to main loop

JZEROWASLOW
      RETURN            ; if it is high, and was high, do nothing.

TIMER1
      CLRF   TMR1H
      INCF   EGGCOUNTER1,1
      BTFSC   EGGCOUNTER1,7
      GOTO    TIMER2
      GOTO    MLOOP

TIMER2
      CLRF   EGGCOUNTER1
      INCF   EGGCOUNTER2,1
      BTFSC   EGGCOUNTER2,7

```

Figure B.3: XY Scanner Motor Control and LCD Display code - 3 of 15

```

GOTO DOEGG
GOTO MLOOP

DOEGG
CLRF EGGCOUNTER1
CLRF EGGCOUNTER2
CLRF TMR1H
CALL OFFSCREEN
CALL JK1
CALL SCROLL_TEXT
MOVLW 0x4F
CALL VLONGDELAY
CALL SCROLL_BACK
GOTO MLOOP

JK1
MOVLW 'S'
CALL LCDWRITE
MOVLW '&'
CALL LCDWRITE
MOVLW 'P'
CALL LCDWRITE
MOVLW ' '
CALL LCDWRITE
MOVLW 'I'
CALL LCDWRITE
MOVLW 'm'
CALL LCDWRITE
MOVLW 'a'
CALL LCDWRITE
MOVLW 'g'
CALL LCDWRITE
MOVLW 'i'
CALL LCDWRITE
MOVLW 'n'
CALL LCDWRITE
MOVLW 'g'
CALL LCDWRITE
CALL LINE2
MOVLW 'S'
CALL LCDWRITE
MOVLW 't'
CALL LCDWRITE
MOVLW 'u'
CALL LCDWRITE
MOVLW 'f'
CALL LCDWRITE
MOVLW 'f'
CALL LCDWRITE
MOVLW ' '
CALL LCDWRITE
MOVLW 's'
CALL LCDWRITE
MOVLW 'i'
CALL LCDWRITE
MOVLW 'n'
CALL LCDWRITE
MOVLW 'c'
CALL LCDWRITE
MOVLW 'e'
CALL LCDWRITE
MOVLW ' '
CALL LCDWRITE
MOVLW '2'
CALL LCDWRITE
MOVLW '0'
CALL LCDWRITE
MOVLW '0'
CALL LCDWRITE
MOVLW '9'
CALL LCDWRITE
RETURN

FULL
BCF PORTC,5 ; set for full steps

```

```

D:\SAMPIC\XY_scanner\xyvarspeed.ASM

BCF    PORTC,2 ; set for full steps
GOTO   MLOOP

HALF|
BSF    PORTC,5 ; set for half steps
BSF    PORTC,2 ; set for half steps
GOTO   MLOOP

ZEROMOVE|
;      CLRWF    TMR1H
;      CLRWF    EGGCOUNTER1
;      CLRWF    EGGCOUNTER2
;      CALL     SHORTDLY
;      BTFSS    PORTA,2
;      RETURN   ; return if clock line not still high after a short wait, attempt to be
noise tolerant|
CALL   CLEARSCREEN
MOVLW '2'
CALL   LCDWRITE
MOVLW 'e'
CALL   LCDWRITE
MOVLW 't'
CALL   LCDWRITE
MOVLW 'o'
CALL   LCDWRITE
MOVLW 'i'
CALL   LCDWRITE
MOVLW 'n'
CALL   LCDWRITE
MOVLW 'g'
CALL   LCDWRITE
MOVLW '.'
CALL   LCDWRITE
MOVLW '.'
CALL   LCDWRITE
MOVLW '.'
CALL   LCDWRITE
MOVLW '.'
CALL   LCDWRITE
MOVLW ' '
CALL   LINE2

GOTOZERO|
CALL   SHORTDLY
CALL   CHECKRIGHTLIM
MOVWF  CHECKW
BTFSC  CHECKW,0
GOTO   RIGHTLIM
CALL   MOVERIGHT
GOTO   GOTOZERO

RIGHTLIM|
CALL   SHORTDLY
CALL   CHECKDOWNLIM
MOVWF  CHECKW
BTFSC  CHECKW,0
GOTO   ENDMOVE
CALL   MOVEDOWN
GOTO   RIGHTLIM

ENDMOVE|
MOVLW 'C'
CALL   LCDWRITE
MOVLW 'o'
CALL   LCDWRITE
CALL   LCDWRITE
MOVLW 'm'
CALL   LCDWRITE
MOVLW 'p'
CALL   LCDWRITE
MOVLW 'i'
CALL   LCDWRITE
CALL   LCDWRITE
MOVLW 'e'
CALL   LCDWRITE
MOVLW 't'
CALL   LCDWRITE
CALL   LCDWRITE
MOVLW 'e'
CALL   LCDWRITE
MOVLW ' '
CALL   LCDWRITE
MOVLW '0x40'

```

Figure B.5: XY Scanner Motor Control and LCD Display code - 5 of 15

```

D:\SAMPIC\XY_scanner\xyvarspeed.ASM

CALL    VLONGDELAY
CALL    STATUSIS
CALL    OK
GOTO    MLOOP
;      BCF    PORTD,1
;      BCF    PORTD,2
RETURN

CLOCKMOVE
CLRFB   EGGCOUNTER1
CLRFB   EGGCOUNTER2
CLRFB   TMR1H
;      CALL   INITLCD
;      MOVLW  'C'
;      CALL   LCDWRITE
;      MOVLW  '1'
;      CALL   LCDWRITE
;      CALL   SHORTDLY
;      BTFSS  PORTA,5
;      RETURN ; return if clock line not still high after a short wait, attempt to be
noise tollerant
;      MOVLW  '2'
;      CALL   LCDWRITE

MOVLM   0x0A ; Assume high speed
MOVWF   SPEEDLOOP ; set speedloop to 10
MOVLM   0x01 ; move 1 to W
BTFSC   PORTE,1 ; check if low speed (low/!high)
MOVWF   SPEEDLOOP ; if flag high, low speed selected, move 01 into loop counter.

BTFSC   PORTA,3
GOTO    XMOVE
GOTO    YMOVE

XMOVE
;      MOVLW  'X'
;      CALL   LCDWRITE
;      BTFSC  PORTA,4
;      GOTO   XPLUS
;      GOTO   XMINUS

YMOVE
;      MOVLW  'Y'
;      CALL   LCDWRITE
;      BTFSC  PORTA,4
;      GOTO   YPLUS
;      GOTO   YMINUS

XMINUS
;      MOVLW  '+'
;      CALL   LCDWRITE
;      CALL   MOVELEFT
;      GOTO   CLKRESET

XPLUS
;      MOVLW  '-'
;      CALL   LCDWRITE
;      CALL   MOVERIGHT
;      GOTO   CLKRESET

YPLUS
;      MOVLW  '+'
;      CALL   LCDWRITE
;      CALL   MOVEUP
;      GOTO   CLKRESET

YMINUS
;      MOVLW  '-'
;      CALL   LCDWRITE
;      CALL   MOVEDOWN
;      GOTO   CLKRESET

CLKRESET
;      MOVLW  'C'
;      CALL   LCDWRITE
;      BTFSC  PORTA,5
;      GOTO   CLKRESET
;      CALL   SHORTDLY
;      BTFSC  PORTA,5

```

Figure B.6: XY Scanner Motor Control and LCD Display code - 6 of 15

```

D:\SAMPIC\XY_scanner\xyvarspeed.ASM

; GOTO CLKRESET
; CALL STATUSIS
; CALL OK
RETURN

;TEST
;
; CALL MOVERIGHT
; GOTO TEST
;
; CALL INITLCD
; MOVLW 'S'
; CALL LCDWRITE
; MOVLW 't'
; CALL LCDWRITE
; MOVLW 'o'
; CALL LCDWRITE
; MOVLW 'p'
; CALL LCDWRITE
; BCF PORTA,0

GOTOFAR
CALL CHECKLEFTLIM
MOVWF CHECKRW
BTFSK CHECKRW,0
GOTO LEFTLIM
CALL MOVELEFT
GOTO GOTOFAR

LEFTLIM
CALL CHECKUPLIM
MOVWF CHECKRW
BTFSK CHECKRW,0
GOTO ENDMOVE
CALL MOVEUP
GOTO LEFTLIM
RETURN

;
; BTFSK PORTC,6
; GOTO UPLIM ;if not left or up, then move both
; BSF PORTD,0 ; go left
; BCF PORTD,3 ; and up
; BCF PORTC,3 ; clock low, now wait 5ms
; BCF PORTC,4 ; clock low, now wait 5ms
; CALL DLYIMS
; BSF PORTC,3 ; clock high, now wait 5ms
; BSF PORTC,4 ; clock high, now wait 5ms
; CALL DLYIMS
; GOTO GOTOZERO
;LEFTLIM
; BTFSK PORTC,6 ; check not up and left, as if that's the case we have finished moving to
zero
; RETURN
; CALL MOVEUP ; otherwise, need to keep moving up
; GOTO LEFTLIM
;UPLIM
; BTFSK PORTC,0
; RETURN
; CALL MOVELEFT
; GOTO UPLIM

CHECKLEFTLIM
BTFSK PORTC,0
RETLW 0x00
CALL DLY
BTFSK PORTC,0
RETLW 0x00
RETLW 0xFF

CHECKRIGHTLIM
BTFSK PORTC,1
RETLW 0x00
CALL DLY

```

Figure B.7: XY Scanner Motor Control and LCD Display code - 7 of 15

```

D:\SAMPIC\XY_scanner\xyvarspeed.ASM

BTFSK PORTC,1
RETLW 0x00
RETLW 0xFF

CHECKUPLIM
BTFSK PORTC,6
RETLW 0x00
CALL DLY
BTFSK PORTC,6
RETLW 0x00
RETLW 0xFF

CHECKDOWNLIM
BTFSK PORTC,7
RETLW 0x00
CALL DLY
BTFSK PORTC,7
RETLW 0x00
RETLW 0xFF

MOVELEFT ; enable using RD1, clock with RC3, direction with RD0 (left is high), test with RC0
BSF PORTD,1
BSF PORTD,0 ; set direction
CALL DLY
CALL CHECKLEFTLIM
MOVWF CHECKW
BTFSK CHECKW,0
GOTO ABORTLEFT ; return early if limit switch is being hit
CALL DLY ; brief delay
BCF PORTC,3 ; clock low, now wait 5ms
CALL DLYIMS
BSF PORTC,3
CALL DLYIMS
DECFSZ SPEEDLOOP
GOTO MOVELEFT

ABORTLEFT
; BCF PORTD,1
RETURN

MOVERIGHT ; test with RC1
BSF PORTD,1
BCF PORTD,0 ; set direction
CALL DLY
CALL CHECKRIGHTLIM
MOVWF CHECKW
BTFSK CHECKW,0
GOTO ABORTRIGHT
CALL DLY ; brief delay
BCF PORTC,3 ; clock low, now wait 5ms
CALL DLYIMS
BSF PORTC,3
CALL DLYIMS
DECFSZ SPEEDLOOP
GOTO MOVERIGHT

ABORTRIGHT
; BCF PORTD,1
RETURN

MOVEUP ; enable using RD2, clock with RC4, direction with RD3 (up is low), test with RC6
BSF PORTD,2 ; enable motor controllers
BCF PORTD,3 ; set direction
CALL DLY
CALL CHECKUPLIM
MOVWF CHECKW
BTFSK CHECKW,0
GOTO ABORTUP
CALL DLY ; brief delay
BCF PORTC,4 ; clock low, now wait 5ms
CALL DLYIMS
BSF PORTC,4
CALL DLYIMS
DECFSZ SPEEDLOOP
GOTO MOVEUP

ABORTUP
; BCF PORTD,2

```

Figure B.8: XY Scanner Motor Control and LCD Display code - 8 of 15

```

D:\SAMPIC\XY scanner\xyvarspeed.ASM

RETURN

MOVEDOWN ; test with RC7
BSF PORTD,2
BSF PORTD,3 ; set direction
CALL DLY
CALL CHECKDOWNLIM
MOVWF CHECKW
BTFSC CHECKW,0
GOTO ABORTDOWN
CALL DLY ; brief delay
BCF PORTC,4 ; clock low, now wait 5ms
CALL DLY1MS
BSF PORTC,4
CALL DLY1MS
DECFSZ SPEEDLOOP
GOTO MOVEDOWN

ABORTDOWN
; BCF PORTD,2
RETURN

; This routine will print to the LCD display the decimal number stored in W
PRINT_NUMBER
CALL CONVERT_BCD
MOVWF DIGIT100S,0
CALL NUMTABLE
CALL LCDWRITE
MOVWF DIGIT10S,0
CALL NUMTABLE
CALL LCDWRITE
MOVWF DIGIT1S,0
CALL NUMTABLE
CALL LCDWRITE
RETURN ; have now printed

;This routine will calculate hundreds from an 8-bit binary Input: w Output: w
CONVERT_BCD
MOVWF TEMP
MOVWF VALUE
CLRF TEMP2

GET100SLOOP
MOVLW D'100'
INCF TEMP2,1 ; count 100s
SUBWF TEMP,1 ; subtract 100
BTFSC STATUS,C ; and check if negative result
GOTO GET100SLOOP ; loop unless negative result
MOVLW D'100'
ADDWF TEMP,1 ; put value in TEMP back so it now contains only 10s and units
parts
DECF TEMP2,0 ; decrement temp2, answer is in W
MOVWF DIGIT100S

;This routine will calculate tens from an 8-bit binary Input: w Output: w and remove them,
leaving only ones
GET_TENS_AND_ONES
CLRF TEMP2

GET10SLOOP
MOVLW D'10'
INCF TEMP2,1
SUBWF TEMP,1
BTFSC STATUS,C
GOTO GET10SLOOP
MOVLW D'10'
ADDWF TEMP,0
MOVWF DIGIT1S
DECF TEMP2,0
MOVWF DIGIT10S
RETURN

; Scrolls text onto screen, ensure you call OFFSCREEN before writing to LCD, then call
SCROLL_TEXT to scroll text into view.
SCROLL_TEXT
MOVLW 0x11
MOVWF SCROLL_COUNTER
SCROLL_TEXT_LOOP
DECFSZ SCROLL_COUNTER,1

```

Figure B.9: XY Scanner Motor Control and LCD Display code - 9 of 15

D:\SAMPIC\XY\_scanner\xyvarspeed.ASM

```

        GOTO    SCROLL
        RETURN
SCROLL
        CALL    LONGDELAY
        CALL    ROTATELEFT
        GOTO    SCROLL_TEXT_LOOP

SCROLL_BACK
        MOVLW   0x11
        MOVWF   SCROLL_COUNTER
SCROLL_TEXT_LOOP2
        DECFSZ  SCROLL_COUNTER,1
        GOTO    SCROLL2
        RETURN
SCROLL2
        CALL    LONGDELAY
        CALL    ROTATERIGHT
        GOTO    SCROLL_TEXT_LOOP2

; Prints an error code stored in W to the display
ERRORCODE
        CALL    INITLCD
        CALL    PRINT_NUMBER
        MOVLW   ' '
        CALL    LCDWRITE
        MOVLW   'E'
        CALL    LCDWRITE
        MOVLW   'x'
        CALL    LCDWRITE
        MOVLW   'x'
        CALL    LCDWRITE
        MOVLW   'o'
        CALL    LCDWRITE
        MOVLW   'x'
        CALL    LCDWRITE
        RETURN

; Initialises PIC and sets register values to ensure correct operation
INITPIC
        BSF    STATUS,RP0 ;select bank 1
        MOVLW  b'00111100'
        MOVWF  TRISA ;set as output
        MOVLW  b'00000111'
        MOVWF  TRISE ;set as output
        MOVLW  b'00000000'
        MOVWF  TRISB ;set as output
        MOVWF  TRISD
        MOVLW  b'11000011'
        MOVWF  TRISC
        MOVLW  b'11000000'
        MOVWF  OPTION_REG
        MOVLW  b'00000110'
        MOVWF  ADCON1

        BCF    STATUS,RP0 ;select bank 0
        MOVLW  b'00010000'
        MOVWF  INTCON
        CLRF   PORTA
        CLRF   PORTE
        CLRF   PORTC
        CLRF   PORTD
        CLRF   EGGCOUNTER1
        CLRF   EGGCOUNTER2
        CLRF   CLOCKWASHIGH
        CLRF   ZEROWASHIGH
        BSF    PORTC,5 ; set for half steps
        BSF    PORTC,2 ; set for half steps
        CALL   DLY
        BSF    PORTC,3
        BSF    PORTC,4 ; set clock lines high, clock by bringing low then high again
        MOVLW  b'00110001'
        MOVWF  TICON
        BCF    SSPCON,5
        RETURN

INITLCD    ;INITIALIZE LCD

```

Figure B.10: XY Scanner Motor Control and LCD Display code - 10 of 15

```

D:\SAMPIC\XY scanner\xyvarspeed.ASM

MOV LW 0xFE ;WAIT LONG
CALL DLY2 ;254 * 0.5 = DELAY OF 127ms
;BUSY FLAG CAN'T BE CHECKED RIGHT NOW

MOV LW B'00111000' ;FUNCTION SET - 8 BIT, BIT_E = HIGH
MOV WF PORTB
BCF PORTB,BIT_E ; BIT_E = LOW

MOV LW 0x0A ;wait for about 5ms
CALL DLY2

MOV LW B'00111000' ;FUNCTION SET - 8 BIT, BIT_E=HIGH
MOV WF PORTB
BCF PORTB,BIT_E

MOV LW 0x02 ;
CALL DLY2

MOV LW B'00111000' ;FUNCTION SET - 8 BIT, BIT_E = high
MOV WF PORTB
BCF PORTB,BIT_E ;BIT_E=LOW
;above i have done same command 3 times, this may be not necessary, i just
followed datasheet
CALL LCDBUSY ;BUSY FLAG CAN BE CHECKED NOW!

MOV LW B'00101000' ;FUNCTION SET - 4 BIT ,BIT_E = HIGH
MOV WF PORTB
BCF PORTB,BIT_E
;.....EVERY INSTRUCTION WILL BE OF 2 CYCLE FROM HERE
CALL LCDBUSY ;..FUNCTION SET..
MOV LW B'00101000'
MOV WF PORTB
BCF PORTB,BIT_E ;1 CYCLE COMPLETE
MOV LW B'10001000'
MOV WF PORTB
BCF PORTB,BIT_E ;2 CYCLE

CALL LCDBUSY ;DISPLAY CONTROL -
MOV LW B'00001000' ; 1ST NIBBLE AND BIT_E=1,BIT_RW=0,BIT_RS=0
MOV WF PORTB
BCF PORTB,BIT_E ;1 CYCLE
MOV LW B'11111000' ;DISPLAY CONTROL NIBBLE (DISP=ON,CURSOR=ON,BLINK=ON) AND
BIT_E=1,BIT_RW=0,BIT_RS=0
MOV WF PORTB
BCF PORTB,BIT_E ;2 CYCLE

CALL LCDBUSY ;CLEAR DISPLAY AND HOME CURSOR
MOV LW B'00001000'
MOV WF PORTB
BCF PORTB,BIT_E
MOV LW B'00011000'
MOV WF PORTB
BCF PORTB,BIT_E

CALL LCDBUSY ;ENTRY SET -
MOV LW B'00001000' ; BIT_E=1,BIT_RW=0,BIT_RS=0
MOV WF PORTB
BCF PORTB,BIT_E ;1 CYCLE
MOV LW B'01101000' ;ENTRY SET - INCREMENT,NO DISP SHIFT(CUR
SHIFT),BIT_E=1,BIT_RW=0,BIT_RS=0
MOV WF PORTB
BCF PORTB,BIT_E ;2 CYCLE

CLRF SCREEN_OFFSET

RETURN

; Checks if the LCD display is busy
LCDBUSY
BSF STATUS,RP0 ;SELECT BANK 1
MOV LW B'11110001'
MOV WF TRISB ;SET RB7-RB4 INPUT

```

Figure B.11: XY Scanner Motor Control and LCD Display code - 11 of 15

```

D:\SAMPIC\XY_scanner\xyvarspeed.ASM

BCF STATUS,RP0 ;SELLECT BANK 0
;
BSF PORTB,BIT_RW
BCF PORTB,BIT_RS
;
BSF PORTB,BIT_E
MOVWF W2
CALL DLY
MOVF W2,0
MOVF PORTB,W ;READ
BCF PORTB,BIT_E ;1 CYCLE complete
BSF PORTB,BIT_RW
BCF PORTB,BIT_RS
BSF PORTB,BIT_E
MOVWF W2
CALL DLY
MOVF W2,0
NOP ;DO NOTHING COZ BUSY FLAG IS IN FIRST NIBBLE
BCF PORTB,BIT_E ;2nd CYCLE complete
;
ANDLW 0x80
BTFSZ STATUS,Z ;CHECK BUSY
GOTO LCDBUSY ;LOOP IF BUSY
;
BCF PORTB,BIT_RW ;**
BSF STATUS,RP0 ;NOT BUSY SO MAKE PORT B O/P
MOVLW b'00000001'
MOVWF TRISB
BCF STATUS,RP0
;
RETURN
; Selects 2nd line of display
; by selecting DDRAM address = 0x40 in case of 16x4 line LCD, see datasheet of HD44780
LINE2
CALL LCDBUSY
MOVLW B'11001000'
ADDWF SCREEN_OFFSET,0 ; adjust for offset
MOVWF PORTB
BCF PORTB,BIT_E
MOVLW B'00001000'
MOVWF PORTB
BCF PORTB,BIT_E
RETURN
; Moves the cursor off screen, use if you plan to scroll text onto the display
OFFSCREEN
CALL LCDBUSY
MOVLW B'10011000'
MOVWF PORTB
BCF PORTB,BIT_E
MOVLW B'00001000'
MOVWF PORTB
BCF PORTB,BIT_E
MOVLW 0x10
MOVWF SCREEN_OFFSET
RETURN
; Rotates all text left
ROTATELEFT
CALL LCDBUSY
MOVLW B'00011000'
MOVWF PORTB
BCF PORTB,BIT_E
MOVLW B'10001000'
MOVWF PORTB
BCF PORTB,BIT_E
RETURN
; Rotates all text left
ROTATERIGHT
CALL LCDBUSY
MOVLW B'00011000'
MOVWF PORTB
BCF PORTB,BIT_E
MOVLW B'11001000'
MOVWF PORTB

```

Figure B.12: XY Scanner Motor Control and LCD Display code - 12 of 15

D:\SAMPIC\XY scanner\xyvarspeed.ASM

```

BCF    PORTB,BIT_E
RETURN

; Switches off the cursor
CURSOROFF
CALL   LCDBUSY
MOVLW B'00001000'
MOVWF  PORTB
BCF    PORTB,BIT_E
MOVLW B'11001000'
MOVWF  PORTB
BCF    PORTB,BIT_E
RETURN

; Clears the display
CLEARSCREEN
CALL   LCDBUSY
MOVLW B'00001000'
MOVWF  PORTB
BCF    PORTB,BIT_E
MOVLW B'00011000'
MOVWF  PORTB
BCF    PORTB,BIT_E

MOVLW B'00001000'
MOVWF  PORTB
BCF    PORTB,BIT_E
MOVLW B'00111000'
MOVWF  PORTB
BCF    PORTB,BIT_E
RETURN

;Writes data/character in W register to selected CG/DD RAM, see its use in START routine
LCDWRITE
MOVWF  TEMP
CALL   LCDBUSY
MOVWF  TEMP,W
ANDLW B'11110000'
IORLW B'00001010' ;BIT_E=1,BIT_RW=0,BIT_RS=1
MOVWF  PORTB
BCF    PORTB,BIT_E ;1 CYCLE COMPLETE
SWAPF TEMP,W ;SWAP NIBBLES AND STORE IN W REGISTER
ANDLW B'11110000'
IORLW B'00001010' ;BIT_E=1,BIT_RW=0,BIT_RS=1
MOVWF  PORTB
BCF    PORTB,BIT_E ;2 CYCLE COMPLETE
MOVLW 0x00
MOVWF  TEMP
RETURN

;Delay routines
;100uS delay with 20MHz
DLY
MOVLW D'160'
MOVWF  V_DLY
DLY_LOOP
DECFSZ V_DLY, F
GOTO   DLY_LOOP
RETURN

SHORTDLY
MOVLW D'20'
MOVWF  V_DLY
SDLY_LOOP
DECFSZ V_DLY, F
GOTO   SDLY_LOOP
RETURN

; w times DLY
DLY1
MOVWF  V_DLY1
DLY1_LOOP
CALL   DLY
DECFSZ V_DLY1, F
GOTO   DLY1_LOOP

```

Figure B.13: XY Scanner Motor Control and LCD Display code - 13 of 15

```

RETURN
DLY1MS
    MOV LW    D'5'
    CALL     DLY1
    RETURN
DLY2MS
    MOV LW    D'10'
    CALL     DLY1
    RETURN
DLY2
    MOV WF    V_DLY1
    MOV LW    D'05'
    MOV WF    V_DLY2
DLY2_LOOP
    MOV F    V_DLY1, 0 ; move back to W
    CALL     DLY1
    DECFSZ   V_DLY2, F ; decrement counter from 5
    GOTO     DLY2_LOOP
    RETURN
DLY20MHZ
    MOV WF    V_DLY20MHZ
    MOV LW    0x10 ; should give a 500uS delay with 20Mhz
    CALL     DLY1
    MOV F    V_DLY20MHZ, 0
    RETURN
LONGDELAY
    MOV WF    TEMP
    MOV LW    0x80
    CALL     DLY1
    RETURN
VLONGDELAY
    ; w^2 * DLY1
    MOV WF    V_DLY3
VDLY_LOOP
    CALL     DLY1
    DECFSZ   V_DLY3, F
    GOTO     VDLY_LOOP
    RETURN
VVLONGDELAY
    ; w^3 * DLY1
    MOV WF    V_DLY4
VVDLY_LOOP
    CALL     VVLONGDELAY
    DECFSZ   V_DLY4, F
    GOTO     VVDLY_LOOP
    RETURN
STATUSIS
    CALL     CLEARSCREEN
    MOV LW    'S'
    CALL     LCDWRITE
    MOV LW    't'
    CALL     LCDWRITE
    MOV LW    'a'
    CALL     LCDWRITE
    MOV LW    't'
    CALL     LCDWRITE
    MOV LW    'u'
    CALL     LCDWRITE
    MOV LW    's'
    CALL     LCDWRITE
    MOV LW    ':'
    CALL     LCDWRITE
    CALL     CURSOROFF
    RETURN

```

OK

D:\SAMPIC\XY scanner\xyvarspeed.ASM

```
MOVLW 'O'  
CALL LCDWRITE  
MOVLW 'K'  
CALL LCDWRITE  
CALL LINE2  
RETURN  
END
```

```

D:\SAMPIC\50Hz100150250_adjusted.asm

;*****
; This program is designed to send data to four AD9833 Waveform *
; generator ICs to control four center frequencies used to control *
; custom sensor feedback networks *
; Inputs ----- *
; *
; Data (7:0) = PortC (7:0) *
; Clock = PortB : 4 *
; Program Enable = PortB : 5 *
; Channel Select (1:0) = PortB 6:7 *
; *
; Outputs ----- *
; *
; SDO = PortA:0 *
; SCLK = PortA:2 *
; !CS = PortA:1 *
; *
; CH1Sel :- PortC:0 *
; CH2Sel :- PortC:1 *
; CH3Sel :- PortC:2 *
; CH4Sel :- PortC:3 *
; *
; SynthSDO :- PortA:0 *
; SynthSCLK :- PortA:2 *
; *
;*****
; *
; Filename:      usbsetvall.asm *
; Date: 19/12/06 *
; File Version: 0.1 *
; *
; Author: Sam Beardsmore-Rust *
; Company: University of Sussex, PEQT Group *
; *
;*****
; *
; Files required: *
; *
; 16F690.lkr (actually seems to cause errors?) *
; *
;*****
list      p=16F690          ; list directive to define processor
#include <pl6F690.inc>      ; processor specific variable definitions

errorlevel -302           ; suppress message 302 from list file

__CONFIG _CP_OFF & _CPD_OFF & _BOR_OFF & _MCLRE_OFF & _WDT_OFF & _PWRTE_ON &
_INTRC_OSC_NOCLKOUT & _FCMEN_OFF & _IESO_OFF

; '_CONFIG' directive is used to embed configuration word within .asm file.
; The tables following the directive are located in the respective .inc file.
; See data sheet for additional information on configuration word settings.

;*****
;RESET_VECTOR CODE 0x005 ; processor reset vector

cblock 0x20
Delay1 ; Define two file registers for the
Delay2 ; delay loop
SENDREG
SENDCOUNT
SENDSLFSF
SENDSMSF
ChipSelect
BITS0to5
BITS6to13
BITS14to19
BITS20to27
endc

Ch1Sel EQU 0
Ch2Sel EQU 1
Ch3Sel EQU 2

```

Figure B.16: Tuned Sensor Controller code - 1 of 5

```

D:\SAMPIC\50Hz100150250_adjusted.asm

Ch4Sel EQU 3

;ChipSelect set 0

SynthSDO EQU 0
SynthSCLK EQU 2

    org 0x005
    GOTO main                ; go to beginning of program

delaysub
    MOVLW 0xFF
    MOVWF Delay1
    MOVLW 0xFF
    MOVWF Delay2 ; setup loop to do 255 * 255 iterations
delaysub2
    DECFSZ Delay1, 1 ; decrement register (and store) and, unless now 0, repeat
    GOTO delaysub2
    DECFSZ Delay2, 1 ;
    GOTO delaysub2
    RETURN

serclock
;CALL delaysub ; wait a minute to make sure output ready
NOP
BCF PORTA, SynthSCLK ; set clock low - data clocked in on falling edge
;CALL delaysub ; wait a sec
NOP
BSF PORTA, SynthSCLK ; set clock high - it idles high
RETURN ; now finished clocking out so return

sendserial
    MOVLW 0x08
    MOVWF SENDCOUNT
mansomnd
    BTFSC SENDREG, 7 ; check MSB of sendreg
    GOTO sersendhigh
sersendlow
    BCF PORTA, SynthSDO ; set bit low
    CALL serclock ; clock low out
    GOTO sersendcheck ; finished sending first bit
sersendhigh
    BSF PORTA, SynthSDO ; set bit high
    CALL serclock ; clock high out
sersendcheck
    RLF SENDREG, 1 ; rotate right to move on to the next bit
    DECFSZ SENDCOUNT, 1
    GOTO mansomnd
;CALL delaysub ; wait a little before returning to ensure a little gap at end of last clock
cycle
NOP
BCF PORTA, 0 ; set SDO low
RETURN ; finished sending all eight bits so now return

senddata
; CALL stage3
    COME ChipSelect, 0
    ANDWF PORTC, 1 ; see notes, this set the relevant chip select pin low and leaves others on
port c unchanged
; BCF PORTC, ChipSelect; set CS pin low to activate programming of digital potentiometers
    MOVF SENDMSF, 0 ; get MSF to send
    MOVWF SENDREG ; prepare to send it
    CALL sendserial ; transmit
    MOVF SENDLSF, 0 ; get second value
    MOVWF SENDREG ; prepare to send
    CALL sendserial
; finished so reset pointer
; BSF PORTC, ChipSelect; set CS pin high to store new values and disable programming
    MOVF ChipSelect, 0 ; move chip select data into W
    IORWF PORTC, 1 ; this sets the relevant chip select pin high again and leaves others unchanged
    RETURN

Transmit
    MOVLW b'00000001' ; reset vector
    MOVWF SENDMSF;

```

Figure B.17: Tuned Sensor Controller code - 2 of 5

```

D:\SAMPIC\50Hz100150250_adjusted.asm

MOVW b'00000000'
MOVWF SENDLSF;
CALL senddata ; transmit reset vector

CALL delaysub

MOVW b'00100000' ; Load two consecutive values to set frequency
MOVWF SENDMSF;
MOVW b'00101000' ; set square wave output (MSB) without diving by 2
MOVWF SENDLSF;
CALL senddata ; transmit reset vector

; First send least significant 14 bits
MOVW BITS14to19,0
MOVWF SENDMSF;
MOVW BITS20to27,0
MOVWF SENDLSF;
CALL senddata

; then send most significant 14 bits
MOVW BITS0to5,0
MOVWF SENDMSF;
MOVW BITS6to13,0
MOVWF SENDLSF;
CALL senddata

; Finally make sure phase registers are zeroed
MOVW b'11000000'
MOVWF SENDMSF;
MOVW b'00000000'
MOVWF SENDLSF;
CALL senddata

RETURN

main
; remaining code goes here
BCF STATUS,RP0 ;Bank 0
BCF STATUS,RP1 ;
CLRF PORTC ;Init PORTC
CLRF PORTA ; Init POPTA
CLRF PORTB ; Init PORTB
BSF STATUS,RP1 ;Bank 2
CLRF ANSEL ;digital I/O
CLRF ANSELH ; digital I/O only
BSF STATUS,RP0 ;Bank 1
BCF STATUS,RP1 ;
MOVW 0xFF ;Hopefully set all of port C and B to be inputs
MOVWF TRISB ; set port B to be inputs
MOVW 0x00 ;
MOVWF TRISA ; Hopefully set all of port A to be outputs (except RA3, always input)
MOVWF TRISC ;
BSF OSCCON, 4
BSF OSCCON, 5
BSF OSCCON, 6

MOVW b'00001010' ;configure Timer0. Sourced from the Processor clock
MOVWF OPTION_REG ;Maximum Prescaler

BCF STATUS,RP0 ;Bank 0
MOVW 0x26
MOVWF FSR ; initialise FSR register to point at array

BSF PORTA, 1; set chip select pin high to deactivate programming of digital pot
BSF PORTA, 4
BSF PORTA, 5 ; set pins 4 and 5 on port a high - using for info LEDs
BSF PORTA, 2 ; set clock high - it will idle high for use with AD9833

BSF PORTC, Ch1Sel
BSF PORTC, Ch2Sel
BSF PORTC, Ch3Sel
BSF PORTC, Ch4Sel ; Set all chip select bits high to disable writing

;CALL stage1

```

Figure B.18: Tuned Sensor Controller code - 3 of 5

D:\SAMPIC\50Hz100150250\_adjusted.asm

```

mainloop
    BTFSS PORTA,3 ; check value of PORTA bit 3, usually 5V, 0V when pressed
    GOTO Buttdown
    GOTO mainloop ; loop if button not being pressed (bit 0 is low)

Buttdown
    MOVLW b'00000010' ; set channel 1 select - 50hz - adjusted up by 12khz
    MOVWF ChipSelect ;
    MOVLW b'01011010' ; First send least significant 14 bits
    MOVWF BITS14to19
    MOVLW b'10011110'
    MOVWF BITS20to27
    MOVLW b'01000000' ; then send most significant 14 bits
    MOVWF BITS0to5
    MOVLW b'00011011'
    MOVWF BITS6to13

    CALL Transmit

    MOVLW b'00000001' ; set channel 2 select - 100hz
    MOVWF ChipSelect ;

    MOVLW b'01110101' ; First send least significant 14 bits
    MOVWF BITS14to19
    MOVLW b'00111100'
    MOVWF BITS20to27
    MOVLW b'01000000' ; then send most significant 14 bits
    MOVWF BITS0to5
    MOVLW b'00110110'
    MOVWF BITS6to13

    CALL Transmit

    MOVLW b'00000100' ; set channel 3 select - 150hz
    MOVWF ChipSelect ;

    MOVLW b'01001111' ; First send least significant 14 bits
    MOVWF BITS14to19
    MOVLW b'11011010'
    MOVWF BITS20to27
    MOVLW b'01000000' ; then send most significant 14 bits
    MOVWF BITS0to5
    MOVLW b'01010010'
    MOVWF BITS6to13

    CALL Transmit

    MOVLW b'00001000' ; set channel 2 select - 250hz
    MOVWF ChipSelect ;

    MOVLW b'01011001' ; First send least significant 14 bits
    MOVWF BITS14to19
    MOVLW b'00000101'
    MOVWF BITS20to27
    MOVLW b'01000000' ; then send most significant 14 bits
    MOVWF BITS0to5
    MOVLW b'10001001'
    MOVWF BITS6to13

    CALL Transmit

Buttonup
    BTFSC PORTA,3 ; check value is high (5V) again
    GOTO mainloop ; if it's 0V, skip this instruction
    GOTO Buttonup ; if not, wait til it is
end

; initialize eeprom locations
EE    CODE    0x2100
DE    0x00, 0x01, 0x02, 0x03

```

Figure B.19: Tuned Sensor Controller code - 4 of 5

D:\SAMPIC\50Hz100150250\_adjusted.asm

```
END ; directive 'end of program'
```

```

D:\SAMPIC\motor controller\motor 03 09 08.asm

;*****
; This program is designed to provide control over a modified A4
; flatbed scanner. Primarily it provides control over the stepper
; motor used to move the head past the sample, as well as interfacing
; through a USB data acquisition card to a Labview VI for computer
; control and data acquisition.
;
;
;*****
;
; Filename:      motor 03 09 08.asm
; Date: 03/09/08
;
; Author: Sam Beardsmore-Rust
; Company: University of Sussex, PEQT Group
;
;
; Files required:
;               16F690.lkr
;*****

list      p=16F690          ; list directive to define processor
#include <pl16F690.inc>     ; processor specific variable definitions

errorlevel -302           ; suppress message 302 from list file

__CONFIG _CP_OFF & _CPD_OFF & _BOR_OFF & _MCLRE_OFF & _WDT_OFF & _PWRTE_ON &
_INTRC_OSC_NOCLKOUT & _FCMEN_OFF & _IESO_OFF

; '__CONFIG' directive is used to embed configuration word within .asm file.
; The labels following the directive are located in the respective .inc file.
; See data sheet for additional information on configuration word settings.

;*****
;RESET_VECTOR CODE 0x005 ; processor reset vector

cblock 0x20
Delay1 ; Define two file registers for the
Delay2 ; delay loop
V_DLY
V_DLY2
DIRECTION
STEPCOUNT
endc

org 0x005
GOTO main ; go to beginning of program

;Delay routines
;500us delay with 4MHz therefore 250us delay with 8MHz
DLY
    MOVLW D'165'
    MOVWF V_DLY
DLY_LOOP
    DECFSZ V_DLY, F
    GOTO DLY_LOOP
    RETURN

DLYp25ms
    MOVLW 0x0A
    MOVWF V_DLY2
DLYp25ms_LOOP
    CALL DLY
    DECFSZ V_DLY2, F
    GOTO DLYp25ms_LOOP
    RETURN

```

Figure B.21: Tuned Sensor Controller code - 1 of 3

D:\SAMPIC\motor controller\motor 03 09 08.asm

```

DLYp250ms
    MOVLW 0x64
    MOVWF V_DLY2
DLYp250ms_LOOP
    CALL DLY
    DECFSZ V_DLY2,F
    GOTO DLYp250ms_LOOP
    RETURN

clockwise
    CLRF PORTB
    BSF PORTB, 4
    BSF PORTB, 7
    CALL DLYp25ms
    BCF PORTB, 7
    BSF PORTB, 6
    CALL DLYp25ms
    BCF PORTB, 4
    BSF PORTB, 5
    CALL DLYp25ms
    BCF PORTB, 6
    BSF PORTB, 7
    CALL DLYp25ms
    CLRF PORTB
    RETURN

anticlockwise
    CLRF PORTB
    BSF PORTB, 5
    BSF PORTB, 7
    CALL DLYp25ms
    BCF PORTB, 7
    BSF PORTB, 6
    CALL DLYp25ms
    BSF PORTB, 4
    BCF PORTB, 5
    CALL DLYp25ms
    BCF PORTB, 6
    BSF PORTB, 7
    CALL DLYp25ms
    CLRF PORTB
    RETURN

gotoreset
    BTFSS PORTA, 0
    RETURN
    CALL clockwise
    GOTO gotoreset
    RETURN

dosweep
    BTFSS PORTA, 1
    RETURN
    CALL anticlockwise
    GOTO dosweep
    RETURN

dostep
    BTFSS PORTA, 5
    GOTO dostep
    MOVLW D'15'
    MOVWF STEPCOUNT
steploop
    BTFSS PORTA, 1
    RETURN
    CALL anticlockwise
    DECFSZ STEPCOUNT
    GOTO steploop
    RETURN

main
; remaining code goes here
BCF STATUS, RP0 ;Bank 0
BCF STATUS, RP1 ;
CLRF PORTC ;Init PORTC

```

Figure B.22: Tuned Sensor Controller code - 2 of 3

D:\SAMPIC\motor controller\motor 03 09 08.asm

```

CLRF PORTA ; Init POPTA
CLRF PORTB ; Init PORTE
BSF STATUS,RP1 ;Bank 2
CLRF ANSEL ;digital I/O
CLRF ANSELH ; digital I/O only
BSF STATUS,RP0 ;Bank 1
BCF STATUS,RP1 ;
MOVLW 0xFF ;Hopefully set all of port C and B to be inputs
MOVWF TRISC ; set port C to be inputs
MOVWF TRISA ; Hopefully set all of port A to be inputs
MOVLW 0x00 ;
MOVWF TRISB ; set port B to be outputs
BSF OSCCON, 4
BSF OSCCON, 5
BSF OSCCON, 6 ; 8 Mhz Clock selected

MOVLW b'00001010' ;configure Timer0. Sourced from the Processor clock
MOVWF OPTION_REG ;Maximum Prescaler

BCF STATUS,RP0 ;Bank 0
CLRF DIRECTION

;CALL stage1

mainloop
; BTFSS PORTA,0
; BSF DIRECTION,0
; BTFSS PORTA,1
; BCF DIRECTION,0
; BTFSS DIRECTION,0
; GOTO clockwise
; GOTO anticlockwise
BTFSS PORTA,4
CALL gotoreset
BTFSS PORTA,5
CALL dostep
BTFSS PORTA,3
CALL dosweep
GOTO mainloop ; otherwise wait forever until that happens
end

; initialize eeprom locations
EE CODE 0x2100
DE 0x00, 0x01, 0x02, 0x03

END ; directive 'end of program'

```

Figure B.23: Tuned Sensor Controller code - 3 of 3